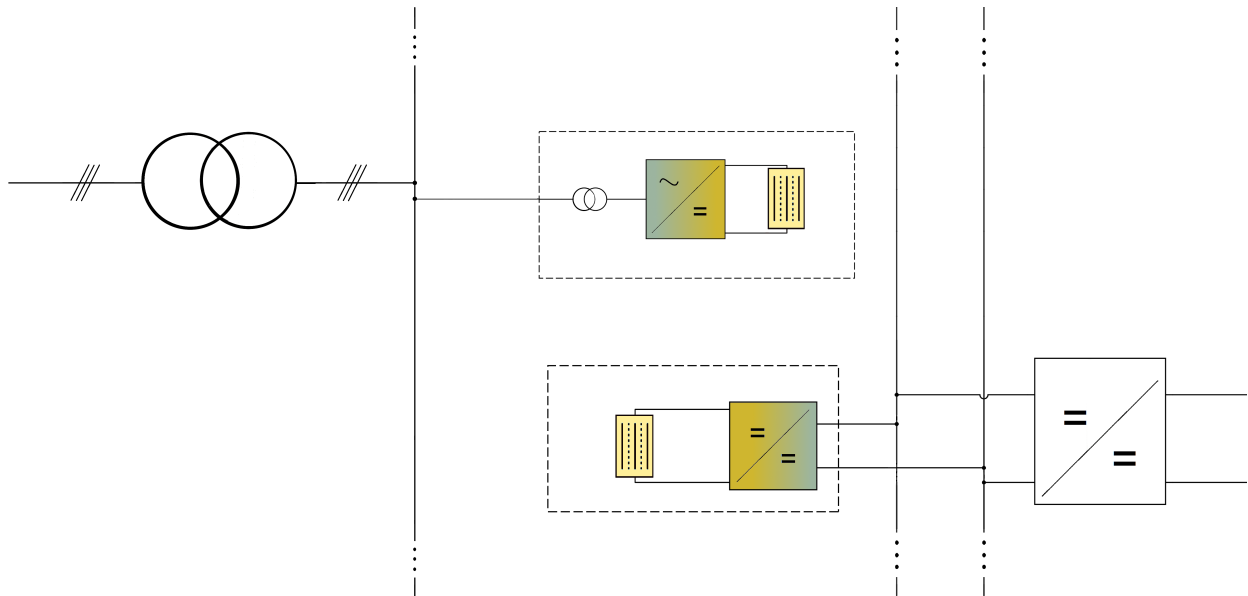




CHALMERS
UNIVERSITY OF TECHNOLOGY



Electric infrastructure for electrolyser systems

Design proposals for AC and DC distribution systems

Master's thesis in Electric Power Engineering

TARIK DERVIŠIĆ AND CARINA ENGSTRÖM

DEPARTMENT OF ELECTRICAL ENGINEERING

CHALMERS UNIVERSITY OF TECHNOLOGY
Gothenburg, Sweden 2021
www.chalmers.se

MASTER'S THESIS 2021

Electric infrastructure for electrolyser systems

Design proposals for AC and DC distribution systems

Tarik Dervišić
Carina Engström



CHALMERS
UNIVERSITY OF TECHNOLOGY

Department of Electrical Engineering
Division of Electric Power Engineering
CHALMERS UNIVERSITY OF TECHNOLOGY
Gothenburg, Sweden 2021

Electric infrastructure for electrolyser systems
Design proposals for AC and DC distribution systems

Tarik Dervišić and Carina Engström

© Tarik Dervišić and Carina Engström, 2021.

Supervisor: Dr. Jan R. Svensson, Research Fellow, Hitachi ABB Power Grids
Examiner: Prof. Massimo Bongiorno, Chalmers University of Technology

Master's Thesis 2021
Department of Electrical Engineering
Division of Electric Power Engineering
Chalmers University of Technology
SE-412 96 Gothenburg
Telephone +46 31 772 1000

Cover: Conceptual drawing of an electrolyser system connected to an AC distribution system and a DC distribution system

Typeset in L^AT_EX
Gothenburg, Sweden 2021

Abstract

The ongoing climate change has resulted in an evolution of the global energy system in which non-fossil fuels should be used. This has resulted in a transition towards renewable energy generation and an electrification of industry processes and loads, in which renewable hydrogen production is a key stone. With electrolyzers and renewable electric power supply, hydrogen can be produced without greenhouse gas emissions. This thesis will introduce different electrolyser technologies with explanation of relevant information and then focus on the proton exchange membrane electrolyser. A short market analysis on hydrogen applications for different sectors and electrolyser manufacturers will be conducted to get an overview of the electrolyser opportunities. The studies showed that renewable hydrogen has a huge potential to support the transition towards the decarbonisation of several sectors. Development efforts by the proton exchange membrane electrolyser manufacturers are also ongoing in order to increase performance and reduce cost. Furthermore, a model of the proton exchange membrane electrolyser will be derived for the analysis of electrolyser properties and for time domain simulations. The operating principle of the electrolyser will be modelled from the electric perspective and will describe how the voltage depends on the current density, the internal resistance, the temperature, and the pressure. A futuristic perspective on how the development of electrolyser stacks could proceed will also be presented. The electrolyser model demonstrated an increase of the cell voltage and a decrease of the efficiency for an increase of the current density. By reducing the internal resistance, increasing the current density or increasing the number of series-connected cells, the electrolyser stack size could be enlarged. Thereafter, the electrolyser model will be connected to an AC distribution system and a DC distribution system. For the AC distribution system case, the voltage level is stepped down and then rectified using a 12-pulse thyristor rectifier. For the DC distribution system case, the voltage is converted with a phase-shifted full-bridge DC/DC converter. The results of the study are that the 12-pulse thyristor rectifier shows good dynamic performance, but is affected negatively by its 11th and 13th order current harmonics because of the increasing reactive power consumption. The phase-shifted full-bridge DC/DC converter has the advantage that no reactive power is consumed. Moreover, it can provide high output current and low output voltage with low ripples while attaining low current flow at a medium-voltage DC-bus as well, therefore appearing as a suitable converter for electrolyser applications. Finally, another futuristic perspective for the coming 30 years on the upscaling of electrolyser stations to gigawatt-scale will conclude the report.

Keywords: Electrolyser, proton exchange membrane, hydrogen, 12-pulse thyristor rectifier, phase-shifted full-bridge DC/DC converter

Acknowledgements

We would like to express our sincere thanks to our supervisor Jan Svensson for the dedication and support of our work. Our weekly conversations and your feedback along the way helped us immensely. Many thanks to our examiner Massimo Bongiorno as well, who was involved during the whole process and made his time available to help us with the work. We would also like to thank Qian Xun for an insightful discussion on the electric properties of fuel cells, which aided in the electrolyser modelling, and Artem Rodionov who introduced the converter modelling tool to us.

Tarik Dervišić and Carina Engström, Gothenburg, 2021.

Contents

| | |
|--|--------------|
| List of Figures | x |
| List of Tables | xvi |
| List of Symbols | xxiii |
| List of Acronyms | xxii |
| 1 Introduction | 1 |
| 1.1 Background | 1 |
| 1.2 Aim | 3 |
| 1.3 Scope | 3 |
| 1.4 Societal, ethical and ecological aspects | 3 |
| 2 Method | 5 |
| 3 Introduction to electrolysers | 7 |
| 3.1 Electrolyser technologies | 7 |
| 3.1.1 Alkaline water electrolysis | 8 |
| 3.1.2 Proton exchange membrane electrolysis | 9 |
| 3.1.3 Solid oxide electrolyser cell electrolysis | 10 |
| 3.1.4 Comparison | 12 |
| 4 Market analysis of hydrogen and electrolysers | 13 |
| 4.1 Hydrogen market | 13 |
| 4.2 Electrolyser manufacturers | 13 |
| 4.2.1 Nel | 13 |
| 4.2.2 McPhy | 16 |
| 4.2.3 ITM Power | 17 |
| 4.2.4 Siemens Energy | 19 |
| 4.2.5 Cummins, formerly Hydrogenics | 20 |
| 5 Hydrogen applications | 23 |
| 5.1 Oil sector | 23 |
| 5.2 Chemical sector | 24 |
| 5.3 Steel- and iron sector | 25 |
| 5.4 Transport sector | 26 |
| 5.4.1 Road transport | 26 |

| | | |
|----------|---|------------|
| 5.4.2 | Maritime | 27 |
| 5.4.3 | Rail | 28 |
| 5.4.4 | Aviation | 28 |
| 5.5 | Power sector | 29 |
| 5.6 | Heating sector | 30 |
| 5.7 | Agriculture- and food sector | 30 |
| 6 | PEM electrolyser model | 31 |
| 6.1 | PEM electrolysis theory | 31 |
| 6.2 | Performance and simulation of PEM model | 32 |
| 6.3 | Future electrolyser trends | 43 |
| 6.4 | Summary | 47 |
| 7 | PEM electrolyser connected to a converter | 49 |
| 7.1 | Thyristor-based AC/DC converter | 51 |
| 7.1.1 | Characteristics of the 12-pulse thyristor rectifier for steady-state electrolyser operation | 53 |
| 7.1.2 | Power requirements and harmonic analysis | 61 |
| 7.1.3 | Dynamic control response of the 12-pulse rectifier | 67 |
| 7.2 | DC/DC converter | 70 |
| 7.2.1 | DC/DC converter topology | 70 |
| 7.2.2 | Phase-shifted full-bridge DC/DC converter module topology | 72 |
| 7.2.3 | Characteristics of the PSFB DC/DC converter for steady-state electrolyser operation | 73 |
| 7.2.4 | Dynamic control response of the PSFB DC/DC converter | 80 |
| 7.2.5 | The effect of leakage inductance on the PSFB DC/DC converter | 84 |
| 7.3 | Summary | 85 |
| 8 | Implementation and structure of electrolyser station on GW-scale | 87 |
| 8.1 | Electrolyser station requirements at PCC | 87 |
| 8.2 | Internal requirements of electrolyser station | 88 |
| 8.3 | Structure of electrolyser station | 89 |
| 8.3.1 | Case 1 | 89 |
| 8.3.2 | Case 2 | 92 |
| 8.3.3 | Case 3 | 93 |
| 8.3.4 | Case 4 | 95 |
| 9 | Conclusion and future work | 99 |
| 9.1 | Conclusion | 99 |
| 9.2 | Future work | 100 |
| | Bibliography | 103 |
| A | Appendix | i |
| A.1 | PEM Electrolyser model | i |
| A.2 | 12-pulse thyristor rectifier model | ii |
| A.3 | Phase-shifted full-bridge DC/DC converter model | iv |

List of Figures

| | | |
|------|--|----|
| 3.1 | Operating principle of an alkaline electrolyser cell [25]. | 8 |
| 3.2 | Common alkaline electrolyser system architecture [25]. | 9 |
| 3.3 | Operating principle of a PEM electrolyser cell [25]. | 10 |
| 3.4 | Common PEM electrolyser system architecture [25]. | 10 |
| 3.5 | Operating principle of a SOEC electrolyser cell [25]. | 11 |
| 3.6 | Common SOEC electrolyser system architecture [25]. | 11 |
| 4.1 | Concept image of Nel’s A485 alkaline electrolyser [30]. | 14 |
| 4.2 | Concept image of Nel’s M400 PEM electrolyser [30]. | 15 |
| 4.3 | Concept image of Nel’s A3880 large scale alkaline electrolyser system [30]. | 15 |
| 4.4 | One of McPhy’s larger electrolysers called McLyzer [31]. | 17 |
| 4.5 | McPhy’s 20 MW electrolyser system consisting of 4 MW modules [31]. . . | 17 |
| 4.6 | Concept image of ITM Power’s HGas2SP electrolyser [32]. | 18 |
| 4.7 | Concept image of ITM Power’s HGasXMW electrolyser [32]. | 19 |
| 4.8 | Concept image of Siemens Silyzer 300 electrolyser with stack size available up to 130 MW [35]. | 19 |
| 4.9 | High pressure, 3.5 kA stacks as installed in Energiepark Mainz in Germany [39]. | 20 |
| 4.10 | Based around a modular 20 MW PEM electrolyser, the new facility in Canada doubles Cummins previous installation size in Japan [47]. | 21 |
| 5.1 | Simplified overview of hydrocracking for higher value oil production. | 23 |
| 5.2 | Simplified overview of hydrogen to ammonia and methanol conversion. . . . | 24 |
| 5.3 | Renewable hydrogen production costs from VRE compared to non- renewable hydrogen production costs within the next 30 years [29]. | 25 |
| 5.4 | Illustration of BF-BOF steel production process and HYBRIT’s renewable DRI-EAF steel production process utilising renewable hydrogen as reducing agent [51]. | 26 |
| 5.5 | Illustration of electrolyser systems integrated in the power grid together with different hydrogen application sectors [26]. | 29 |
| 6.1 | Overview of the PEM electrolyser model with input and output variables. . | 34 |
| 6.2 | Electrolyser model in Figure 6.1 described as resistors. | 34 |
| 6.3 | Cell voltage V_{cell} of the electrolyser model. | 36 |
| 6.4 | LHV efficiency η^{LHV} of the electrolyser model. | 36 |
| 6.5 | The cell overvoltages of the electrolyser model. | 37 |
| 6.6 | Electrolyser model resistance. | 37 |
| 6.7 | The power P_0 of the electrolyser model. | 38 |

| | | |
|------|--|----|
| 6.8 | The power losses $P_{0,\text{loss}}$ of the electrolyser model. | 38 |
| 6.9 | The output voltage V_0 and the output current I_0 as a function of the hydrogen production rate v_{H_2} | 39 |
| 6.10 | Cell voltage V_{cell} of the electrolyser model for different temperature cases. | 39 |
| 6.11 | LHV efficiency η^{LHV} of the electrolyser model for different temperature cases. | 40 |
| 6.12 | Cell voltage V_{cell} of the electrolyser model for different pressure cases. | 40 |
| 6.13 | LHV efficiency η^{LHV} of the electrolyser model for different pressure cases. | 41 |
| 6.14 | Cell voltage V_{cell} of the electrolyser model for different membrane thickness cases. | 41 |
| 6.15 | LHV efficiency η^{LHV} of the electrolyser model for different membrane thickness cases. | 42 |
| 6.16 | Electrolyser hydrogen production rate v_{H_2} as a function of membrane area A_{mem} and electrolyser voltage V_0 for current density of $J=3$ A/cm ² with $J_1=5$ A/cm ² | 44 |
| 6.17 | Electrolyser power P_0 as a function of membrane area A_{mem} and electrolyser voltage V_0 for current density of $J=3$ A/cm ² with $J_1=5$ A/cm ² | 44 |
| 6.18 | Electrolyser power losses $P_{0,\text{loss}}$ as a function of membrane area A_{mem} and electrolyser voltage V_0 for current density of $J=3$ A/cm ² with $J_1=5$ A/cm ² | 45 |
| 6.19 | Electrolyser hydrogen production rate v_{H_2} as a function of membrane area A_{mem} and electrolyser voltage V_0 for current density of $J=4$ A/cm ² with $J_1=5$ A/cm ² | 45 |
| 6.20 | Electrolyser power P_0 as a function of membrane area A_{mem} and electrolyser voltage V_0 for current density of $J=4$ A/cm ² with $J_1=5$ A/cm ² | 46 |
| 6.21 | Electrolyser power losses $P_{0,\text{loss}}$ as a function of membrane area A_{mem} and electrolyser voltage V_0 for current density of $J=4$ A/cm ² with $J_1=5$ A/cm ² | 46 |
| 7.1 | Electrolyser station comprised of system modules, connected to a HVAC line via a transformer. | 49 |
| 7.2 | Electrolyser station comprised of system modules, connected to a HVAC line via a rectifier. | 50 |
| 7.3 | Electrolyser station comprised of system modules, connected to a HVDC line via a DC/DC converter. | 50 |
| 7.4 | Schematic diagram of the six-pulse thyristor rectifier, shown with a voltage step-down transformer and an output filter inductor connected to the electrolyser. | 51 |
| 7.5 | Schematic diagram of the 12-pulse thyristor rectifier. The 12-pulse is comprised of a Y Δ y transformer to step down the voltage level and cancel 5 th and 7 th order harmonics, two six-pulse rectifiers in parallel output configuration to increase the total current rating and an output filter inductance for each rectifier. | 52 |
| 7.6 | a) Block scheme of the pulse generation for rectifier 1 with voltage measurement through a PLL, and b) current control block scheme with anti-windup. The generated controlled firing angle α varies as a response to the input current reference, which in turn decided the commutation delay of each thyristor. Pulse generation is synchronised with the measured voltage phase angle φ_{AC} . A similar control system can be drawn for rectifier 2. | 53 |
| 7.7 | Phase voltages at the grid for hydrogen production rate reference of a) 25% and b) 75%. | 56 |

| | | |
|------|---|----|
| 7.8 | Phase currents at the grid for hydrogen production rate reference of a) 25% and b) 75%. | 56 |
| 7.9 | Rectifier 1 phase voltages v_{ac1} for hydrogen production rate reference of a) 25% and b) 75%. The irregular spike behaviour is due to the commutation of the current via the Δ -connected transformer leakage inductance L_{R_s} . . . | 57 |
| 7.10 | Rectifier 1 phase currents i_{ac1} for hydrogen production rate reference of a) 25% and b) 75%. | 57 |
| 7.11 | Rectifier 2 phase voltages v_{ac2} for hydrogen production rate reference of a) 25% and b) 75%. The irregular spike behaviour is due to the commutation of the current via the y -connected transformer leakage inductance L_{R_s} . . . | 58 |
| 7.12 | Rectifier 2 phase currents i_{ac2} for hydrogen production rate reference of a) 25% and b) 75%. | 58 |
| 7.13 | Rectifier 1 DC current I_{dc1} for hydrogen production rate reference of a) 25% and b) 75%. | 59 |
| 7.14 | Rectifier 2 DC current I_{dc2} for hydrogen production rate reference of a) 25% and b) 75%. | 59 |
| 7.15 | Output current I_0 for hydrogen production rate reference of a) 25% and b) 75%. | 60 |
| 7.16 | Output voltage V_0 for hydrogen production rate reference of a) 25% and b) 75%. | 60 |
| 7.17 | The active power P_{AC} and the reactive power Q_{AC} that is required at the PCC as a function of the hydrogen production rate. | 61 |
| 7.18 | The amplitude of the harmonic currents at PCC as a function of hydrogen production rate. | 63 |
| 7.19 | Power at PCC as a function of varying grid strength in a) for active power P_{AC} and in b) for reactive power Q_{AC} with a hydrogen production demand of 75%. | 65 |
| 7.20 | Harmonic current amplitudes $\hat{I}_{AC_f(n)}$ at PCC for different SCR with a hydrogen production demand of 75%. | 66 |
| 7.21 | Dynamic simulation of the output current I_0 and the output current reference $I_{0,ref}$ for hydrogen production rate reference of 10%, 50% and 100%. . | 67 |
| 7.22 | Dynamic simulation of the output voltage V_0 and the output voltage reference $V_{0,ref}$ for hydrogen production rate reference of 10%, 50% and 100%. . | 68 |
| 7.23 | Dynamic simulation of the hydrogen production rate v_{H_2} and the hydrogen production rate reference $v_{H_2,ref}$ for hydrogen production rate reference of 10%, 50% and 100%. | 68 |
| 7.24 | Output voltage V_0 in blue, and the converter voltage $V_{0,1}$ and $V_{0,2}$ in black for hydrogen production rate reference of a) 10%, b) 50% and c) 100%. . . | 69 |
| 7.25 | Schematic diagram of the PSFB DC/DC converter topology interconnecting the distribution DC-bus and the electrolyser system. The schematics of the PSFB DC/DC converter module can be seen in Figure 7.26. | 71 |
| 7.26 | Schematic diagram of the PSFB DC/DC converter module. | 72 |
| 7.27 | Detailed view of the medium frequency transformer model in Figure 7.26. . | 72 |
| 7.28 | Schematic diagram of the control system used for the PSFB DC/DC converter. | 74 |
| 7.29 | Filter inductor current I_{L_f} for hydrogen production rate reference of a) 25% and b) 75%. | 76 |

| | | |
|------|--|----|
| 7.30 | Output current I_0 for hydrogen production rate reference of a) 25% and b) 75%. | 76 |
| 7.31 | Primary transformer current I_p for hydrogen production rate reference of a) 25% and b) 75%. | 77 |
| 7.32 | Secondary transformer current I_s for hydrogen production rate reference of a) 25% and b) 75%. | 77 |
| 7.33 | Diode current I_{D_1} for hydrogen production rate reference of a) 25% and b) 75%. | 77 |
| 7.34 | Capacitor current I_{C_0} for hydrogen production rate reference of a) 25% and b) 75%. | 78 |
| 7.35 | Output voltage V_0 for hydrogen production rate reference of a) 25% and b) 75%. | 78 |
| 7.36 | Primary transformer voltage V_p for hydrogen production rate reference of a) 25% and b) 75%. | 78 |
| 7.37 | Secondary transformer voltage V_s for hydrogen production rate reference of a) 25% and b) 75%. | 79 |
| 7.38 | Dynamic simulation of the output current I_0 and the output current reference $I_{0,ref}$ for hydrogen production rate reference of 10%, 50% and 100%. | 81 |
| 7.39 | Dynamic simulation of the output voltage V_0 and the output voltage reference $V_{0,ref}$ for hydrogen production rate reference of 10%, 50% and 100%. | 82 |
| 7.40 | Dynamic simulation of the hydrogen production rate v_{H_2} and the hydrogen production rate reference $v_{H_2,ref}$ for hydrogen production rate reference of 10%, 50% and 100%. | 82 |
| 7.41 | Dynamic simulation of the hydrogen production rate reference $v_{H_2,ref}$ and the output current reference $I_{0,ref}$ for hydrogen production rate reference of 10%, 50% and 100%. | 83 |
| 7.42 | Output power P_0 as a function of the leakage inductance L_R ratio when the hydrogen production rate reference value is 25%. | 85 |
| 8.1 | Schematic view of an electrolyser station connected to PCC. | 87 |
| 8.2 | The structure of the electrolyser station and its integration to the sub-transmission or the transmission grid for case 1. | 90 |
| 8.3 | The nominal current at the 33 kV bus $I_{n,bus}$ and the SCC I_{SCC} as a function of the number of transformers connected to the 150 kV bus x for case 1. | 91 |
| 8.4 | The structure of the electrolyser station and its integration to the sub-transmission or the transmission grid for case 2. | 92 |
| 8.5 | The nominal current at the 66 kV bus $I_{n,bus}$ and the SCC I_{SCC} as a function of the number of transformers connected to the 150 kV bus x for case 2. | 93 |
| 8.6 | The structure of the electrolyser station and its integration to the sub-transmission or the transmission grid for case 3. | 94 |
| 8.7 | The nominal current at the 33 kV bus $I_{n,bus}$ and the SCC I_{SCC} as a function of the number of transformers connected to one of the 150 kV buses x for case 3. | 95 |
| 8.8 | The structure of the electrolyser station and its integration to the sub-transmission or the transmission grid for case 4. | 96 |
| 8.9 | The nominal current at the 66 kV bus $I_{n,bus}$ and the SCC I_{SCC} as a function of the number of transformers connected to one of the 150 kV buses x for case 4. | 97 |

| | | |
|-----|---|----|
| A.1 | The PEM electrolyser model as modelled in MATLAB Simulink. | ii |
| A.2 | The 12-pulse thyristor rectifier model as modelled in PLECS in a), with the two six-pulse rectifiers demonstrated in b). | iv |
| A.3 | The PSFB DC/DC converter model as modelled in PLECS in a), with the PSFB DC/DC converter module model demonstrated in b). | vi |

List of Tables

| | | |
|-----|--|----|
| 3.1 | Comparison of different parameters between alkaline, PEM and SOEC electrolyzers [3], [25], [28]. | 12 |
| 4.1 | Annual revenues for Nel between 2015-2020 [30]. | 14 |
| 4.2 | Technical specifications for Nel's largest electrolyser systems [30]. | 15 |
| 4.3 | Annual revenues for McPhy between 2015-2020 [31]. | 16 |
| 4.4 | Technical specifications for McPhy's largest electrolyser systems [31]. | 16 |
| 4.5 | Annual revenues for ITM Power between 2015-2020 [32]. | 18 |
| 4.6 | Technical specifications for ITM Power's largest electrolyser systems [32]. | 18 |
| 4.7 | Technical specifications for Siemens Silyzer electrolyser systems. The Silyzer 300 is intended for modular installation, that is combining several electrolyzers to achieve a desired output. | 20 |
| 4.8 | Annual revenues for Hydrogenics between 2015 - 2018 and Cummins Electronics and Fuel systems segment in 2019 and 2020. Cummins Electronics and Fuel Systems also includes other technologies such as control units, software and diesel fuel injection systems, but separate revenue for hydrogen-related technology was not represented in financial reports [40],[42],[43],[44]. | 21 |
| 6.1 | Different parameter values of the 2 MW PEM electrolyser model [25], [28], [56], [57], [58], [61]. | 33 |
| 6.2 | Universal constant values. | 33 |
| 7.1 | Parameter values for the 12-pulse thyristor rectifier, which have been kept constant for all simulation cases within Section 7.1.1. | 54 |
| 7.2 | The output current I_0 , output voltage V_0 , output current ripple ΔI_0 , output voltage ripple ΔV_0 , hydrogen production rate v_{H_2} , electrolyser efficiency η^{LHV} , active output power P_0 and energy consumption E_0 for hydrogen production rate reference values of 10%, 25%, 50%, 75% and 100%. | 55 |
| 7.3 | Grid inductance values (identical value on all three phases) with corresponding SCR. | 62 |
| 7.4 | Fundamental current and current harmonics for different SCR's. | 63 |
| 7.5 | Fundamental current and current harmonics for 5 th , 7 th , 11 th , 13 th , 17 th and 19 th for hydrogen production rate reference values of 10%, 25%, 50%, 75% and 100%. Simulated for a strong grid (zero line impedance). | 64 |
| 7.6 | PSFB DC/DC converter parameter values. | 74 |

| | | |
|------|--|----|
| 7.7 | The filter inductor current I_{L_f} , the output voltage V_0 , the filter inductor current ripple ΔI_{L_f} and the output voltage ripple ΔV_0 of one PSFB DC/DC converter module for hydrogen production rate reference value of 25% and 75%. | 75 |
| 7.8 | The output current I_0 , the output current ripple ΔI_0 , the input current I_{in} , the hydrogen production rate v_{H_2} , the electrolyser efficiency η^{LHV} , the output power P_0 and the energy consumption E_0 of the PSFB DC/DC converter and the electrolyser for hydrogen production rate reference value of 25% and 75%. | 75 |
| 7.9 | The output current I_0 , the output voltage V_0 , the input current I_{in} , the output current ripple ΔI_0 , the output voltage ripple ΔV_0 , the hydrogen production rate v_{H_2} , the electrolyser efficiency η^{LHV} , the output power P_0 and the energy consumption E_0 of the PSFB DC/DC converter and the electrolyser for hydrogen production rate reference value of 10%, 50% and 100%. | 80 |
| 7.10 | The output current reference $I_{0,ref}$, the output voltage reference $V_{0,ref}$ and the hydrogen production rate reference $v_{H_2,ref}$ of the PSFB DC/DC converter and the electrolyser for hydrogen production rate reference value of 10%, 50% and 100%. | 81 |
| 7.11 | The filter inductor current I_{L_f} , the output voltage V_0 , the filter inductor current ripple ΔI_{L_f} and the output voltage ripple ΔV_0 of one PSFB DC/DC converter module for different leakage inductance values when the hydrogen production rate reference value is 25%. | 84 |
| 7.12 | The output current I_0 , the output current ripple ΔI_0 , the hydrogen production rate v_{H_2} , the output power P_0 and the energy consumption E_0 of the PSFB DC/DC converter and the electrolyser for different leakage inductance values when the hydrogen production rate reference value is 25%. | 85 |
| 8.1 | Structure comparison of electrolyser station cases 1-4. | 96 |

List of Symbols

| | | |
|-------------------------|---|--------------------|
| A_{mem} | Membrane area | [cm ²] |
| α | Firing angle | [-] |
| α_{an} | Anode charge transfer coefficient | [-] |
| α_{ca} | Cathode charge transfer coefficient | [-] |
| C_0 | Filter capacitance | [F] |
| C_{oss} | Switch output capacitance | [F] |
| C_{T} | Transformer capacitance | [F] |
| D | Duty cycle | [-] |
| ΔG | Gibbs free energy | [J/mol] |
| ΔH | Change of enthalpy | [J/mol] |
| ΔI_0 | Output current ripple | [A] |
| ΔI_{L_f} | Filter inductor current ripple | [A] |
| ΔS | Change of entropy | [J/(mol · K)] |
| ΔV_0 | Output voltage ripple | [V] |
| δ_{mem} | Membrane thickness | [cm] |
| E_0 | Electrolyser energy consumption | [J] |
| E_{R} | Leakage inductor energy | [J] |
| η^{LHV} | Electrolyser efficiency | [-] |
| F | Faraday constant | [C/mol] |
| f | Grid frequency (source setting) | [Hz] |
| f_{sw} | Switching frequency | [Hz] |
| φ_0 | Grid offset angle (source setting) | [rad] |
| φ_{AC} | Phase signal (estimated) | [rad] |
| I | Current | [A] |
| I_0 | Output current | [A] |
| I_2 | Current through the transistors | [A] |
| $I_{\text{AC}_f(n)}$ | The n:th frequency of harmonic current | [A] |
| I_{DC} | Current sensor signal | [A] |
| I_{DC}^* | Current reference signal | [A] |
| I_{dc1} | First rectifier output current | [A] |
| I_{dc2} | Second rectifier output current | [A] |
| I_{L_f} | Filter inductor current | [A] |
| $I_{\text{n,bus}}$ | Nominal bus current of electrolyser systems | [A] |
| I_{SCC} | Short-circuit current | [A] |
| i_{ac} | Grid current | [A] |
| i_{ac1} | Secondary transformer side (Δ) current | [A] |
| i_{ac2} | Secondary transformer side (y) current | [A] |

| | | |
|--------------------------|--|----------------------|
| i_{sec} | Secondary transformer side current | [A] |
| J | Current density | [A/cm ²] |
| $J_{0,\text{an}}$ | Anode exchange current density | [A/cm ²] |
| $J_{0,\text{ca}}$ | Cathode exchange current density | [A/cm ²] |
| J_1 | Limiting current density | [A/cm ²] |
| k_i | Controller integration constant | [-] |
| k_p | Controller proportional constant | [-] |
| L_f | Filter inductance | [H] |
| L_g | Line impedance | [H] |
| L_M | Magnetization inductance | [H] |
| L_R | Leakage inductance | [H] |
| L_{R_p} | Leakage inductance primary side | [H] |
| L_{R_s} | Leakage inductances secondary side | [H] |
| L_{out} | Output filtering inductance | [H] |
| L_T | Equivalent transformer inductance | [H] |
| λ | Water content of the membrane | [-] |
| n | Transformer turn ratio | [-] |
| n_s | Number of cells connected in series | [-] |
| P_{AC} | Active power drawn from the grid | [W] |
| P_0 | Output power | [W] |
| p | Pressure | [bar] |
| p_{H_2} | Partial pressure of hydrogen | [bar] |
| $p_{\text{H}_2\text{O}}$ | Partial pressure of water | [bar] |
| p_{O_2} | Partial pressure of oxygen | [bar] |
| Q_{AC} | Reactive power drawn from the grid | [var] |
| R | Universal gas constant | [J/(mol · K)] |
| R_u | Universal gas constant | [bar · L/(mol · K)] |
| R_{el} | Electrode resistance | [Ω] |
| R_{ion} | Ionic resistance | [Ω] |
| R_{R_p} | Leakage reactance primary side | [Ω] |
| R_{R_s} | Leakage reactance secondary side | [Ω] |
| $S_{n,\text{el}}$ | Rated apparent power of electrolyser station | [VA] |
| $S_{n,T}$ | Rated apparent power of transformers | [VA] |
| σ_{mem} | Membrane conductivity | [S/cm] |
| T | Temperature | [K] |
| V_0 | Output voltage | [V] |
| V_{act} | Activation overvoltage | [V] |
| V_{bus} | Bus voltage of the electrolyser systems | [V] |
| V_{cell} | Cell voltage | [V] |
| V_{con} | Concentration overvoltage | [V] |
| $V_{\text{dc,bus}}$ | Distribution DC-bus voltage | [V] |
| V_F | Fault voltage | [V] |
| V_{in} | Input voltage | [V] |
| $V_{L_{\text{out}}}$ | DC reactor voltage | [V] |
| V_{ohm} | Ohmic overvoltage | [V] |
| V_{rev} | Reversible voltage | [V] |
| v_{AC} | Voltage sensor signal | [V] |

| | | |
|---------------|---|--------------|
| v_{ac} | Grid voltage | [V] |
| v_{ac1} | Secondary transformer side (Δ) voltage | [V] |
| v_{ac2} | Secondary transformer side (y) voltage | [V] |
| v_{H_2} | Hydrogen production rate | [L/s] |
| v_m | Molar volume | [L/mol] |
| v_{sec} | Secondary transformer side voltage | [V] |
| x | Number of 150/33 kV or 150/66 kV transformers | [-] |
| Z_B | Base impedance | [Ω] |
| Z_F | Fault impedance | [Ω] |
| Z_{T_1} | 400/150 kV transformer impedance | [Ω] |
| $Z_{T_1,tot}$ | Total 400/150 kV transformer impedance | [Ω] |
| Z_{T_2} | 150/33 kV or 150/66 kV transformer impedance | [Ω] |
| z | Number of electron moles | [-] |

List of Acronyms

| | |
|----------------|---|
| AC | Alternating current |
| BEV | Battery electric vehicle |
| BF-BOF | Blast furnace/basic oxygen furnace |
| CC | Current control |
| CAPEX | Capital expenditures |
| DC | Direct current |
| DRI | Direct reduction of iron |
| EAF | Electric arc furnace |
| EMI | Electromagnetic interference |
| FCEV | Fuel cell electric vehicle |
| H ₂ | Hydrogen |
| HHV | Higher heating value |
| HVAC | High voltage alternating current |
| HVDC | High voltage direct current |
| ICE | Internal combustion engine |
| IEA | The International Energy Agency |
| IRENA | The International Renewable Energy Agency |
| KOH | Potassium hydroxide |
| LHV | Lower heating value |
| OH | Hydroxide |
| OPEX | Operating expenditures |
| PCC | Point of common coupling |
| PI | Proportional integral |
| PLL | Phase-locked loop |
| PEM | Proton exchange membrane |
| PFSA | Perfluorosulfonic acid |
| PSFB | Phase-shifted full-bridge |
| rms | root mean square |
| SCC | Short-circuit current |
| SCR | Short-circuit ratio |
| SOEC | Solid oxide electrolyser cell |
| VRE | Variable renewable energy |
| ZVS | Zero voltage switching |

1

Introduction

1.1 Background

In the classical power system, large power plants at remote locations far from the customer have been the norm. Moreover, driving a vehicle to the gas station to refill the fuel tank has been the normal behaviour. A paradigm shift is approaching in how the world's energy needs will be met in order to supply all consumers with electricity and fuel, while at the same time ensure that the energy is non-fossil. Securing reliability in combination with sustainability raises the questions: How should a large and increasing number of dispersed power generation units be handled? What kind of fuels will be used for the transportation fleet of tomorrow?

The world's energy consumption is mainly supplied from fossil fuels which is not sustainable due to the emissions of greenhouse gases and other pollutants such as nitrogen oxide (NO_x) [1]. It is expected that the global energy consumption will increase by 77% in the next 30 years [2], and therefore solutions to generate renewable electric energy is of great importance. An issue with variable renewable energy (VRE) sources such as solar and wind power is that they are intermittent and do not have the capability of storing energy [1]. By implementing electrolyzers in the power system, the excess energy from VRE sources could be used to produce hydrogen, thus providing flexibility services to the power grid [3]. Hydrogen storage systems and fuel cells could then be used to supply power to the grid during peak periods, increasing the reliability and stability of the power grid as well [4]. Hydrogen storage is also capable of long-period storage with high robustness, thus making it very suitable for decentralised power systems [5]. Moreover, hydrogen has the potential to replace natural gas in existing gas turbines, which stands for 23% of the worlds power generation, enabling the use of today's infrastructure for the future power grid [6]. Hydrogen could also enable more long distance power transmission as it either can be transported in existing gas pipelines or by other means due to its long-period storage capabilities. This could be economically beneficial compared to building new grid infrastructure when the power generation capacity is too low or when installing submarine cables [3]. Transportation vehicles also contribute to a large amount of the global carbon dioxide emissions, which could be reduced immensely if replaced with hydrogen as fuel instead of gasoline or diesel [7]. Thus hydrogen can have an important role in the reduction of fossil fuels by enabling increased utilisation of renewable and sustainable energy as well as replacing fossil fuels in the transport sector, contributing to a sustainable future without greenhouse gas emissions and pollutants [8].

Hydrogen has high energy density (120–142 MJ/kg), but low volumetric density, which requires larger compressed gas or liquid tank systems. All stationary applications where space is available will be less concerned by the volumetric density (2 - 8 MJ/litre) [9]. In applications where size needs to be minimised, the competitor Li-ion batteries has an advantage. However, due to a comparably low energy density (0.36–0.95 MJ/kg) in recent Li-ion batteries [10], and the need to recycle batteries while hydrogen is automatically recycled on use, hydrogen as energy storage is an attractive option. The typical discharge time of batteries is also under 5 hours while a typical hydrogen storage can last more than 1000 hours, enabling long-period storage [3]. Finally, Li-ion batteries degrade after 2-3 years, which is shorter than the lifetime of hydrogen storage tanks that last more than 8 years [5]. Supercapacitors have a shorter lifetime and discharge faster than hydrogen as well [4]. Long-period storage is beneficial to countries such as Germany that can have a 50% lower renewable power generation but a 30% higher load demand during the winter compared to the summer. Therefore, hydrogen would be more optimal for energy storage where long-period storage is needed [3]. Pumped hydro storage is well established and a widely used energy storage system today with long-period storage as well. However, the technology has low energy density and is very dependent on suitable geological locations, which is why hydrogen could be more beneficial as an energy storage system [11].

Steam methane reforming (SMR) alongside partial oxidation (POX) process (gasification) in natural gas and coal industry are the most common hydrogen production techniques, but they utilise fossil fuels which produces carbon dioxide emissions [8]. Electrolysis of water is emerging in the industry, as well as thermolysis and photoelectrolysis, with hopes of offering opportunities for synergy with variable power generation. Several other methods are in development such as pyrolysis, fermentation, photosynthetic algae and nuclearcycle-assisted systems [12]. These more futuristic methods do not produce hydrogen with the help of a power electronic system. The two resulting elements when electrolysis of water is performed are pure oxygen and hydrogen, which comes from the input of water and electricity. The electric energy must originate from renewables if the aim is to have a completely sustainable hydrogen production by electrolysis [2]. Otherwise, electrolysis could contribute to higher emissions than SMR or ROX. There are different electrolyser technologies such as alkaline based and proton exchange membrane (PEM) electrolysers, the most common ones, as well as solid oxide electrolysis cells (SOEC), which is the least developed one. Alkaline based has the lowest initial cost but the highest operating costs due to the lowest efficiency. SOEC has the highest efficiency, but does however have issues regarding corrosion, seals and thermal cycling. Finally, PEM has higher efficiency and is more expensive than alkaline based electrolysers. Efficiencies of 56-73% can be reached with electrolysis, which result in an approximate energy conversion between 70.1-53.4 kWh/kg hydrogen. Electrolysis is, compared to other hydrogen production techniques such as SMR or POX, expensive [7]. Thus, the cost of electrolysis with renewable energy sources must be reduced to be preferred over hydrogen production techniques that are common today. The choice of converter topology as well as the electric infrastructure in the electrolyser system could minimise the electricity consumption and therefore the costs, as the electricity consumption stands for 30% of the hydrogen cost [3], [13].

1.2 Aim

The aim of the work, which has resulted in this report, is to dynamically model the electrolyser together with different converter topologies. The functionality of the converter topology models as well as their influence on the dynamic electrolyser model will be analysed and determined. Moreover, the global hydrogen market of today and the future as well as its applications today and potential applications in the future will be investigated in order to determine the manufacturers and customers of hydrogen. Finally, an investigation of electrolyser stations on GW-scale will be conducted to present the main requirements and viable structure designs.

1.3 Scope

The hydrogen market as well as the customers and manufacturers of hydrogen will be analysed. Moreover, manufacturers of electrolysers and their products will be investigated. The analysis will also focus on applications of hydrogen in near-time as well as future perspective.

There are different electrolyser technologies. However, only one electrolyser technology will be considered in the simulations to verify the functionality of the converter topologies. The electrolyser which is deemed the most suitable and efficient one for power system applications will be modelled after the literature study on electrolyser modelling is complete. Only the electrolyser will be modelled, excluding other common components in an electrolyser system such as feed water supply, gas separator and compressor. Moreover, the components inside the electrolyser will only be modelled as overvoltages, where a more complex model would consider choice of material for the electrodes and membrane.

Voltage and current ratings will be determined for the different parts of the electrolyser and thereafter the dynamic models of the respective converter topologies for an AC distribution system and a DC distribution system will be designed with focus on functionality. Other factors such as thermal properties, cost and volume will not be included in the design. Also, only one converter topology for each grid case will be investigated.

Four structure designs of electrolyser stations on GW-scale will be presented with simplified assumptions to propose what a viable option could be. A detailed analysis including accurate data of the electrolyser station transformers and the reactive power consumption of the station will not be conducted. Furthermore, only transformers in the proposed electrolyser station designs will be included, excluding components such as switchgears, relays, current and voltage transformers.

1.4 Societal, ethical and ecological aspects

Effects on society and environment as well as ethical dilemmas should always be taken into consideration throughout the thesis work and thereafter in employment, simply because technology affects the many and not just the developers of it [14]. While promoting increased use of electrolytic hydrogen which comes with a number of benefits

like enabling fuel cell vehicles [15], replacing natural gas for some uses so that nations are not dependant on one specific country [16] and net zero emission-enabling [17],[18], the one clear issue with hydrogen is its tendency to enter a combustion reaction and produce flames or explosions (with added initial energy).

There are a number of modern incidents in which workers have been injured or killed [19], [20], [21]. Death as a hazard of enabling more electrolytic hydrogen is never acceptable. All companies that promote hydrogen should always ensure that a suitable amount of funding is directed towards leakage detection equipment and early warning systems as well as manufacturing of high quality storage tanks and gas pipes. It is also suggested that close family of a deceased receive compensation. With the aforementioned in mind, workplace accidents occur across other energy sector related jobs as well, with fossil fuels having the highest mortality rate (deaths per produced kWh) [22]. If safety concerns are met, market introduction is not a problem and publicly perceived safety increases with increased use of hydrogen appliances [23].

Finally, all parts of this thesis is carried out remotely due to COVID-19. Not being close to the physical circumstances which are explored risk some disconnection from issues which would otherwise be more apparent.

2

Method

In order to understand the role hydrogen has today and the potential role hydrogen could have for renewables and a sustainable future, its applications had to be investigated. The requirements on the converter system are dependent on the size of the electrolyser system, which is dependent on the hydrogen demand. Therefore, the global hydrogen market was analysed. As a result, customers and manufacturers of hydrogen were also determined. Finally, since the converter topology interconnects the electrolyser to the power grid, the capabilities of the electrolyser products are also important factors to consider for the converter requirements. Thus, electrolyser manufacturers were determined along with their products. The above mentioned investigations and analyses were conducted through literature studies and by investigating the top global electrolyser manufacturer companies.

A dynamic model of an electrolyser system had to be made in order to connect the chemical modelling with the electric modelling. Therefore, literature studies were conducted to understand how it should be modelled properly and which electrolyser technology should be modelled. In addition to literature studies, there was also an interview conducted with a researcher at Chalmers University of Technology in order to aid with the electrolyser modelling. The electrolyser was modelled in MATLAB Simulink. Once the model was complete, simulations were conducted to analyse the behaviour of the system and what influence parameter changes would have.

The electrolyser model was connected to a converter model for two different grid types, one for an AC distribution system and one for a DC distribution system. For the AC distribution system, the usual converter topology for electrolyser applications was selected which is a transformer connected to a rectifier. However, for the DC distribution system a literature study had to be conducted to investigate which topology was most suitable for electrolyser applications connected to a DC grid. The requirements for a DC/DC converter topology were listed and thereafter the most suitable converter topology was selected. Subsequently, further literature studies were conducted for each converter topology to understand the theory as well as the functionality so that they could be modelled properly.

After the converter topology analyses were complete, the modelling began. The simulation program PLECS was used for the converter modelling which could be connected together with a MATLAB Simulink model. After each converter topology was modelled, simulations were performed to verify their function. Once the models worked properly, they were connected to the electrolyser model. Adaptations and iterations to the converter topologies had to be made until the dynamic models were considered to

operate accordingly together with the electrolyser model as well. Thereafter dynamic simulations were conducted to evaluate and verify the functionality of the models as well as to evaluate the influence that the converter topologies has on the electrolyser model.

Finally, an investigation on the implementation and structure of electrolyser station on GW-scale was conducted. Both the main external and internal requirements were presented to demonstrate what must be considered before the construction of an electrolyser station on GW-scale. Thereafter, four viable structure designs were presented and evaluated.

3

Introduction to electrolysers

Jan Rudolph Deiman and Adriaan Paets van Troostwijk were the first persons to introduce water electrolysis in 1789. This was performed by submerging two gold electrodes in water and generating an electrostatic discharge between them. In the beginning of the 19th century, Alessandro Volta invented the battery which was used by Johann Wilhelm Ritter for electrolysis advancements. Dmitry Lachinov then developed a method to produce hydrogen and oxygen from electrolysis in 1888, and at the beginning of 20th century over 400 alkaline units were operational [24], primarily for ammonia production but also for chlorine production as well. The first pressurised alkaline electrolysers were later announced in 1948 [25]. General Electric demonstrated the first PEM fuel cell technology in the 1960s which was used for electricity generation to the Gemini Space program, leading to the development of the PEM electrolyser technology [24]. PEM electrolysers, unlike alkaline, could have clean water without any solutions as well as higher power densities and efficiencies due to the membrane material which has good ionic transport capacity. After the 1980s and during the next three decades, PEM were further developed to be utilised in other applications. This meant an increase in the scale to hundreds of kW, efficiency, lifetime and lower investment costs. Alkaline electrolysers were also developed in a way that smaller units were created for lower hydrogen production applications. Finally, from 2010 to today much solar and wind power were installed which decreased the costs immensely. This was a milestone for electrolysers as that meant that the costs for renewable hydrogen decreased as well, since the electricity costs decreased. Furthermore, due to the climate change issue, the development and utilisation of electrolysers has increased much in order to help the transition towards the decarbonisation of several sectors. With an increase in the global electrolyser capacity, the investment costs decrease which makes them more competitive compared to other less expensive carbon-based hydrogen production technologies [25].

3.1 Electrolyser technologies

Today there are three main technologies where alkaline is fully commercialised while PEM is being more utilised and SOEC is still in early development stages [26]. The simplified working principle of an electrolyser is that two electrodes, an anode and a cathode, are submerged into an electrolyte. When the electrolyte is electrified a reaction process will occur that will form water molecules into oxygen molecules at the anode and hydrogen molecules at the cathode. The cell efficiency can be calculated in two different ways, either as the ratio between the higher heating value (HHV) voltage divided with the cell voltage or as the ratio between the lower heating heating value (LHV) voltage divided with the cell voltage. Furthermore, there is also the Faradaic efficiency which is the

ratio between the amount of hydrogen produced divided with the calculated theoretical hydrogen production [27].

3.1.1 Alkaline water electrolysis

As mentioned, alkaline electrolysers are commercialised and the most utilised electrolyser technology today. As can be seen in Figure 3.1, the electrodes are submerged in a high concentration electrolyte solution of potassium hydroxide (KOH) with a diaphragm in between. Furthermore, in the hydrogen production process there are four hydroxide (OH) ions at the anode that form two water molecules, one oxide molecule and four electrons. These four electrons then travel from the anode to the cathode where they react with four water molecules to form two hydrogen molecules and four hydroxide ions which travel to the anode through the diaphragm. Alkaline electrolyser have an operating temperature and pressure of 70-90°C and 1-30 bar respectively [25]. Furthermore, alkaline electrolysers have an efficiency between 63% and 70% as well as an operating stack lifetime of 60000-90000 hours. The load range is between 10-110% of the nominal load, where the start up and shutdown time is between 1-10 minutes with a ramp up and down speed of 0.2-20% per second [3], [28]. This is a technology that is reliable with a simple system architecture and manufacturing process [25]. It also has the advantage over the other technologies that it is well-developed and therefore less expensive, having a CAPEX of 500-1400\$/kW_e. However, it has disadvantages such as low current density as well as being incapable of high pressure operation [24], [28]. Moreover, an illustration of an alkaline electrolyser system is shown in Figure 3.2. As can be seen, alkaline systems have many components. Due to the usage of the electrolyte solution KOH, a gas-water separator is needed as well as an electrolyte tank. The electrolyte also needs to be recirculated into the electrolyser, which will lower the efficiency [25].

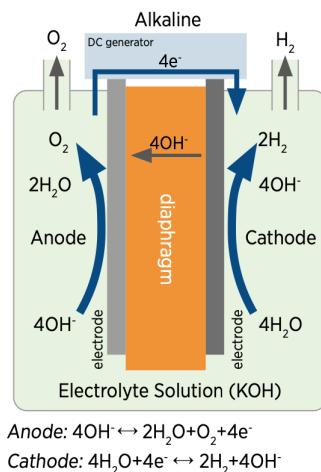


Figure 3.1: Operating principle of an alkaline electrolyser cell [25].

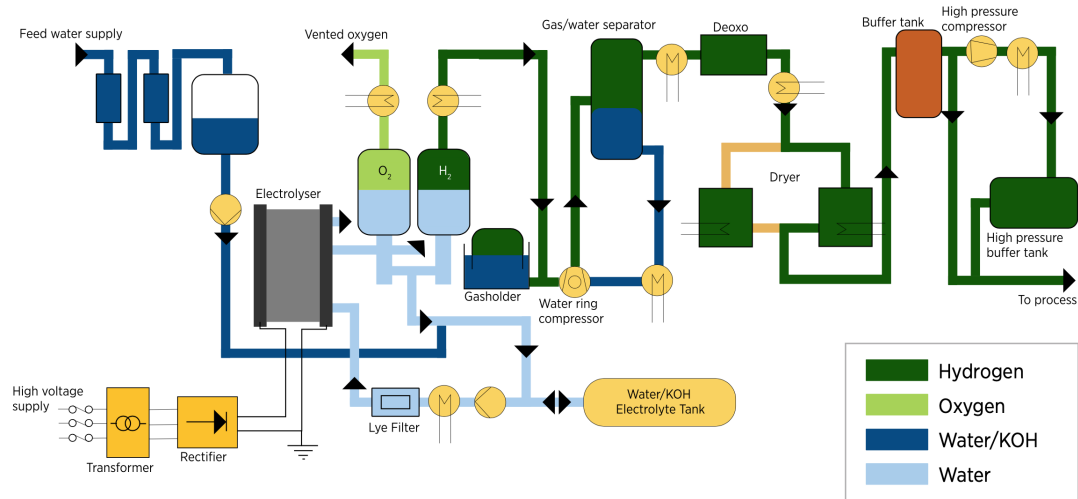


Figure 3.2: Common alkaline electrolyser system architecture [25].

3.1.2 Proton exchange membrane electrolysis

The PEM electrolyser uses perfluorosulfonic acid (PFSA) membrane instead of a diaphragm between the electrodes as the alkaline electrolyser. Pure water is also enough as an electrolyte for PEM electrolyser cells. As can be seen in Figure 3.3, two hydrogen molecules form one oxygen molecule, four hydrogen ions and four electrons at the anode. The hydrogen ions then travel through the membrane to the cathode while the electrons travel from the anode to the cathode through the electrodes, which will then create a reaction and form two hydrogen molecules at the cathode. This electrolyser technology has an operating temperature and pressure of 50-80°C and between 30-80 bar respectively [25], [28]. The efficiency is around 56-60% with an operating stack lifetime of 30000-90000 hours [28]. PEM electrolyzers have a faster start up and shutdown time as well as ramp up and down speed compared to alkaline. The start up time is between 1 second and 5 minutes while the shutdown time last only for a few seconds, and the ramp up and ramp down speed is 100% per second [3]. The load range, which is between 0-160% of nominal load, is higher as well. But, the disadvantage is that PEM electrolyzers are more expensive, with a CAPEX of 1100-1800 \$/kW_e [28]. An illustration of a common PEM electrolyser system architecture is illustrated in Figure 3.4 as well. As can be seen, the system requires less components compared to the alkaline system in Figure 3.2, which is due to the ability to utilise pure water instead of KOH as an electrolyte solution [25].

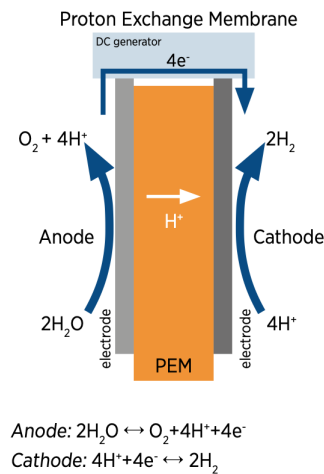


Figure 3.3: Operating principle of a PEM electrolyser cell [25].

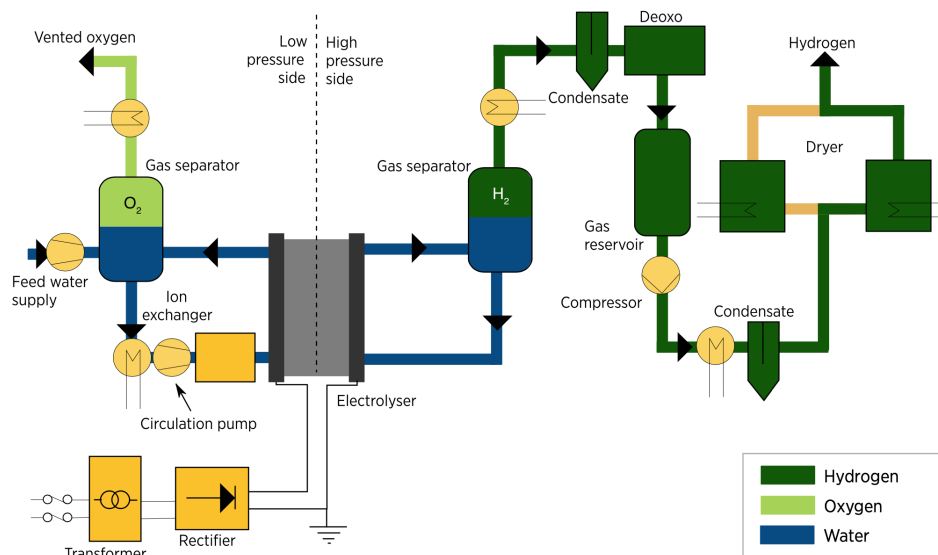


Figure 3.4: Common PEM electrolyser system architecture [25].

3.1.3 Solid oxide electrolyser cell electrolysis

Out of these three electrolyser technologies, SOEC is the least developed one and still in early development stages. As can be seen in Figure 3.5, two oxygen ions form one oxygen molecule and four electrons at the anode. The electrons then travel from the anode to the cathode and react with two water molecules, forming two hydrogen molecules and two oxygen ions which travel to the anode through the solid ceramic membrane. Aside from the reaction process, SOEC also differs from alkaline and PEM electrolyzers by operating at high temperatures of 700-850°C. The advantage of high temperature operation is that less expensive electrodes can be utilised, but also that the electricity demand is decreased which increases the efficiency [25]. SOEC electrolyzers have efficiencies of 74-81% which is higher than both alkaline and PEM electrolyzers [28]. The disadvantage with these temperatures is shorter lifespans due to a higher degradation rate because of the thermochemical cycling [25], with an operating stack lifetime of 10000-30000 hours. The load range is between 20 and 100% of nominal load and they operate at atmospheric pressure. Since SOEC is also in early development stage, they are quite expensive with a CAPEX

of 2800-5600 $\$/kW_e$ [28]. Finally, the common architecture of a SOEC electrolyser system is illustrated in Figure 3.6. Since the SOEC operates at high temperatures, different components are required compared to alkaline and PEM electrolyser systems such as a heater, evaporator and pre-heater for the steam and air [25].

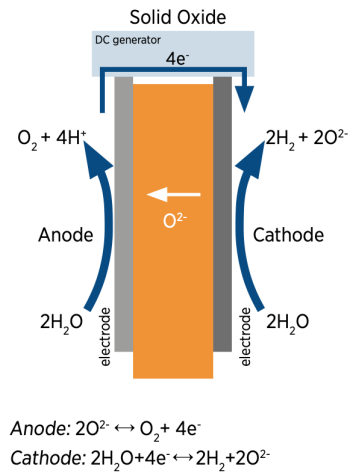


Figure 3.5: Operating principle of a SOEC electrolyser cell [25].

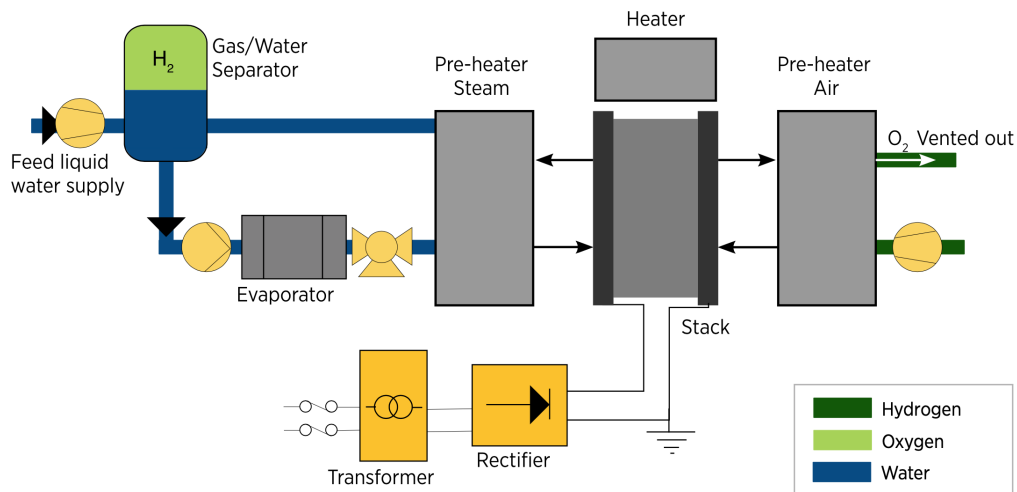


Figure 3.6: Common SOEC electrolyser system architecture [25].

3.1.4 Comparison

A comparison between alkaline, PEM and SOEC electrolysers is presented in Table 3.1. As can be seen, SOEC operates on higher temperatures compared to alkaline and PEM electrolysers, which is why the efficiency is higher as well. However, alkaline has both lower investment costs and higher operating stack lifetime compared to the other two because it is a more mature technology. Finally, PEM electrolysers are more efficient when comparing the start up and shutdown time, ramp up and ramp down speed as well as the load range of the nominal load. The current density of PEM is also higher compared to alkaline and SOEC. With the ongoing development efforts of the electrolyser manufacturers, the less matured PEM electrolyser will probably be improved on the lifetime and on the CAPEX to reach closer to alkaline electrolyser performance.

For power system applications with VRE integration, PEM electrolysers seem to be a better option due to the faster start up and shutdown time as well as the faster ramp up and ramp down speed. These characteristics are advantageous since VRE sources are intermittent and the power generation can change unexpectedly. Furthermore, PEM electrolysers are more flexible regarding the load range compared to alkaline. Another benefit is that water is utilised as an electrolyte instead of KOH.

Table 3.1: Comparison of different parameters between alkaline, PEM and SOEC electrolysers [3], [25], [28].

| Parameter description | Alkaline | PEM | SOEC |
|----------------------------|----------------------------|-----------------------------|-----------------------------|
| Temperature | 70-90°C | 50-80°C | 700-850°C |
| Pressure | 1-30 bar | 30-80 bar | 1 bar |
| Current density | 0.2-0.8 A/cm ² | 1-2 A/cm ² | 0.3-1 A/cm ² |
| Efficiency (LHV) | 63-70% | 56-60% | 74-81% |
| CAPEX | 500-1400\$/kW _e | 1100-1800\$/kW _e | 2800-5600\$/kW _e |
| Operating stack lifetime | 60000-90000 h | 30000-90000 h | 10000-30000 h |
| Load range of nominal load | 10-110% | 0-160% | 20-100% |
| Start up time | 1-10 min | 1 s-5 min | - |
| Shutdown time | 1-10 min | Seconds | - |
| Ramp up speed | 0.2-20%/s | 100%/s | - |
| Ramp down speed | 0.2-20%/s | 100%/s | - |

4

Market analysis of hydrogen and electrolysers

To have a rough estimate, an analysis of the market opportunities related to hydrogen and electrolysers has been investigated. The aim has been to look at the current situation as well as future predictions.

4.1 Hydrogen market

Today the annual hydrogen production amounts to approximately 120 million metric tons, with almost 80 million tons consisting of pure hydrogen production and the remaining production is a mixture with other gases. This equals to a total energy content of 14.4 EJ (exajoules). 95% of the global hydrogen is produced from production technologies that consume natural gas and coal, while the rest is produced from electrolysis [29] and only 0.7% is produced from renewable production technologies [28]. In a future scenario case made by IRENA, with the Paris agreement into consideration, the global hydrogen energy content from renewable electrolysis could potentially increase to 3 EJ by 2030, 8 EJ by 2040 and finally 19 EJ by 2050. A global hydrogen production equal to an energy content of 19 EJ by 2050 would require approximately 1700 GW of electrolyser capacity and 4 TW of renewable power generation capacity [29].

The hydrogen demand today is mostly used for feedstock in industrial sectors such as oil refineries (33%), ammonia production (27%), methanol production (11%) and steel production (3%). In the future however, hydrogen could have a potential increase in other sectors such as the transport, power and heating sector [28].

4.2 Electrolyser manufacturers

The top global electrolyser manufacturers that have been identified are Nel, McPhy, ITM Power, Siemens Energy and Cummins (Hydrogenics). Information on company background, goal, revenue and technical specifications of their products will be presented in the following subsections.

4.2.1 Nel

Nel is a Norwegian company that was founded in 1927 and specialised in alkaline electrolysers [30]. In 2015, the company obtained H2 Logic A/S, a world leading hydrogen

fueling technology company. Two years later Nel also obtained Proton Energy Systems Inc, a world leading PEM electrolyser technology company. Thus, after acquiring these companies, Nel manufactures hydrogen production as well as hydrogen fueling technologies and sell their products to companies within the energy, gas and industry sector. More than 3500 units have been delivered, where more than 2700 of them are PEM electrolysers and more than 800 of them are alkaline electrolysers. There are two manufacturing facilities for the electrolyser production, one in Wallingford, USA that focuses on PEM electrolyser manufacturing and another in Notodden/Herøya, Norway that manufactures alkaline electrolysers. The manufacturing facilities in USA and Norway both have a production capacity of 40 MW/year. However, the manufacturing facility in Norway is expanding and will have a production capacity of 500 MW/year ready in Q3 2021, with the possibility to expand further to a production capacity of 2 GW/year. The annual revenue of Nel is presented in Table 4.1, which shows that their revenue and growth is high, with an increase of 659% since 2015.

The largest alkaline electrolyser and PEM electrolyser products of Nel are displayed in Table 4.2, where the alkaline electrolyser A485 and the PEM electrolyser M400 are illustrated in Figure 4.1 and Figure 4.2 respectively. The large scale 17.6 MW alkaline electrolyser system A3880, which consists of eight A485 stacks, is illustrated in Figure 4.3 as well.

Table 4.1: Annual revenues for Nel between 2015-2020 [30].

| Year | Revenue |
|------|-----------------|
| 2015 | 100 million NOK |
| 2016 | 115 million NOK |
| 2017 | 302 million NOK |
| 2018 | 489 million NOK |
| 2019 | 570 million NOK |
| 2020 | 659 million NOK |

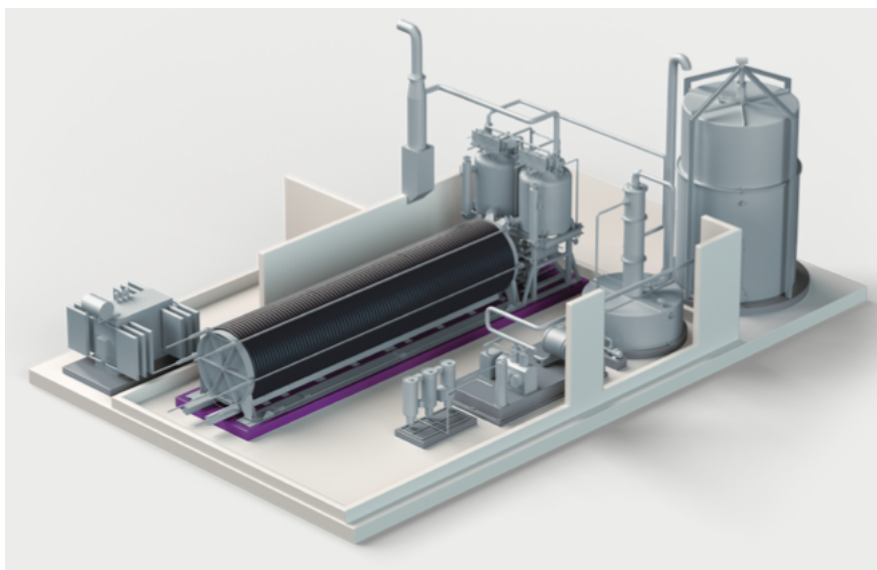


Figure 4.1: Concept image of Nel’s A485 alkaline electrolyser [30].



Figure 4.2: Concept image of Nel's M400 PEM electrolyser [30].

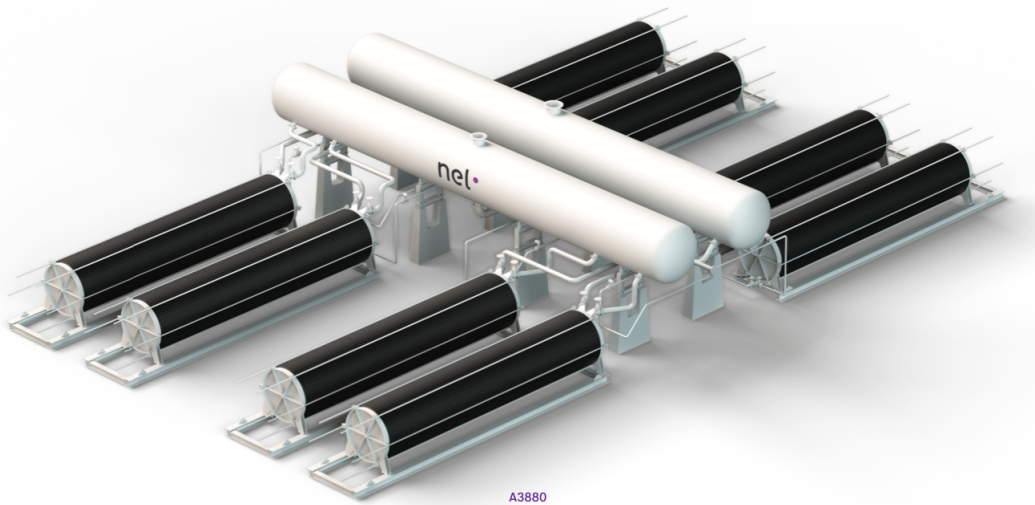


Figure 4.3: Concept image of Nel's A3880 large scale alkaline electrolyser system [30].

Table 4.2: Technical specifications for Nel's largest electrolyser systems [30].

| Model | Technology | Size | H ₂ production | Energy consumption |
|-------|------------|---------|---------------------------|--------------------|
| A485 | Alkaline | 2.2 MW | 43.6 kg/h | 49.4 kWh/kg |
| A1000 | Alkaline | 4.4 MW | 87.3 kg/h | 49.4 kWh/kg |
| A3880 | Alkaline | 17.6 MW | 348.9 kg/h | 49.4 kWh/kg |
| M400 | PEM | 2.0 MW | 36.8 kg/h | 50.9 kWh/kg |
| M4000 | PEM | 20.0 MW | 356.0 kg/h | 50.9 kWh/kg |
| MC500 | PEM | 2.5 MW | 44.3 kg/h | 50.4 kWh/kg |

The projects that Nel has recently announced are the Iberdrola project and Fredericia hydrogen project. The Iberdrola project is a purchase order from the electricity company Iberdrola and the fertiliser manufacturer company Fertiberia to develop a 20 MW PEM electrolyser solution for the production of renewable fertiliser in Puertollano, Spain and was valued €13.5 million. The other project, called the Fredericia hydrogen project, aims to develop a 20 MW electrolyser solution as well, but for the production of renewable hydrogen. It is a €7.2 million project which will be installed in Fredericia, Denmark to one of Shell's facilities. Another worth-mentioning purchase order is the \$30 million worth

purchase order of 85 MW alkaline electrolyzers from Nikola Motor for the development of their large hydrogen fueling stations project.

4.2.2 McPhy

In 2008 the french company McPhy was founded with a focus on hydrogen solid-state storage technology [31]. Piel, an electrolysis development company, was acquired in 2012 by McPhy, adding hydrogen production technology to their area of expertise. A year later the company created a partnership with Enertrag AG, forming a new company called McPhy Deutschland that would focus on the development of large-scale electrolyser systems on MW-scale. Today, the company specialises in high-pressure alkaline electrolyzers as well as hydrogen station solutions. However, they started on the development of PEM electrolyser systems as well in 2017. McPhy sell their products and system solutions to customers within the industry, mobility and energy market. The manufacturing and engineering facility for their electrolyzers is located in San Miniato, Italy, and has an annual manufacturing capacity of 300 MW. This manufacturing capacity is expected to be valid between 2020 and 2023. The engineering facility for McPhy Deutschland, which develops large-scale electrolyzers, is located in Wildau, Germany. McPhy does not have as high revenue as Nel, displayed in Table 4.3, but there has still been a 351% increase since 2015.

Table 4.3: Annual revenues for McPhy between 2015-2020 [31].

| Year | Revenue |
|------|---------------|
| 2015 | €3.9 million |
| 2016 | €7.5 million |
| 2017 | €10.1 million |
| 2018 | €8.0 million |
| 2019 | €11.4 million |
| 2020 | €13.7 million |

McPhy’s larger alkaline electrolyzers are called McLyzer, where the different models are presented in Table 4.4. The appearance of one of their larger electrolyser systems is also shown in Figure 4.4. Furthermore, McPhy’s 20 MW electrolyser system is also illustrated in Figure 4.5 which consists of 4 MW McLyzer 800-30 modules. These high power electrolyser modules have utilised advanced electrodes that can withstand current densities twice as high as ordinary electrodes.

Table 4.4: Technical specifications for McPhy’s largest electrolyser systems [31].

| Model | Technology | Size | H ₂ production | Energy consumption |
|----------------|------------|--------|---------------------------|--------------------|
| McLyzer 100-30 | Alkaline | 0.5 MW | 8.9 kg/h | 50.6 kWh/kg |
| McLyzer 200-30 | Alkaline | 1.0 MW | 17.8 kg/h | 50.6 kWh/kg |
| McLyzer 400-30 | Alkaline | 2.0 MW | 35.6 kg/h | 50.6 kWh/kg |
| McLyzer 800-30 | Alkaline | 4.0 MW | 71.2 kg/h | 50.6 kWh/kg |

Two major projects that are on-going for McPhy are the Djewels project and the zero emission valley project. The Djewels project is the development and installation



Figure 4.4: One of McPhy's larger electrolyzers called McLyzer [31].

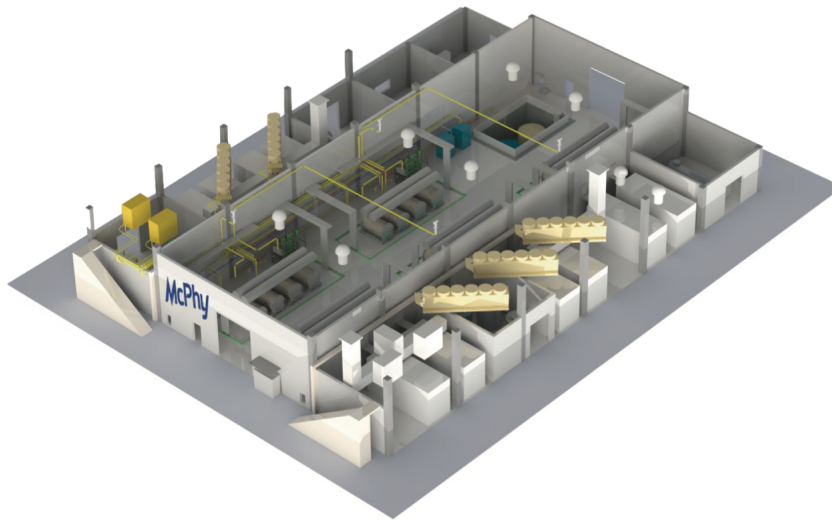


Figure 4.5: McPhy's 20 MW electrolyzer system consisting of 4 MW modules [31].

of a 20 MW electrolysis solution located in Delfzijl, The Netherlands. The project was launched by the companies Nouryon and Gasunie with the purpose of producing renewable hydrogen-based methanol. The funds for this project came from the Fuel Cells and Hydrogen Joint Undertaking (FCH-JU) as well as from the Waddenfonds, worth €11 million and €5 million respectively. Furthermore, the zero emission valley project, worth over €11 million, was launched by the Auvergne-Rhône-Alpes Regional council in France, with the aim to install up to 20 hydrogen fueling stations and a 37 MW electrolyzer solution.

4.2.3 ITM Power

ITM Power is a company that was founded in 2001, United Kingdom and develops PEM electrolyzer system and hydrogen station solutions [32]. In 2019 a joint venture was

formed with Linde AG, a global company that focus on industrial gases and engineering technologies for gas processing, creating the company ITM Linde Electrolysis GmbH that will be responsible for industrial scale projects which require renewable hydrogen production capacity of more than 10 MW. Bessemer Park is ITM Power’s manufacturing facility located in Sheffield, England with an annual production capacity of 1 GW, making it the world’s largest electrolyser manufacturing facility. ITM Power’s revenue is quite low but has grown 206% since 2015, as presented in Table 4.5.

The different sizes of ITM Power’s PEM electrolyser systems are presented in Table 4.6, with a concept image of the HGas2SP model illustrated in Figure 4.6. A concept image of the HGasXMW model is also illustrated in Figure 4.7, which is a 10.1 MW electrolyser system consisting of 15 stacks.

Table 4.5: Annual revenues for ITM Power between 2015-2020 [32].

| Year | Revenue |
|------|--------------|
| 2015 | £1.6 million |
| 2016 | £1.9 million |
| 2017 | £2.4 million |
| 2018 | £3.3 million |
| 2019 | £4.6 million |
| 2020 | £3.3 million |

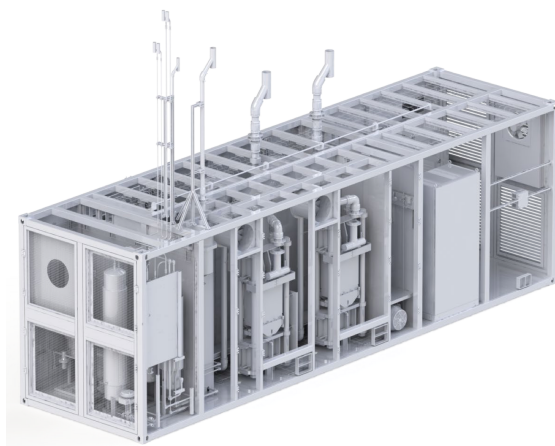


Figure 4.6: Concept image of ITM Power’s HGas2SP electrolyser [32].

Table 4.6: Technical specifications for ITM Power’s largest electrolyser systems [32].

| Model | Technology | Size | H ₂ production | Energy consumption |
|---------|------------|---------|---------------------------|--------------------|
| HGas1SP | PEM | 0.7 MW | 11.0 kg/h | 63.6 kWh/kg |
| HGas2SP | PEM | 1.39 MW | 22.0 kg/h | 63.2 kWh/kg |
| HGas3SP | PEM | 2.35 MW | 36.0 kg/h | 65.3 kWh/kg |
| HGasXMW | PEM | 10.1 MW | 168.8 kg/h | 59.7 kWh/kg |

ITM Power has announced three projects which are called the REFHYNE project, HyDeploy and H2Mobility. While HyDeploy is a project to enable a 20% hydrogen blend in gas turbines and H2Mobility is the installation of hydrogen refuelling stations, the

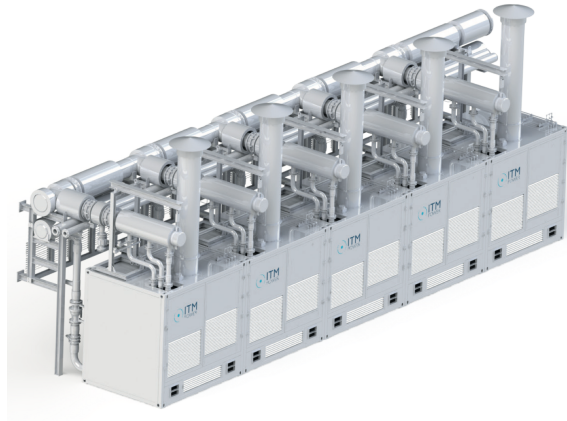


Figure 4.7: Concept image of ITM Power's HGasXMW electrolyser [32].

REFHYNE project is the development of a 10 MW electrolyser solution for renewable hydrogen production. The electrolyser solution will be installed for Shell's refinery located in Wesseling, Germany and is funded by FCH-JU.

4.2.4 Siemens Energy

Being active for more than 170 years, Siemens is one of the oldest technology companies. Early on Siemens made notable contributions such as the discovering of the dynamo-electric principle (1866) [33]. Siemens began exploring fuel cell technology in 1994 with a ceramic high-temperature SOFC (Solid Oxide Fuel Cell), which was able to output 1.8 kW (breaking the previous record of 1.3 kW) [34]. Recently, Siemens created a subsidiary, called Siemens Energy in order to better focus its efforts in generation, transmission, industrial applications, renewable energy and new energy, where new energy includes electrolyser technology. This split of a separate Siemens energy company started in March 2020 and was finalised in September 2020. Technical specifications for Siemens electrolyser models are presented in Table 4.7, where the Silyzer 300 electrolyser is also displayed in Figure 4.8.

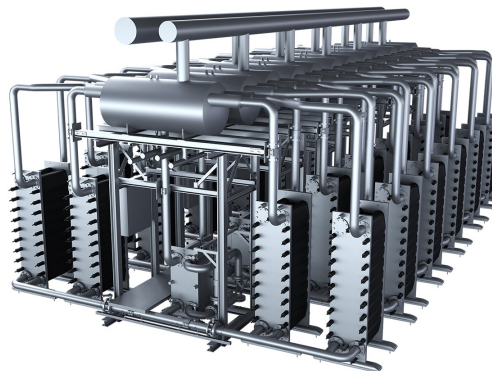


Figure 4.8: Concept image of Siemens Silyzer 300 electrolyser with stack size available up to 130 MW [35].

The Siemens Gamesa project, offshore green hydrogen production powered by wind, was announced in January 2021 where full scale off-shore demonstration is going to be

Table 4.7: Technical specifications for Siemens Silyzer electrolyser systems. The Silyzer 300 is intended for modular installation, that is combining several electrolyzers to achieve a desired output.

| Model | Technology | Size | H ₂ production |
|-------------|------------|---------|---------------------------|
| Silyzer 200 | PEM | 1.25 MW | 19 kg/h |
| Silyzer 300 | PEM | 130 MW | 100-2000 kg/h |



Figure 4.9: High pressure, 3.5 kA stacks as installed in Energiepark Mainz in Germany [39].

available in 2025/2026. An electrolyser array is to be placed at the base of the offshore wind turbine, where the ability to run the electrolyser array off-grid lowers hydrogen production cost [36].

A plant with the capacity of 200 MW is to be installed in Normandy in France (announced in February 2021). The project will apply for funds from Important Project of Common European Interest (IPCEI) as part of the European Green Deal [37].

Siemens also invests in the large project called Energiepark Mainz in Germany, together with the Linde Group, RheinMain University of Applied Sciences and Stadtwerke Mainz. Each stack at the plant, shown in Figure 4.9 has continuous operation at 1.3 MW and peak power operation at 2 MW. This is for high pressure operation at 35 bar and with a converter setup consisting of a transformer with filter circuits, which is supplied directly from a 20 kV medium voltage grid and with a DC current output maximum of 3.5 kA [38]. For larger plant capacity in the 100 MW range, modular design with current electrolyser units is a reliable option [39].

The company aims to become completely climate neutral by 2030, and in 2023 all own power consumption should originate from green electricity. Focusing the New Energy business sector on enabling the green hydrogen economy and promoting decarbonisation, Siemens will continue to develop their electrolyzers further [35].

4.2.5 Cummins, formerly Hydrogenics

Hydrogenics was an initiative started in 1995, and did since its initiation grow steadily with a focus on converting renewable energy to hydrogen with design and manufacture of generators and fuel cells. Hydrogenics electrolysis technology was mainly PEM-based and the company entered into a couple of mutually beneficial agreements, examples are Enbridge Inc. (industrial pipelines) and CommScope Inc. (backup power for communication networks) [40]. In September 2019, Hydrogenics with its technology and all assets was acquired by Cummins whom continue to develop fuel cell technology for powertrain



Figure 4.10: Based around a modular 20 MW PEM electrolyser, the new facility in Canada doubles Cummins previous installation size in Japan [47].

systems in trains, cars and trucks as well as electrolyser technology [41].

Table 4.8: Annual revenues for Hydrogenics between 2015 - 2018 and Cummins Electronics and Fuel systems segment in 2019 and 2020. Cummins Electronics and Fuel Systems also includes other technologies such as control units, software and diesel fuel injection systems, but separate revenue for hydrogen-related technology was not represented in financial reports [40],[42],[43],[44].

| Year | Revenue |
|------|----------------|
| 2015 | N/A |
| 2016 | N/A |
| 2017 | \$48.1 million |
| 2018 | \$33.9 million |
| 2019 | \$236 million |
| 2020 | \$317 million |

As can be noted in Table 4.8, the revenue of Hydrogenics went down during 2018 to that of financial values from six years prior. This was due to a decline of shipments for industrial electrolysers and fewer shipments of power systems to China, according to Hydrogenics themselves [42]. A financial backlash which likely led to Cummins buying the majority of Hydrogenics. By 2025, Cummins predicts that their earnings from electrolysers and fuel cell systems in trains will be \$400 million. The company made this prediction based on assuming 3.5 GW electrolyser sales and a price of \$750 000 per MW on electrolysers, in combination with a hundred trains being provided with fuel cell systems [45]. Cummins continues to acquire new assets in addition to Hydrogenics. A joint venture with NPROXX whom develops hydrogen storage pressure tank solutions was closed in November 2020, and the company seems set on continuing to invest in electrolyser and fuel cell technologies for hydrogen [46].

A recent project by Cummins and Air Liquide is one of the worlds largest hydrogen electrolyser sites, located in Bécancour, Canada. Site installation is comprised of four 5 MW HyLYZER 1000-30 units, displayed in Figure 4.10, which totals a facility of 20 MW and a production rate of up to 8.2 tonnes of hydropowered hydrogen per day [47].

5

Hydrogen applications

In this chapter hydrogen applications will be presented, both in near-time and future perspective. As mentioned in Section 4.1, the global hydrogen demand is dominated in oil refineries, ammonia production, methanol production and steel production. How hydrogen is used today and will be used in the future in these sectors will be presented. Other sectors in which the hydrogen demand is very low today but could see a large increase in the future are the transport, power, heating and agriculture sector.

5.1 Oil sector

Oil refining is responsible for 33% of the global hydrogen demand, where it is mostly used for hydrocracking and hydrotreatment processes [28]. An overview of hydrocracking can be seen in Figure 5.1 to illustrate how hydrogen is utilised in the process [29]. Hydro-

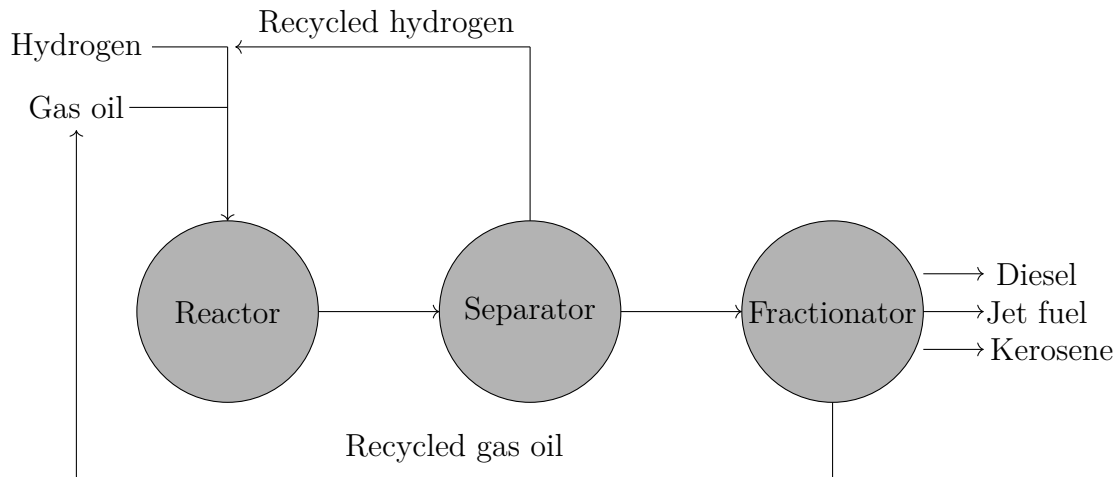


Figure 5.1: Simplified overview of hydrocracking for higher value oil production.

cracking is used to produce lighter oils of higher value from residual heavy oils. As the heavy residual oil demand is decreasing and the higher value oil demand is increasing, hydrocracking process usage and the associated hydrogen demand is expected to increase. The other process called hydrotreatment is utilised to remove or reduce contamination in oils such as sulphur. Crude oils contain sulphur where over 70% is removed through hydrotreatment processes due to air quality regulations. These regulations will most likely become more strict in the near future which will require higher hydrogen demand to remove more of the sulphur in crude oils [28]. Furthermore, both the hydrogen demand for oil refineries and the oil demand is expected to increase 7% by 2030 [28], [48]. Countries

with growing markets such as China, India, South East Asia and Sub-Saharan Africa are most likely to be the cause of the expected increase in oil demand. However, after 2030 the oil demand is expected to decrease with 30% over the two following decades. The reason is the coming electrification of the transport sector but also because of engine efficiency advancements [48].

5.2 Chemical sector

The chemical sector accounts for 40% of the global hydrogen demand, with ammonia and methanol production alone accounting for 93% of that hydrogen demand. The production of fertilisers as well as industrial applications such as synthetic fibers and explosives require 80% and 20% of the ammonia demand respectively. Methanol is mostly used for the production of industrial applications such as formaldehyde and methyl methacrylate among other chemicals, but also for production of gasoline in a process called methanol-to-gasoline, which does not require oil. The hydrogen to ammonia and methanol conversion is illustrated in Figure 5.2. Between 2018 and 2030, ammonia and methanol demand for

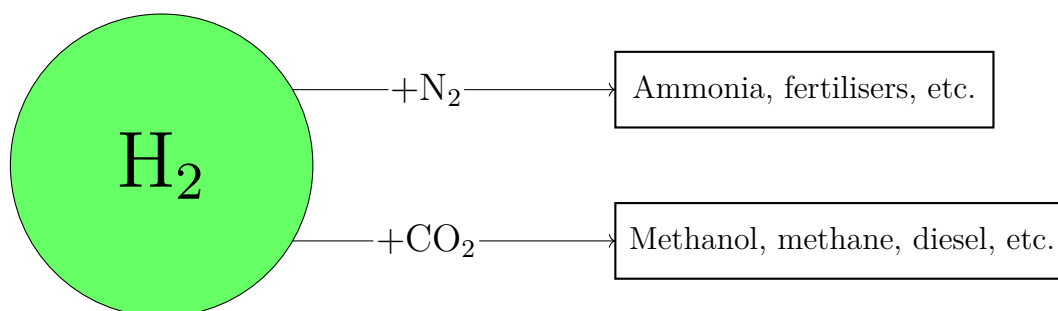


Figure 5.2: Simplified overview of hydrogen to ammonia and methanol conversion.

applications today is expected to increase 1.7% and 3.6% every year respectively [28]. In order to reduce the greenhouse gas emissions, the non-renewable hydrogen used as feedstock could be replaced with renewable hydrogen without any significant changes to the infrastructure. The current major limitation is that renewable ammonia and methanol production is around three times more expensive than non-renewable production [49]. As can be seen in Figure 5.3, renewable hydrogen production cost is more expensive compared to non-renewable hydrogen production cost, which is why renewable ammonia and methanol production is more expensive as well. It can be seen that renewable hydrogen production from both solar and wind power generation could become competitive between 2035 and 2040 compared to non-renewable hydrogen production. However, in best case scenario this could occur by 2025 [29].

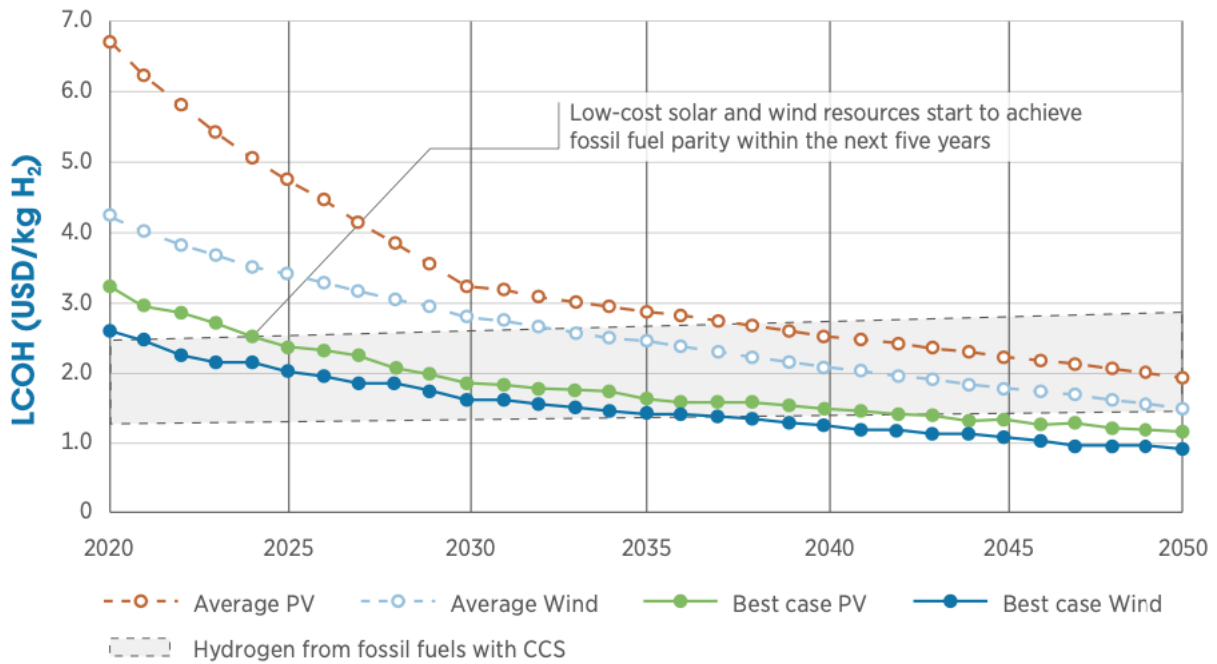


Figure 5.3: Renewable hydrogen production costs from VRE compared to non-renewable hydrogen production costs within the next 30 years [29].

5.3 Steel- and iron sector

Blast furnace/basic oxygen furnace (BF-BOF) is a steel production technology within the steel industry, with coal and coke as reducing agent, that accounts for 71% of the global steel production. The rest is produced by using steel scraps in an electric arc furnace (EAF) [50]. Moreover, there is also a technology called direct reduction of iron (DRI), where combined with EAF becomes DRI-EAF and accounts for over 5% of the global steel production. Hydrogen and carbon monoxide in a mixture is used as a reducing agent to produce steel in DRI-EAF and accounts for over 3% of the global hydrogen consumption. However, the hydrogen is non-renewable in today's DRI-EAF applications. But there are several projects today developing renewable steel production by using renewable hydrogen as reducing agent in DRI-EAF, such as the Swedish project HYBRIT and the German project SALCOS [28]. This is viewed as the technology with highest potential to decarbonise the steel industry [50]. An illustration is shown in Figure 5.4, where the ordinary BF-BOF steel production process is compared to HYBRIT's DRI-EAF renewable steel production process utilising renewable hydrogen as a reducing agent. As can be seen, the process of ironmaking and steelmaking differs between the two production technologies [51]. According to IEA, the DRI-EAF technology is set to double by 2030 as well, which would also double the hydrogen demand [28].

Renewable hydrogen can further be implemented in other sectors within the steel- and iron sector such as a reducing agent in smelting plants as well as fuel for steel heating. The recycling of zinc uses coal as reducing agent today, where research is being conducted to replace coal with renewable hydrogen. Another option could be to implement ammonia instead, where it is already being used as a reducing agent for copper production in Rönnskärs smelting plant located in Sweden. Finally, natural gas and gasoline are used for the heating of steel, but could be replaced with renewable hydrogen to reduce the emis-

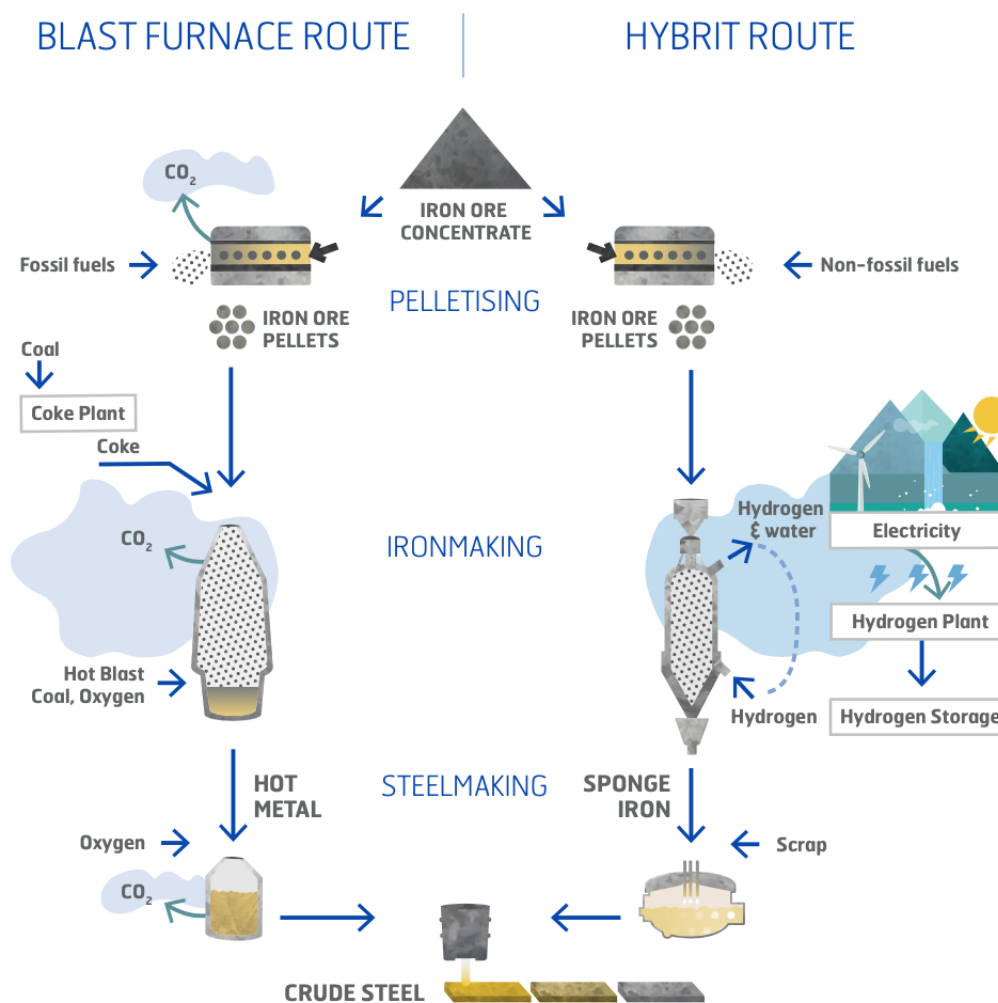


Figure 5.4: Illustration of BF-BOF steel production process and HYBRIT's renewable DRI-EAF steel production process utilising renewable hydrogen as reducing agent [51].

sions. This has been demonstrated by the Swedish steel company Ovako in 2020. Ovako's strategy by 2022 is to implement electrolyser systems of 16 MW to produce renewable hydrogen and replace the current fuel usage, potentially decreasing their emissions in Sweden with 50% [52].

5.4 Transport sector

Hydrogen is not highly applied in the transport sector. However, there has been an increase over the past years and the hydrogen demand is believed to increase even further in the future due to its potential in aiding with the decarbonisation of the transport sector. Transportation can be divided into road, maritime, rail and aviation transport.

5.4.1 Road transport

In 2018 there were over 1 billion cars, 190 million trucks and 25 million buses but only 11200 cars, 400 trucks and 500 buses were fuel cell electric vehicles (FCEV). Compared to the 5.1 million battery electric vehicles (BEV) existing today, there are not many

FCEV. However, FCEV have been deployed with a high increase lately, with 56% more fuel cell cars in 2018 compared to 2017. FCEV have been highly deployed in industries that require forklifts, with over 25000 forklifts today. The reason being is that forklifts are highly utilised in industries and require fast refuel time, giving FCEV an advantage over BEV. Moreover, the number of road transport vehicles is expected to grow in the future, both for trucks and personal cars, which enables a potential to implement more fuel cell trucks and battery electric cars in order to decarbonise the road transport sector [28].

The reason why BEV is a more attractive option for cars today is because the total cost of ownership is less expensive compared to FCEV. In order for FCEV to be cost-competitive in the future for ranges over 400 km, there would need to be more hydrogen fuel station installments as well as a decrease in fuel cells and storage costs. But, for short distances below 400 km, BEV is considered to be the most suited option, both today and in the future [28]. However, long range, heavy duty and high utilisation vehicles, such as forklifts, trucks and buses, require low refuel time and higher energy capacity compared to cars, which is hard requirements to be fulfilled by batteries alone. Therefore, FCEV is considered a more suitable and competitive option in this case [26]. Even for the high fuel cell costs today, FCEV are considered preferable over BEV for heavy-duty applications that has travel distances above 600 km [28]. Thus could FCEV complement BEV in the future decarbonisation of both short-range and long-range as well as light-duty and heavy-duty road transport [26].

5.4.2 Maritime

International shipping corresponds to 80% of the shipment in the maritime sector and is responsible for 2.5% of the global carbon dioxide (CO₂) emissions. If no actions are taken, the environmental impact will only increase as shipping is expected to increase 45% by 2030 and 300% by 2050. In order to decarbonise the maritime sector, low-carbon alternatives must replace heavy fuel oil that is mostly used today [28]. Batteries are not a viable option for deep-sea ships, because they require high energy demand and need to travel far distances. Since hydrogen requires high storage space, it is also not a viable option for deep-sea ships, because it is of high importance to optimise the freight space. However, batteries and fuel cells could both have a potential to replace oil in short-distance shipping such as ferries as they are usually smaller. Another reason is also because the energy consumption is mostly varying in short-sea ships due to them travelling in varying velocities, dissimilar to deep-sea ships that travel with steady velocity, which is suitable for electric- and fuel cell systems [53].

Fuel candidates that have the potential to replace oil in deep-sea shipping are bio-fuels, ammonia and hydrogen-based synthetic fuels such as diesel, methane and methanol. Biofuels are considered a viable option to replace oil because it can be used in internal combustion engines (ICE) and does not require large modifications to the existing system infrastructure. Renewable ammonia is a hydrogen-based fuel that does not have the same storage difficulties as hydrogen, which makes it more attractive as fuel replacement. However, there are no engines today that can utilise ammonia as combustion fuel, but there are a few under development. It is still considered as a viable replacement for oil fuel in ships due to the existing infrastructure for transportation and

storage of ammonia. Although, the infrastructure must be advanced further for ammonia to be utilised as fuel. Finally, hydrogen-based synthetic fuels such as diesel, methane and methanol are similar to biofuels in the way that they require low modifications to the infrastructure system and can be used in ICE's. However, these carbon-based fuels are only renewable if the carbon was obtained in a sustainable manner so the emissions are included in the natural carbon cycle. For these fuels to become competitive, the electricity costs must decrease since the production of synthetic fuels are energy-demanding and therefore expensive. According to DNV GL, carbon-based synthetic fuels are considered as suitable alternatives for the transition towards renewable maritime transport [53].

As mentioned in Section 5.4.1, fuel cells could be a more viable option compared to batteries for high utilised and heavy-duty vehicles that require short refuel time, which makes it suitable to replace oil-based forklifts and trucks operating at harbours [28]. This could especially be a preferable option over electrifying harbours if installing electrical lines is more expensive [26].

5.4.3 Rail

The railway network is the most electrified transport network today. However, Germany and France are two countries where 80% of the rail traffic is on electrified tracks, while more than 50% of the railway network is not electrified. This indicates that these countries, and others, have an extensive railway network which is not used to its full potential. More countries are continuing to expand the electrification of the railway network, but other technologies that have shown potential are fuel cell and battery trains. These can be used on non-electrified railways and replace diesel trains in cases where electrifying railway tracks is too expensive. This was the case in Germany, which has two hydrogen trains and has ordered several more from the french company Alstom. Hydrogen trains is considered to be preferable for large trains that travel far distances and which are not utilised in the rail network frequently, which is usual for rail freight [28]. For the future however, a hybrid of hydrogen and battery trains could be most beneficial whenever the cost of electrifying the railway network is too expensive. The hybrid trains could be powered from the fuel cells and the batteries which recharge through regenerative braking [54].

5.4.4 Aviation

The aviation sector is responsible for 2.8% of the global greenhouse gas emissions. It is the transport sector that is expected to grow the most in the future with twice as much air traffic by 2050. Expected fuels that could replace jet fuel based on fossil fuels are biofuels and hydrogen-based synthetic fuels. Pure hydrogen is not considered a viable option for the aviation sector as it requires large infrastructure changes in the storage and refueling system on airports as well as aircraft architecture changes. However, there are some on-going projects for battery aircraft development, but there are difficulties with electrification of the aviation sector due to the immense weight and cost for the amount of battery capacity needed to provide enough power for flight [28].

Biofuels as well as hydrogen-based synthetic fuels have the advantage over pure hydrogen that they require no modifications to the refueling and storing infrastructure

as well as the aircraft architecture [28]. Hydrogen-based fuels could compliment biofuels as replacement fuels or as blending fuels for jet fuels, supporting the transition towards the decarbonisation of the aviation sector [49]. The issue is that the production of hydrogen-based fuels is energy-demanding and expensive, resulting in 4-6 times higher costs compared to ordinary jet fuel today. In order to be competitive in the future, the production costs of hydrogen-based synthetic fuels must decrease [28].

5.5 Power sector

With a global power generation capacity of 7 TW, approximately 15% consists of solar and wind power [29]. The result of implementing more variable renewable energy (VRE) systems into the global power grid is that the power generation will be intermittent and therefore unable to supply the load demand. The availability of VRE systems can be increased with the help of flexibility services, helping to reduce VRE curtailment and improve load balancing [49]. Excess power generation can be used to produce hydrogen through electrolysis which can then be stored [3]. In Figure 5.5, an illustration

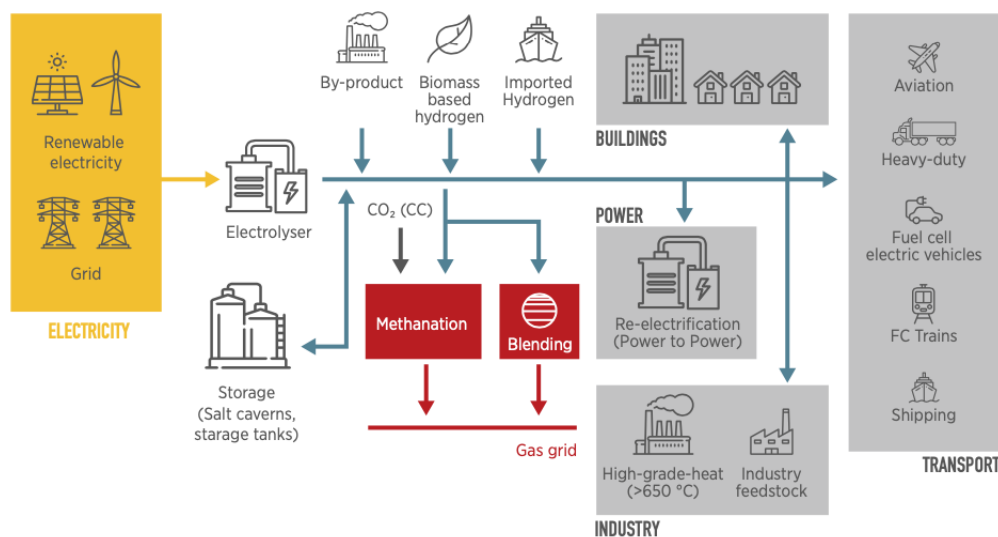


Figure 5.5: Illustration of electrolyser systems integrated in the power grid together with different hydrogen application sectors [26].

of electrolyser systems connected to the power grid and hydrogen application sectors is shown. As can be seen, hydrogen can be produced from renewable electricity through electrolysis which can be stored or even re-electrified with fuel cells [26]. Energy storage is an essential part in VRE systems, and hydrogen storage in combination with batteries could enable energy storage from a few seconds to several months [52]. The reason why hydrogen storage would be a well-suited complement is because batteries self-discharge and are less suitable for long-term storage as well as large storage capacity, since the cost increases linearly with the storage capacity [26]. Hydrogen storage is more advantageous for long-term seasonal storage as it can store energy for several weeks due to its no self-discharge capabilities. Another advantage with the long-term storage capabilities of hydrogen is that other countries can export excess energy to countries with high load demand but low energy production, reducing seasonal supply and demand imbalances [3].

Fuel cells together with hydrogen storage can also be used for decentralised power systems as well for back-up power generation. Diesel generators are mostly used today for back-up power supply, which could be replaced with fuel cells to reduce the emissions but also because it is more robust compared to a system of batteries [26].

5.6 Heating sector

The building sector today has a global energy demand of nearly 30% and accounts for the same amount of the global greenhouse gas emissions. Natural gas could be replaced with renewable hydrogen for heating of buildings where it can be used in the existing natural gas infrastructure. However, this would require advancements to the infrastructure and could be costly. Another solution to help the transition towards reducing the global emissions from the heating sector is by blending renewable hydrogen or even use synthetic methane, as it would not require significant changes to the infrastructure. However, since the maximum blending percentage is 20% today, it would only reduce the emissions and not remove them. Furthermore, fuel cells could be used for heating buildings and could be a viable solution as well. Hydrogen could be more beneficial than total electrification due to seasonal imbalance demands. Many countries today that need heating due to extreme climates have buildings that are older than 25 years old and require more energy to be heated. Even buildings that are not as old will require more energy as they become older in the future, which makes hydrogen for heating as a viable option to reduce the emissions from the heating sector [28]. It can also complement heat pumps if there are difficulties in the transition from today's heating systems to heat pumps, such as in dense cities with several commercial and apartment buildings [55].

5.7 Agriculture- and food sector

Mineral nitrogen fertilisers are produced from ammonia, which could be replaced with renewable ammonia produced from renewable hydrogen. Large farming vehicles such as tractors could also begin implementing fuel cells to reduce the emissions as it is suitable for heavy-duty vehicles. Decentralised hydrogen production from VRE such as solar and wind power has been considered by the agriculture and food sector as well [52].

6

PEM electrolyser model

In this chapter the theory regarding PEM electrolysis will be presented [56], [57], [58], [59], [60]. Furthermore, simulation results and discussion of the electrolyser model as well as future electrolyser trends will be presented.

6.1 PEM electrolysis theory

The voltage of a PEM electrolyser cell can be expressed as

$$V_{\text{cell}} = V_{\text{rev}} + V_{\text{act}} + V_{\text{ohm}} + V_{\text{con}} \quad (6.1)$$

where V_{rev} is the reversible voltage and V_{act} , V_{ohm} and V_{con} are the activation, ohmic and concentration overvoltages respectively. The reversible voltage is the required voltage to initiate electrolysis and can be calculated with Gibbs free energy ΔG and the Faraday constant F as

$$V_{\text{rev}} = V_{\text{rev},0} + \frac{R \cdot T}{z \cdot F} \cdot \ln\left(\frac{p_{\text{H}_2} \sqrt{p_{\text{O}_2}}}{p_{\text{H}_2\text{O}}}\right) \quad (6.2a)$$

$$V_{\text{rev},0} = \frac{\Delta G}{z \cdot F} \quad (6.2b)$$

where $V_{\text{rev},0}$ is the initial reversible voltage, R is the universal gas constant, T is the temperature and z is equal to 2 which represents the number of electron moles that are transferred to produce one hydrogen mole. The parameters p_{H_2} , p_{O_2} and $p_{\text{H}_2\text{O}}$ are the partial hydrogen pressure, partial oxygen pressure and partial water pressure respectively. Gibbs free energy ΔG can be expressed as

$$\Delta G = \Delta H - \Delta S \cdot T \quad (6.3)$$

where ΔH and ΔS are the process enthalpy- and entropy change respectively. The current density at the electrode surface will result in an activation overvoltage which can be calculated for the anode and cathode separately as

$$V_{\text{act}} = V_{\text{act,an}} + V_{\text{act,ca}} \quad (6.4a)$$

$$V_{\text{act,an}} = \frac{R \cdot T}{\alpha_{\text{an}} \cdot F} \cdot \sinh^{-1}\left(\frac{J}{2 \cdot J_{0,\text{an}}}\right) \quad (6.4b)$$

$$V_{\text{act,ca}} = \frac{R \cdot T}{\alpha_{\text{ca}} \cdot F} \cdot \sinh^{-1}\left(\frac{J}{2 \cdot J_{0,\text{ca}}}\right) \quad (6.4c)$$

where J is the current density and α as well as J_0 are the transfer coefficient and the exchange current density respectively. Furthermore, the ohmic overvoltage is due to the ionic resistance of the ion flow in the electrolyte R_{ion} and the resistance of the electrodes R_{el} , and can be expressed as

$$V_{\text{ohm}} = (R_{\text{ion}} + R_{\text{el}}) \cdot I \quad (6.5)$$

where I is the current. The ionic resistance R_{ion} can further be calculated as

$$R_{\text{ion}} = \frac{\delta_{\text{mem}}}{A_{\text{mem}} \cdot \sigma_{\text{mem}}} \quad (6.6)$$

where δ_{mem} , A_{mem} and σ_{mem} are the thickness, area and conductivity of the membrane respectively. The conductivity can also be expressed according to

$$\sigma_{\text{mem}} = (0.005139 \cdot \lambda - 0.00326) \cdot e^{(1268 \cdot (\frac{1}{303} - \frac{1}{T}))} \quad (6.7)$$

where λ is the water content of the membrane. Finally, there are limitations in the mass transportation for high current densities due to the accumulation of oxygen gas bubbles on the membrane. This will result in a concentration overvoltage which can be expressed as

$$V_{\text{con}} = -\frac{R \cdot T}{z \cdot F} \cdot \ln\left(1 - \frac{J}{J_1}\right) \quad (6.8)$$

where J_1 is the limiting current density. The hydrogen production rate v_{H_2} in litres per second for one cell can also be calculated as

$$v_{\text{H}_2} = \frac{v_{\text{m}} \cdot I}{z \cdot F} \quad (6.9)$$

where v_{m} is one molar volume which can be expressed as

$$v_{\text{m}} = \frac{R_{\text{u}} \cdot T}{p} \quad (6.10)$$

where R_{u} also is the universal gas constant as R but in another unit and p is the operating pressure of the electrolyser. The LHV cell efficiency of the electrolyser can be calculated according to

$$\eta^{\text{LHV}} = \frac{V_{\text{rev}}}{V_{\text{cell}}} \quad (6.11)$$

Finally, in order to calculate the total electrolyser output voltage and hydrogen production rate, the values of one cell should be multiplied with the number of cells, n_{s} , that are connected in series in an electrolyser system.

6.2 Performance and simulation of PEM model

An overview of the electrolyser model, with input and output variables, is illustrated in Figure 6.1. Furthermore, the inside of the electrolyser block in Figure 6.1 is illustrated in Figure 6.2 which shows the voltage components that the voltage V_0 across the electrolyser consists of. The parameter values that were used to model a 2 MW PEM electrolyser model are presented in Table 6.1 and were derived from [25], [28], [56], [57], [58], [61]. As can be seen, the maximum current $I_{0,\text{max}}$ is 3750 A and the maximum output voltage $V_{0,\text{max}}$ will result in 533 V. Note that n_{s} electrolyser cells have been connected in series.

Table 6.1: Different parameter values of the 2 MW PEM electrolyser model [25], [28], [56], [57], [58], [61].

| Parameter description | Parameter value |
|-----------------------------|------------------------|
| T | 80° C |
| p | 30 bar |
| α_{an} | 0.5 |
| α_{ca} | 0.5 |
| $J_{0,\text{an}}$ | 0.01 A/cm ² |
| $J_{0,\text{ca}}$ | 10 A/cm ² |
| J_1 | 3 A/cm ² |
| λ | 18 |
| δ_{mem} | 127 μm |
| A_{mem} | 1250 cm ² |
| R_{el} | 0 Ω |
| n_s | 277 |
| $I_{0,\text{max}}$ | 3750 A |
| $V_{0,\text{max}}$ | 533 V |
| $v_{\text{H}_2,\text{max}}$ | 37.8 kg/h |

Table 6.2: Universal constant values.

| Constant description | Constant value |
|----------------------|---|
| R | 8.314 J/(mol· K) |
| R_u | 8.314· 10 ⁻² bar· L/(mol· K) |
| F | 96485 C/mol |
| ΔH | 285.84 kJ/mol |
| ΔS | 163.2 J/(mol· K) |

This will also result in a maximum hydrogen production rate $v_{\text{H}_2,\text{max}}$ of 37.8 kg/h and maximum cell voltage of $V_{\text{cell,max}}$ equal to 1.92 V.

The cell voltage V_{cell} as a function of the current density J is illustrated in Figure 6.3. As can be seen, the cell voltage V_{cell} increases with the current due to the increase of the overvoltages in Figure 6.5. The anode activation overvoltage $V_{\text{act,an}}$ is the largest contributor, especially for low current densities, with the ohmic overvoltage V_{ohm} being the second largest. It can also be seen that the cathode activation overvoltage $V_{\text{act,ca}}$ is close to negligible while the concentration overvoltage V_{con} contributes as most for large current densities. The electrolyser efficiency η^{LHV} is also illustrated in Figure 6.4, where it decreases with the current density J . It is because it is inversely proportional to the cell voltage V_{cell} according to (6.11) and because the reversible voltage V_{rev} is constant. Moreover, the electrolyser model can be viewed as a resistive load and is illustrated in Figure 6.6. As can be seen, the resistance decreases with an inverse exponential rate for an increase in the current density J , and moves towards infinity for very low current densities. This behaviour is expected since the voltage does not increase linearly with the current density J as shown in Figure 6.3, which it would if the resistance was constant. Furthermore, the power P_0 and the power losses $P_{0,\text{loss}}$ are illustrated in Figure 6.7 and Figure 6.8 respectively. As can be seen, both the power P_0 and the power losses $P_{0,\text{loss}}$

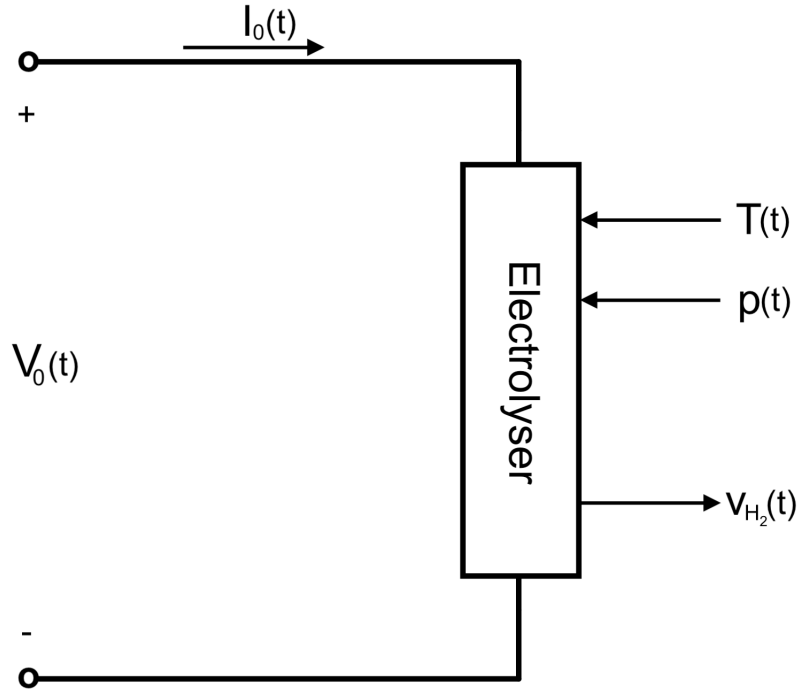


Figure 6.1: Overview of the PEM electrolyser model with input and output variables.

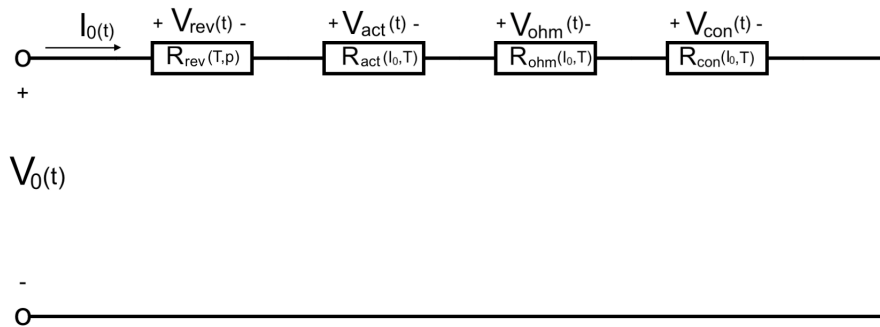


Figure 6.2: Electrolyser model in Figure 6.1 described as resistors.

increase similarly as a function of the current density J . For a power of 2 MW, the power losses are approximately 750 kW which is high. Therefore, there will be a need for a cooling system due to the heat generation produced from the high power losses. Finally, the output voltage V_0 and the output current I_0 are displayed in Figure 6.9 as a function of the hydrogen production rate v_{H_2} . The output current I_0 has a linear increase with the hydrogen production rate v_{H_2} , as expected according to (6.9). This is the reason why the output voltage V_0 has the same behaviour with an increase of the hydrogen production rate v_{H_2} as the cell voltage V_{cell} has with an increase of the current density J , as illustrated in Figure 6.3. The difference between the output voltage V_0 and the cell voltage V_{cell} is the amplitude, which is a factor of the number of cells connected in series n_s higher for the output voltage V_0 .

In Figure 6.10 and Figure 6.11, the cell voltage V_{cell} and the electrolyser efficiency η^{LHV} were plotted as a function of the current density J for different temperatures. As can be seen, increased temperature will result in lower cell voltage, which is because the reversible voltage V_{rev} and the ohmic overvoltage V_{ohm} decrease more than the

activation overvoltage V_{act} and the concentration overvoltage V_{con} increase with increased temperature T . However, as can be seen in Figure 6.11, the electrolyser efficiency is only higher for higher temperatures when the current density is above 1.2 A/cm^2 . The reason for this is when the electrolyser operates in the activation region, a temperature increase will result in a higher proportional decrease on the reversible voltage compared to the total cell voltage, which is why the efficiency decreases as well according to (6.11). But as soon as the electrolyser start to operate in the ohmic region, then the total cell voltage will proportionally decrease more than the reversible voltage did, which is why the efficiency will increase.

The cell voltage V_{cell} and the electrolyser efficiency η^{LHV} were also plotted for different pressures. As can be seen in Figure 6.12 and Figure 6.13, an increase in the pressure will result in an increase in the cell voltage and the efficiency. This is because the reversible voltage V_{rev} is the only voltage affected by the pressure p , which increases with increased pressure. Therefore, even though the cell voltage V_{cell} increases, the electrolyser efficiency η^{LHV} will increase as well because the reversible voltage V_{rev} will proportionally increase more than the cell voltage V_{cell} . Moreover, it can also be noticed that changing the pressure does not make significant changes to either the cell voltage or the efficiency.

Finally, in Figure 6.14 and Figure 6.15 the cell voltage V_{cell} and electrolyser efficiency η^{LHV} were plotted for different membrane thicknesses. A decrease in the membrane thickness δ_{mem} will result in a decrease of the cell voltage and therefore an increase of the electrolyser efficiency. This is because the ionic resistance R_{ion} will decrease according to (6.6), which will decrease the ohmic overvoltage V_{ohm} .

The simulation results of the PEM electrolyser model were compared to [57] and had similar behaviour. This can therefore verify that the model behaved as expected.

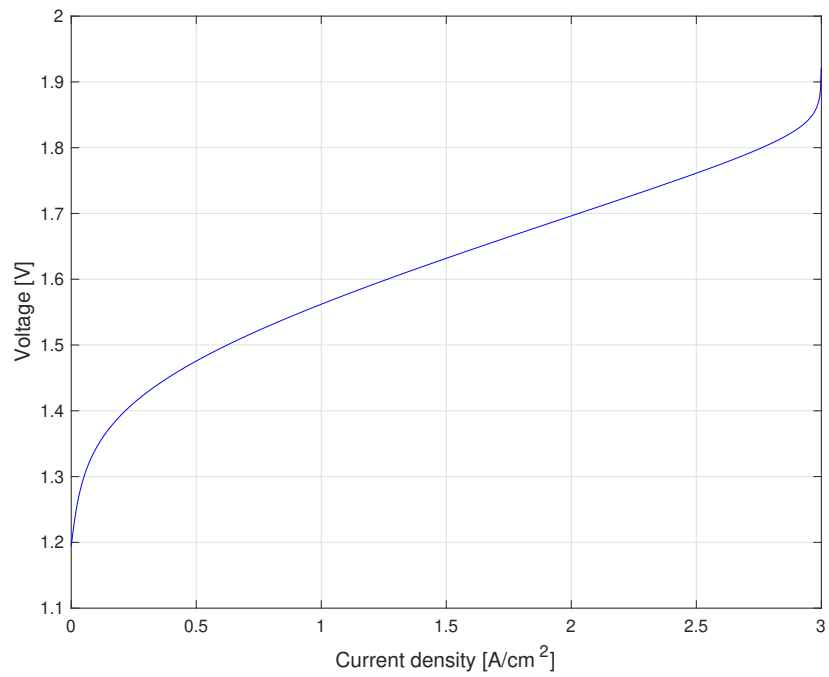


Figure 6.3: Cell voltage V_{cell} of the electrolyser model.

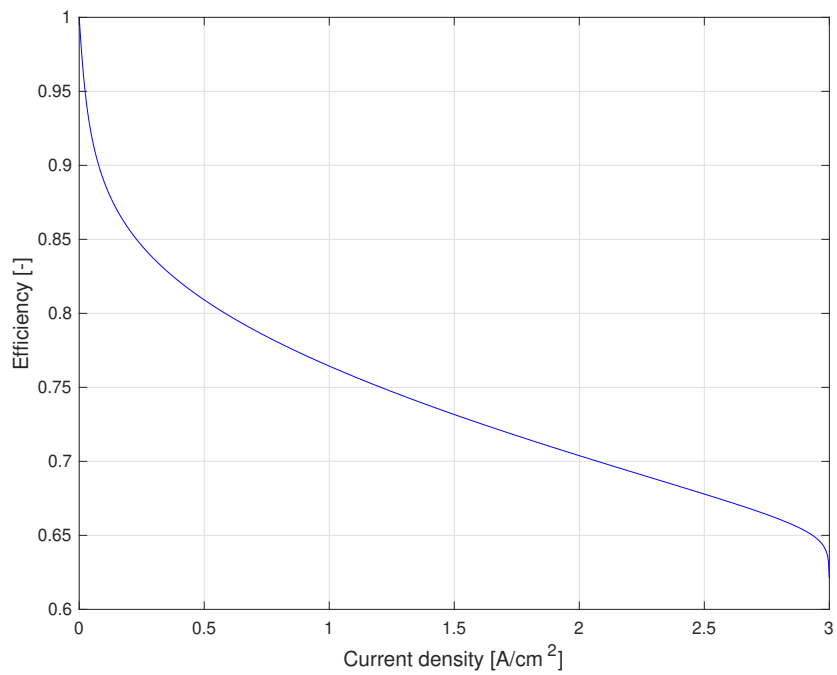


Figure 6.4: LHV efficiency η^{LHV} of the electrolyser model.

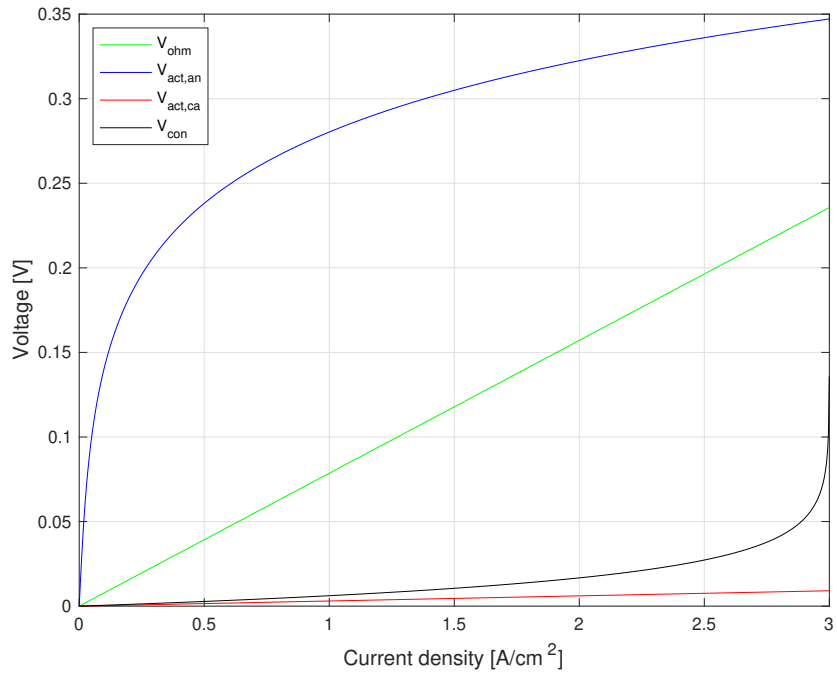


Figure 6.5: The cell overvoltages of the electrolyser model.

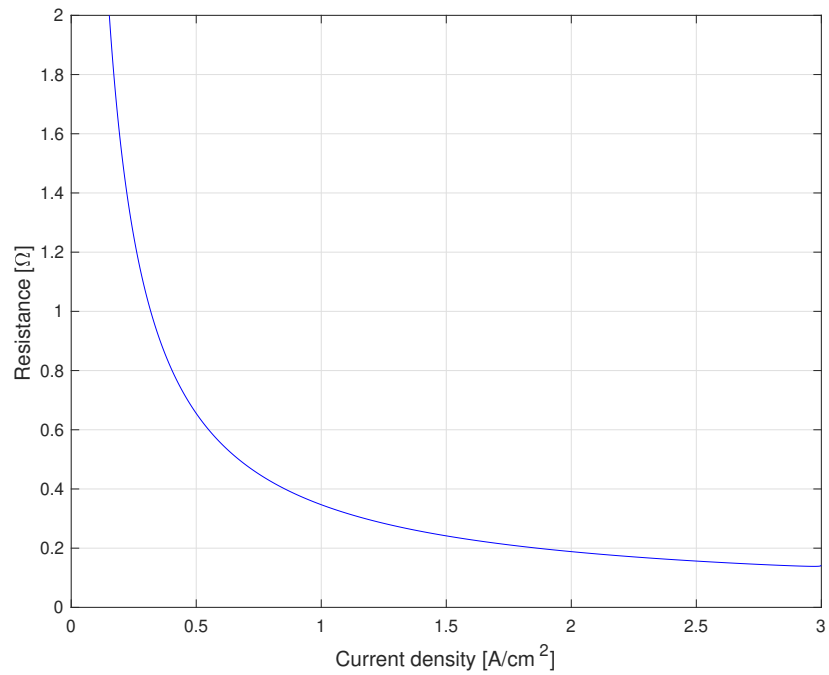


Figure 6.6: Electrolyser model resistance.

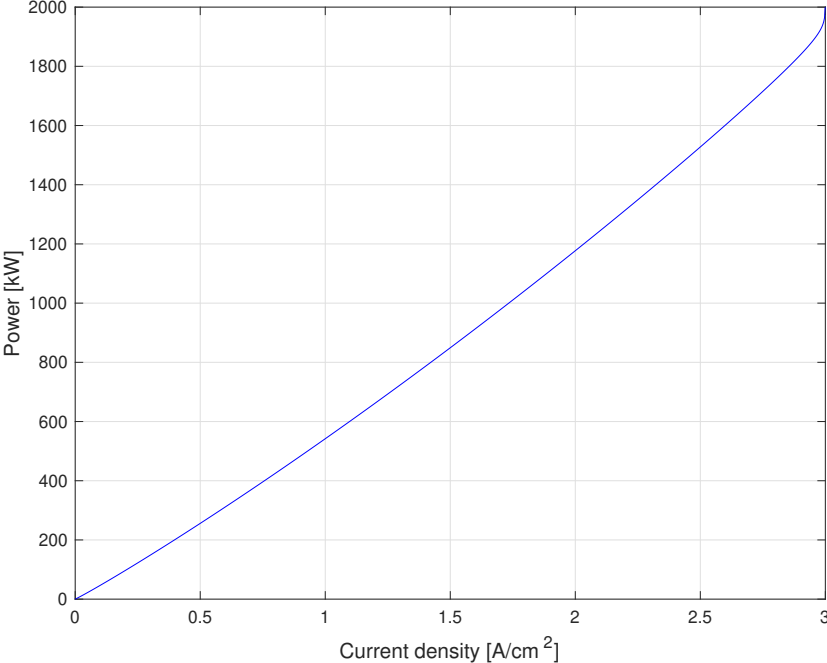


Figure 6.7: The power P_0 of the electrolyser model.

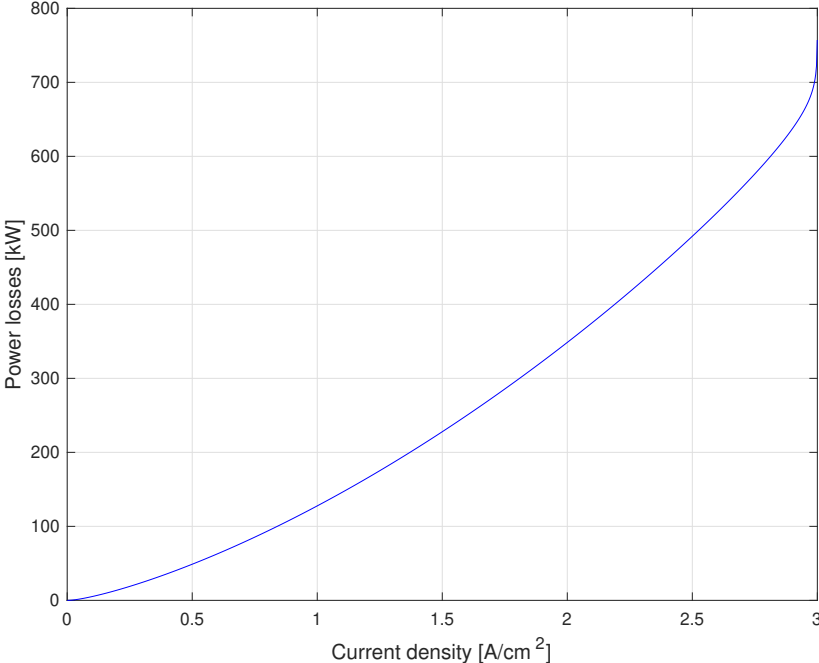


Figure 6.8: The power losses $P_{0,loss}$ of the electrolyser model.

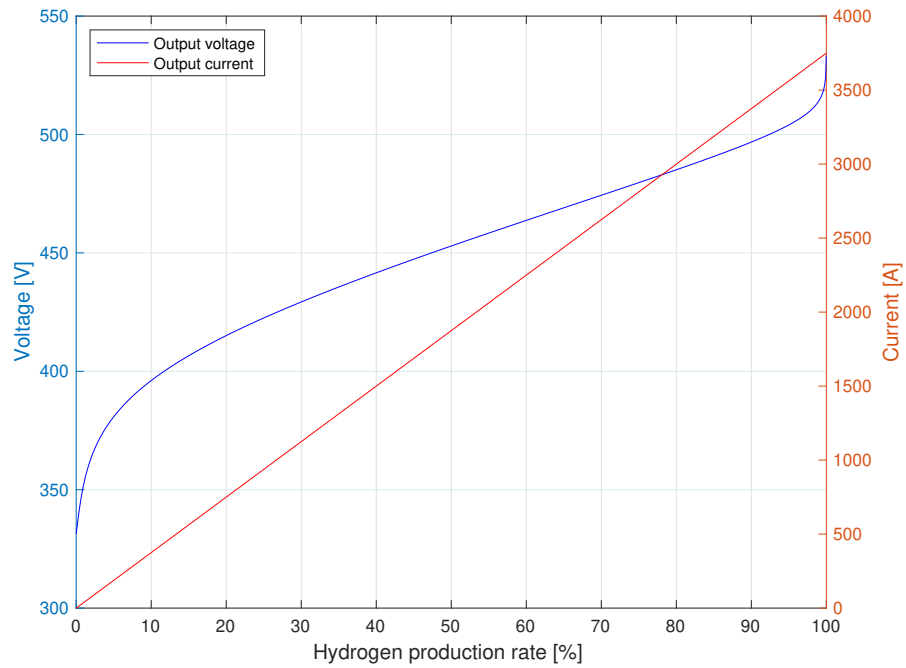


Figure 6.9: The output voltage V_0 and the output current I_0 as a function of the hydrogen production rate v_{H_2} .

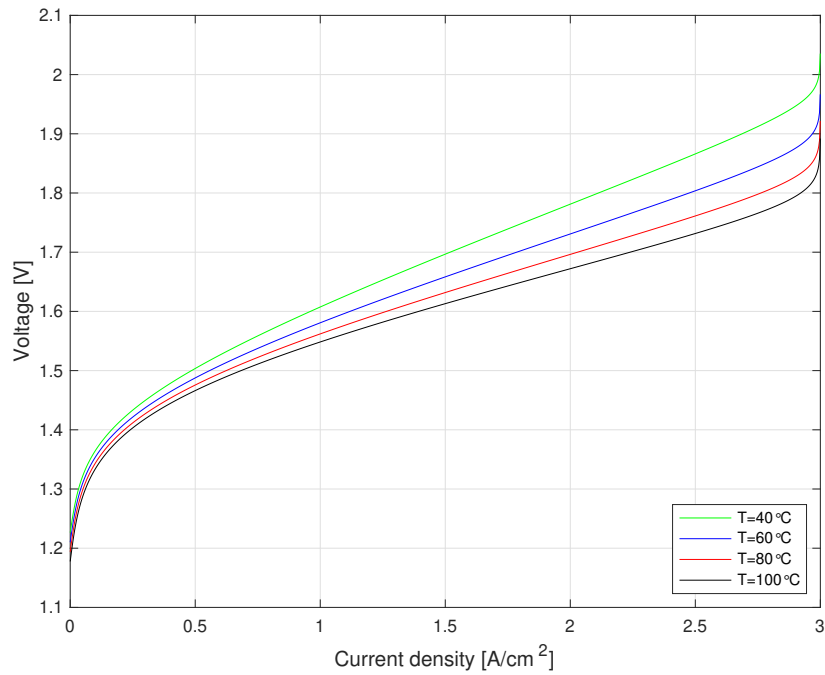


Figure 6.10: Cell voltage V_{cell} of the electrolyser model for different temperature cases.

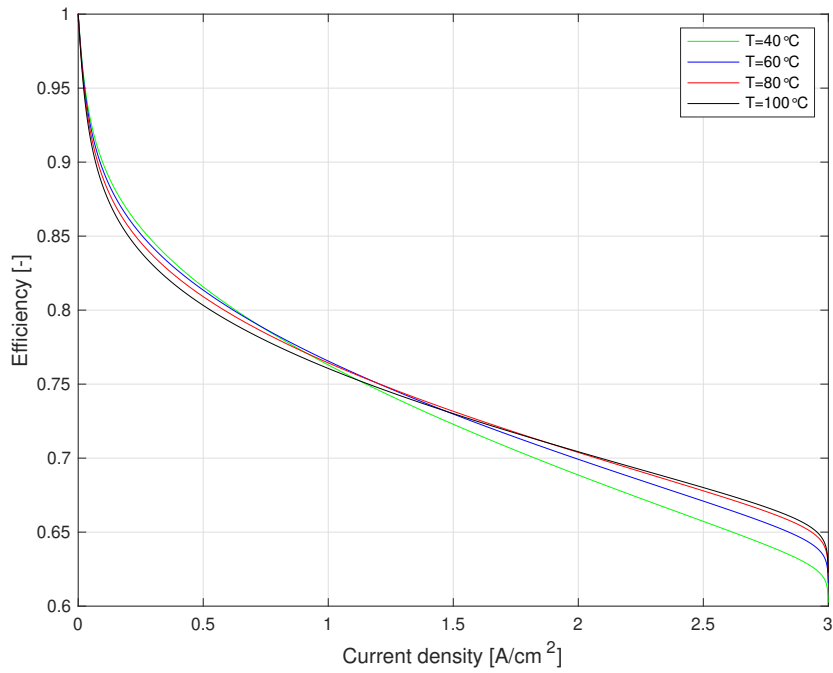


Figure 6.11: LHV efficiency η^{LHV} of the electrolyser model for different temperature cases.

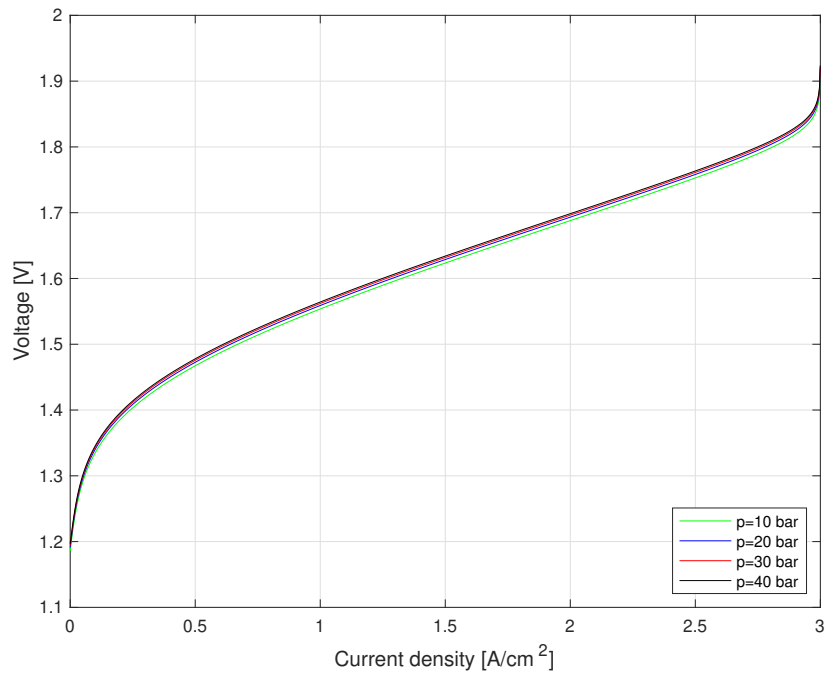


Figure 6.12: Cell voltage V_{cell} of the electrolyser model for different pressure cases.

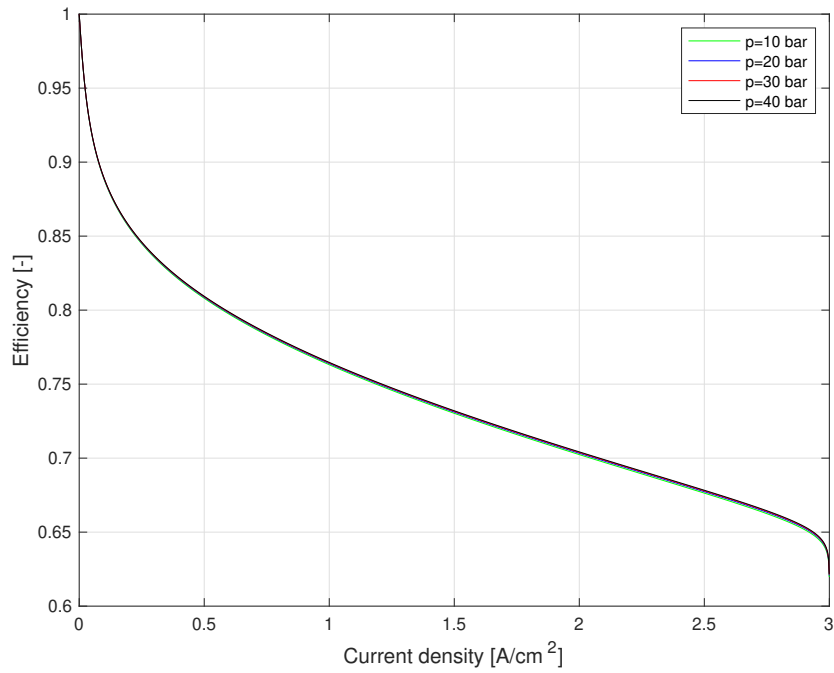


Figure 6.13: LHV efficiency η^{LHV} of the electrolyser model for different pressure cases.

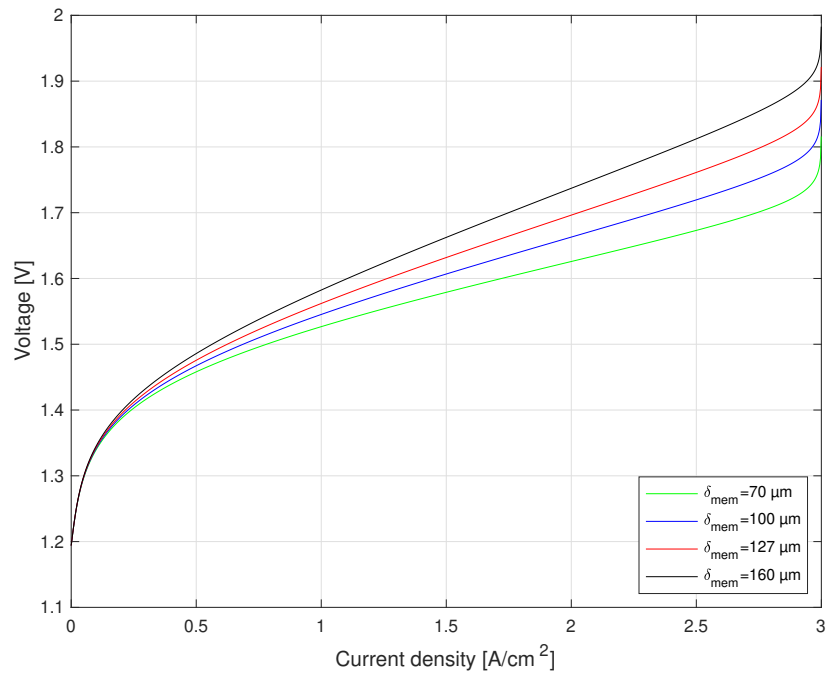


Figure 6.14: Cell voltage V_{cell} of the electrolyser model for different membrane thickness cases.

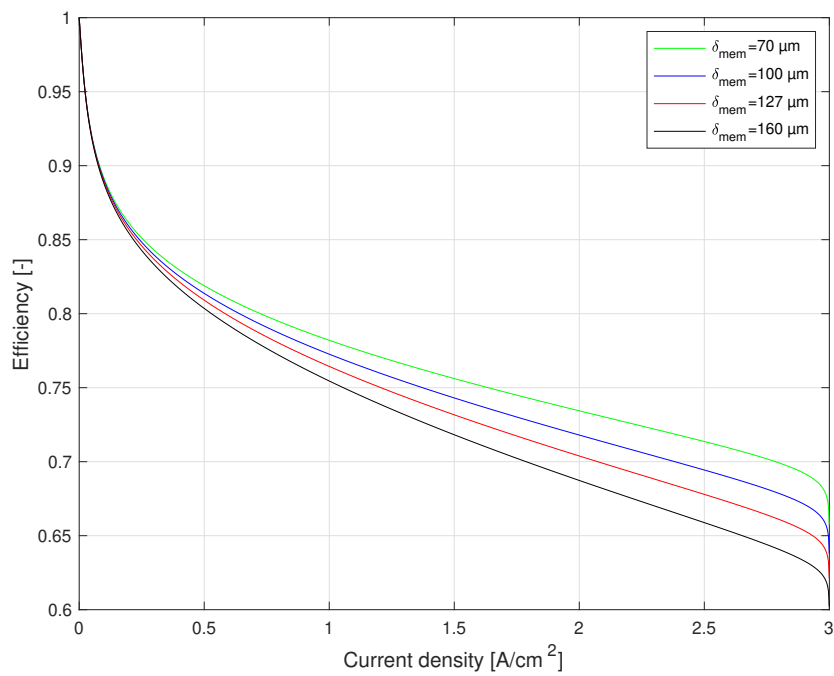


Figure 6.15: LHV efficiency η^{LHV} of the electrolyser model for different membrane thickness cases.

6.3 Future electrolyser trends

There are several parameters that can and should be improved with PEM electrolyzers in order to make them more competitive and efficient regarding the hydrogen production rate in the future. Firstly, the number of cells connected in series can be increased, as long as it can be done without compromising the reliability of the system. The maximum voltage of the stack will probably be below 1.5 kV, since that is the limit for low DC voltage. Secondly, as can be seen in Figure 6.14 and Figure 6.15, the membrane thickness should be decreased without compromising the durability of the membrane. This will help improve the overall electrolyser efficiency. Furthermore, the membrane area can be increased by improving the cell design and utilise an improved membrane as well which will result in higher hydrogen production rate as more current can flow through the electrolyser. Finally, another option to increase the current is to increase the current density. In Figure 6.16-6.21, a case has been made where the limiting current density J_1 has been increased from 3 A/cm² to 5 A/cm² in order to be able to increase the current density without operating in the concentration region. This would be preferable since the voltage increases exponentially in the concentration region, which means that the power consumption increases far more than if the electrolyser operated in the ohmic region. The hydrogen production rate as well as the power are plotted as a function of the membrane area and the electrolyser voltage, where the electrolyser voltage is increased as a function of the number of cells connected in series. As can be seen in Figure 6.16 and Figure 6.19 as well as Figure 6.17 and Figure 6.20, both the hydrogen production rate and the power increase with the membrane area and the voltage as a function of the number of cells connected in series respectively. Finally, by comparing Figure 6.16 and Figure 6.17 to Figure 6.19 and Figure 6.20, it can be seen that an increase in the current density from 3 A/cm² to 4 A/cm² will result in an increase of the hydrogen production rate and power as well. The same behaviour applies for the power losses as for the hydrogen production rate and the power when the membrane area and the voltage as a function of the number of cells connected in series increase, as illustrated in Figure 6.18 and Figure 6.21. When the maximum power is equal to 13.5 MW and 18 MW for the current density J of 3 A/cm² and 4 A/cm² respectively, the maximum power losses will reach 4.5 MW and 6.7 MW respectively. These are very high power losses which will result in very high heat generation and therefore demand high requirements on the cooling system. Nevertheless, future electrolyser systems will be designed to fulfill the requirements at a minimum cost. Therefore, the optimal operating point of the electrolyser can be at a partial load in order to maximise the total system at a minimum cost.

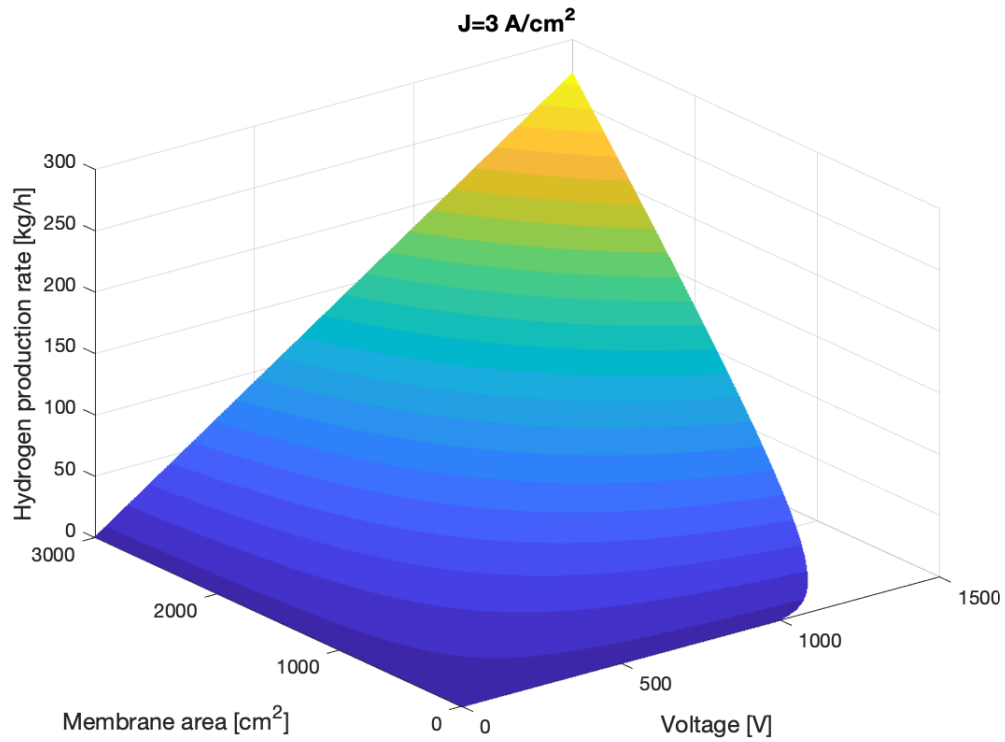


Figure 6.16: Electrolyser hydrogen production rate v_{H_2} as a function of membrane area A_{mem} and electrolyser voltage V_0 for current density of $J=3$ A/cm² with $J_1=5$ A/cm².

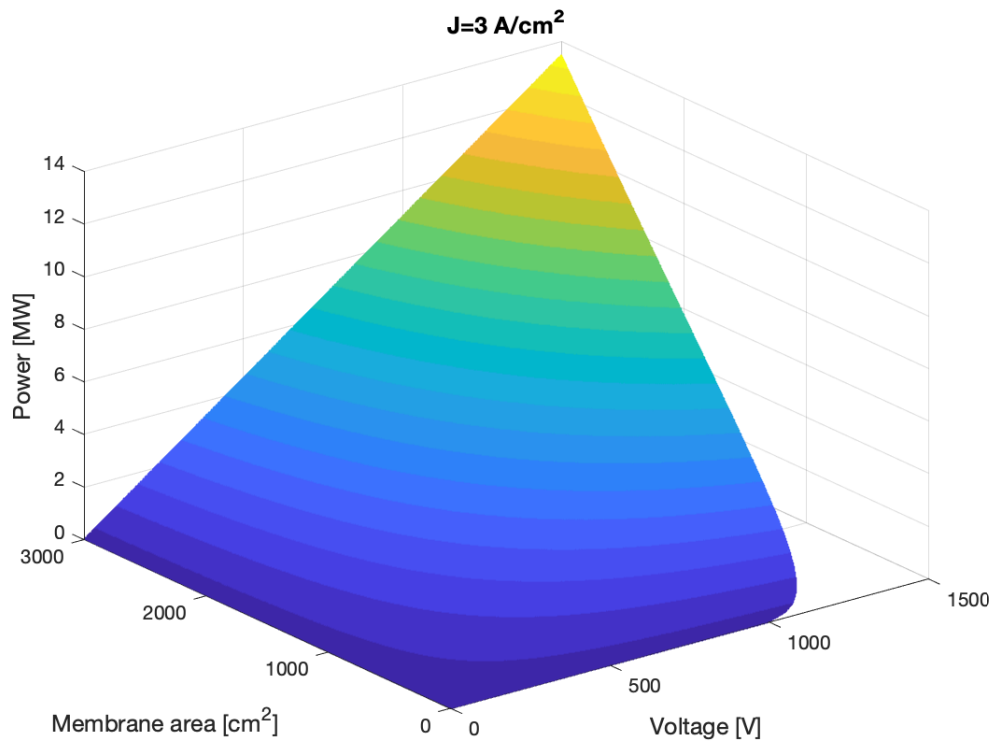


Figure 6.17: Electrolyser power P_0 as a function of membrane area A_{mem} and electrolyser voltage V_0 for current density of $J=3$ A/cm² with $J_1=5$ A/cm².

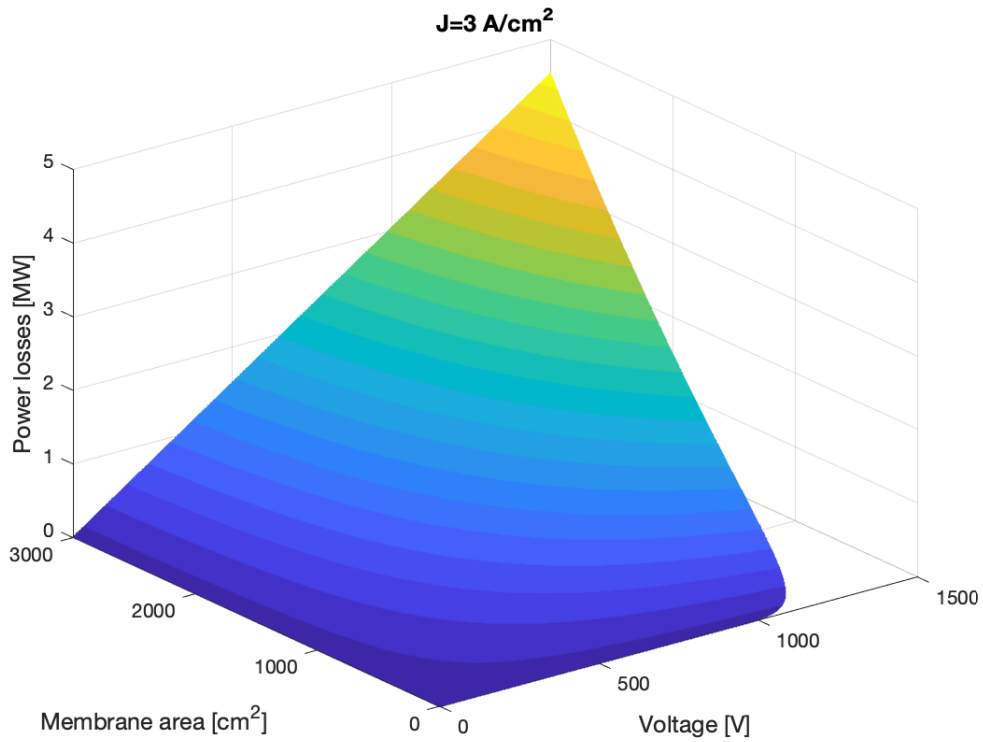


Figure 6.18: Electrolyser power losses $P_{0,\text{loss}}$ as a function of membrane area A_{mem} and electrolyser voltage V_0 for current density of $J=3 \text{ A/cm}^2$ with $J_1=5 \text{ A/cm}^2$.

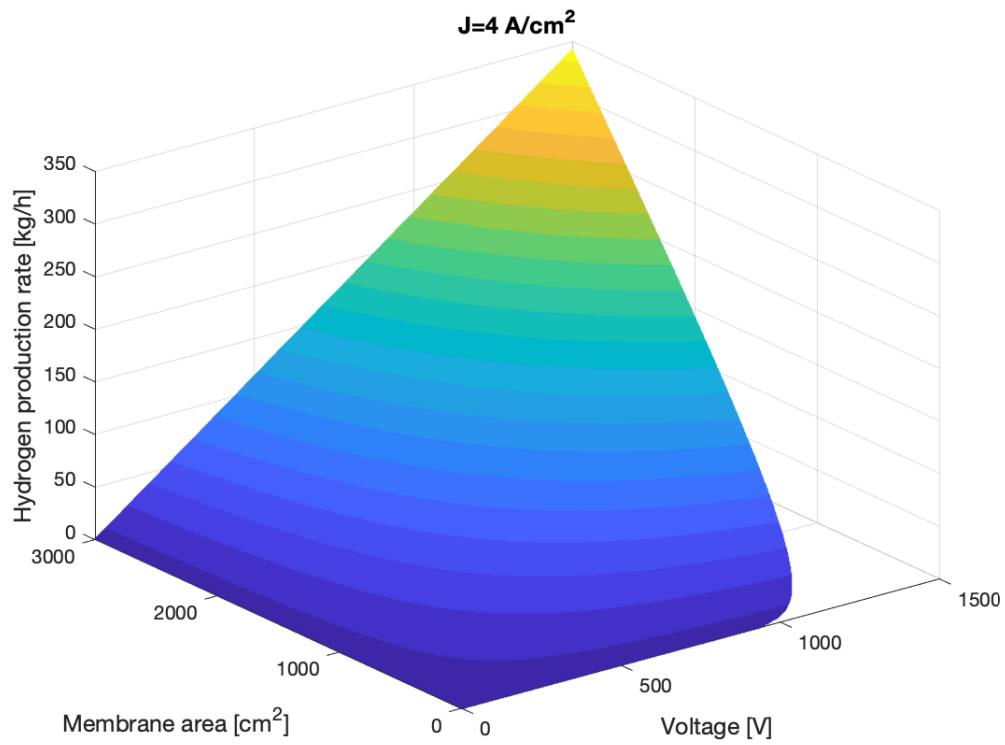


Figure 6.19: Electrolyser hydrogen production rate v_{H_2} as a function of membrane area A_{mem} and electrolyser voltage V_0 for current density of $J=4 \text{ A/cm}^2$ with $J_1=5 \text{ A/cm}^2$.

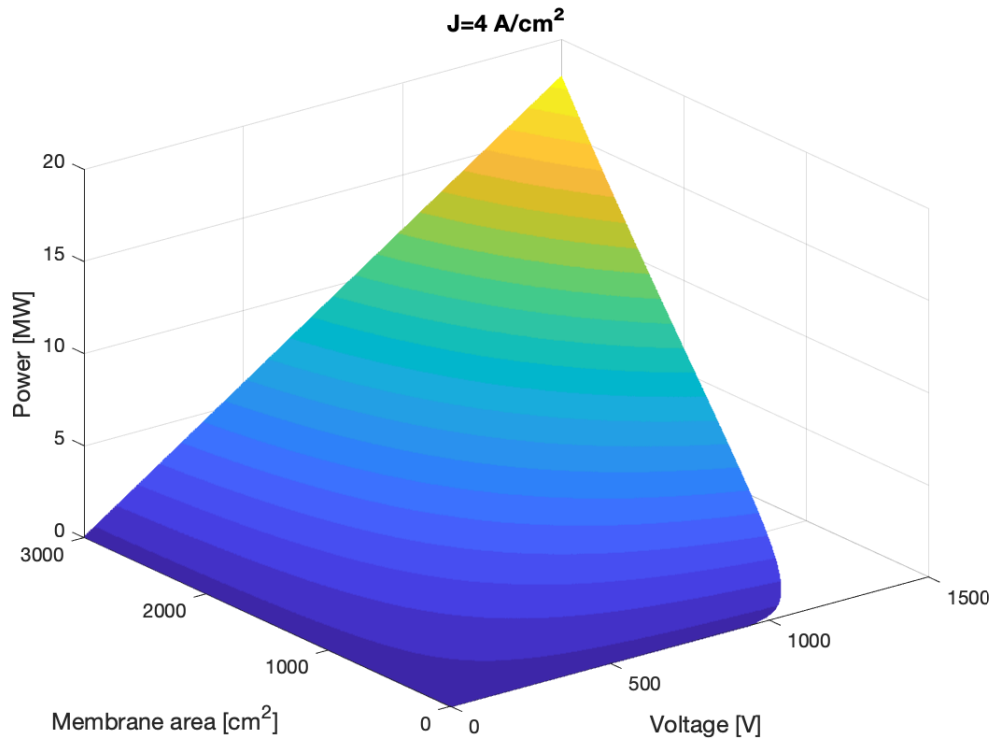


Figure 6.20: Electrolyser power P_0 as a function of membrane area A_{mem} and electrolyser voltage V_0 for current density of $J=4 \text{ A/cm}^2$ with $J_1=5 \text{ A/cm}^2$.

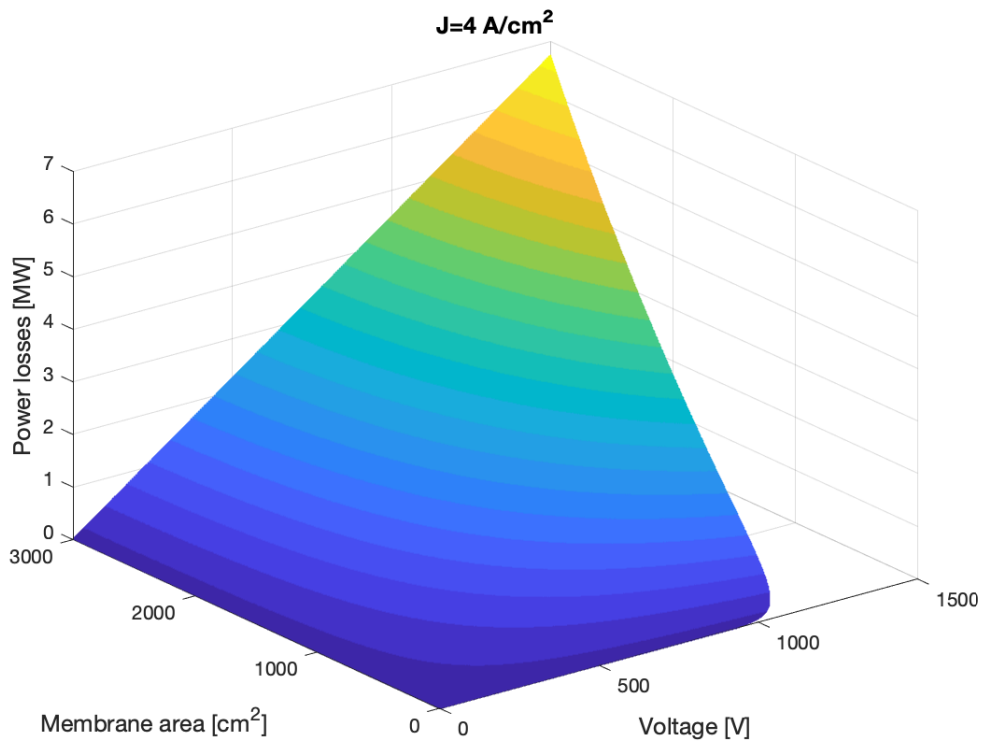


Figure 6.21: Electrolyser power losses $P_{0,\text{loss}}$ as a function of membrane area A_{mem} and electrolyser voltage V_0 for current density of $J=4 \text{ A/cm}^2$ with $J_1=5 \text{ A/cm}^2$.

6.4 Summary

The cell voltage V_{cell} increases with the current density J where the largest contributors are the anode activation overvoltage $V_{\text{act,an}}$ and the ohmic overvoltage V_{ohm} . The electrolyser efficiency η^{LHV} is inversely proportional to the cell voltage V_{cell} which is why it decreases with an increase in the current density J . Moreover, as the current density J increases, the power P_0 and the power losses $P_{0,\text{loss}}$ increase as well. It was also observed that the power losses can reach up to 750 kW if the electrolyser power is 2 MW. Hence, a cooling system will be required due to the high heat generation. Furthermore, an increase in the temperature T and a decrease in the membrane thickness δ_{mem} will result in a significant increase of the efficiency η^{LHV} . However, an increase in the pressure p did not increase the efficiency η^{LHV} as much.

For future performance and efficiency improvements of PEM electrolyser systems, development to increase the number of cells connected in series, decrease the membrane thickness, increase the membrane area and increase the current density should be considered. These advancements will result in the possibility to develop larger electrolyser stacks which will increase the hydrogen production rate immensely. However, the total electrolyser system optimisation will determine the electrolyser design and operating point.

7

PEM electrolyser connected to a converter

The traditional system setup is to connect the electrolyser station to an incoming HVAC line. The electrolyser station consists of a step-down transformer that feed power to an AC distribution system. A number of electrolyser systems are parallel-connected to the AC distribution system, as displayed in Figure 7.1. The larger power rating of the electrolyser station, the higher voltage level for the incoming HVAC line is needed to handle the power demand. The electrolyser system consists of a step-down transformer and a rectifier connected to the electrolyser stack or stacks. An alternative system setup is to use a DC distribution system. The distribution grid can be connected to one large rectifier that is connected to an incoming HVAC line, as shown in Figure 7.2. Another alternative is that the DC distribution system is connected to a HVDC line via a large DC/DC converter as displayed in Figure 7.3. The electrolyser systems consists of a DC/DC-converter that steps down the voltage and is connected to the electrolyser stack or stacks.

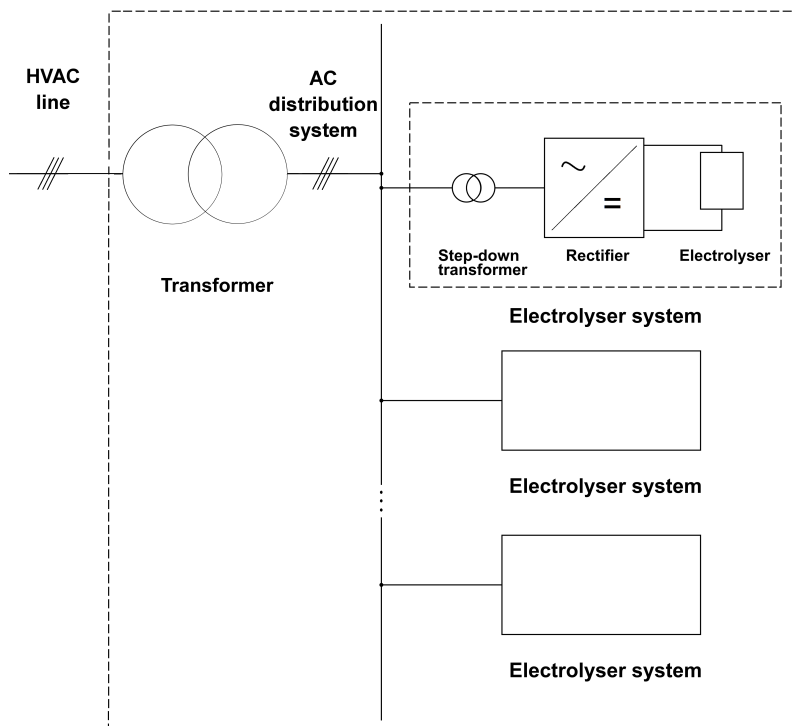


Figure 7.1: Electrolyser station comprised of system modules, connected to a HVAC line via a transformer.

7. PEM electrolyser connected to a converter

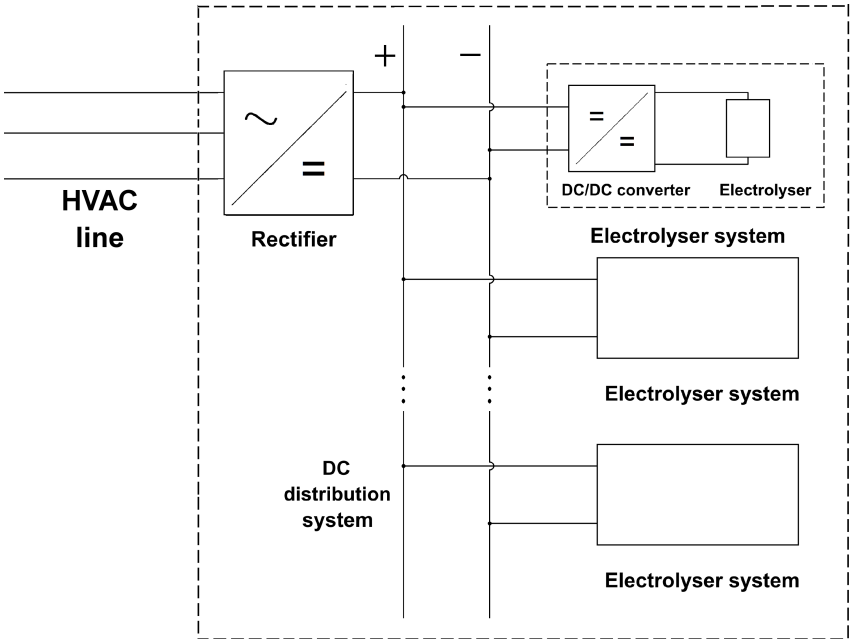


Figure 7.2: Electrolyser station comprised of system modules, connected to a HVAC line via a rectifier.

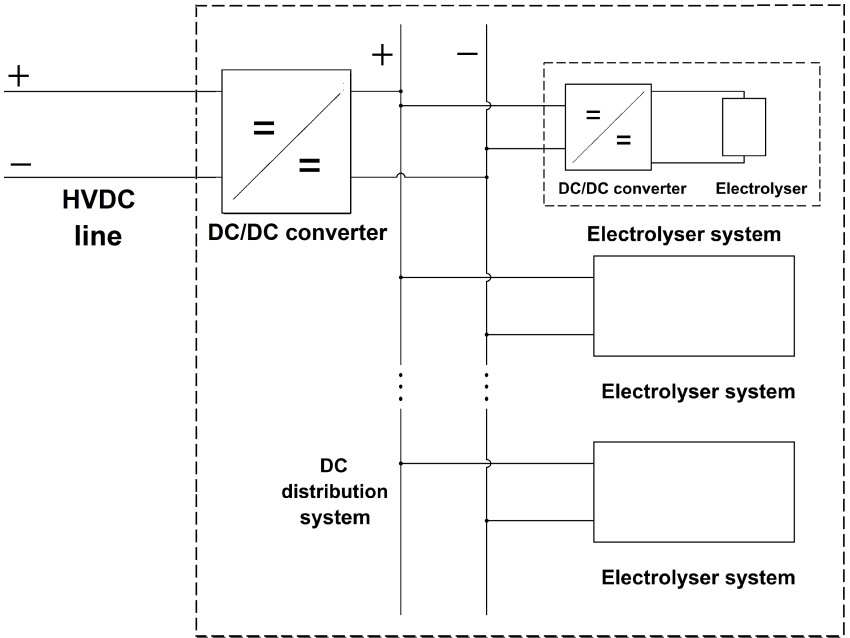


Figure 7.3: Electrolyser station comprised of system modules, connected to a HVDC line via a DC/DC converter.

7.1 Thyristor-based AC/DC converter

An electrolyser requires relatively high current at a low voltage, both which needs to be direct and not alternating. Considering an AC distribution grid, a transformer can be used to step down the voltage from a high to a low voltage, and then a rectifying converter can be used to produce the direct current and voltage.

The thyristor rectifier is a robust solution. Its design allows operation at a given maximum power level as well as for lower levels [62]. A thyristor six-pulse rectifier is the least complex solution in the case of an electrolyser in an industrial operation connected to a three-phase AC distribution grid. A schematic diagram of the six-pulse rectifier with transformer, grid and electrolyser is presented in Figure 7.4.

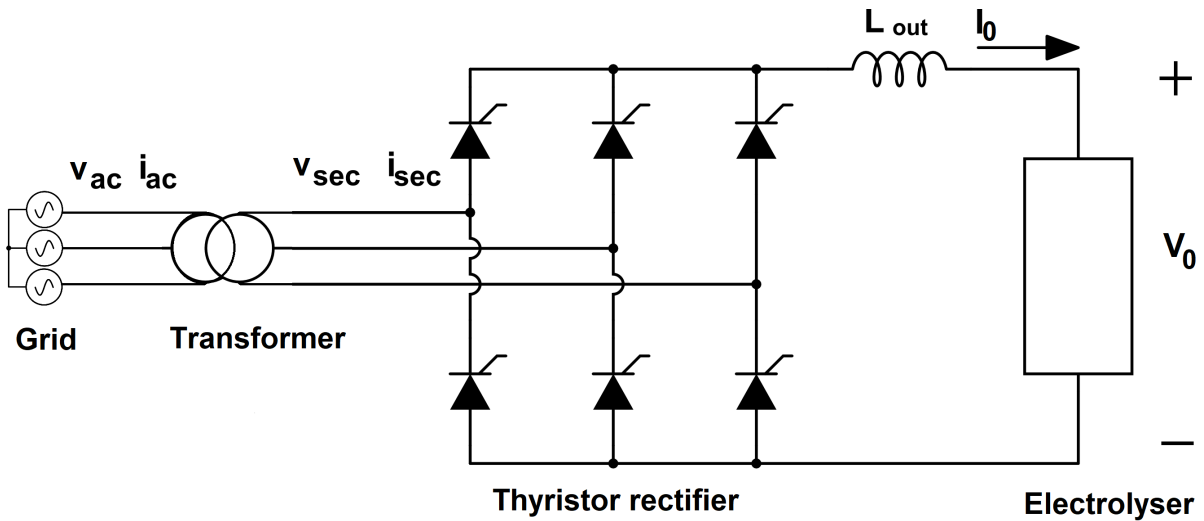


Figure 7.4: Schematic diagram of the six-pulse thyristor rectifier, shown with a voltage step-down transformer and an output filter inductor connected to the electrolyser.

For loads that consume a high current, such as a PEM electrolyser, a six-pulse thyristor connection becomes impractical as the amount of reactive power Q_{AC} and harmonic currents increase by a large proportion [63]. Each nontriplen odd harmonic ($6n \pm 1$ where $n = 1, 2, 3, \dots$) contributes to the total harmonic current by the inverse proportion of their harmonic order.

A useful cancellation technique for low-order harmonics is to pair two six-pulse thyristor rectifiers with a three-winding transformer. This shifts the phase relationship at the converter input between the two parallel-connected rectifiers. The harmonic currents can be “trapped” (kept in circulation) inside the transformer connection of the 12-pulse converter illustrated in Figure 7.5. The 3rd harmonic is already cancelled out for a three-phase six-pulse converter [62]. The 5th harmonic appear inside the currents at $5\omega t$, and with the same harmonic amplitude value on all phases, it can be derived to a negative sequence current in the Yy connection. The 7th harmonic is calculated in a similar way to the 5th harmonic, and turns out to be a positive sequence current in the Yy connection. The same derivation has to be done once for the Yy connection, and once for the Y Δ connection. Lastly, the phasor diagrams of the 5th and 7th harmonic Yy and Y Δ are compared, and since they are opposites they will cancel each other out [62].

This is typically applied in high-power systems considering that the other alternative would be to use tuned LC-filters. With the power levels in a high-power system, the filter size would become large in order to perform harmonic cancellation, and thus very expensive which is undesirable. Choosing if the converter outputs towards the load should be series or parallel-connected depends on which quantity, voltage or current, is intended to be the higher one. For a large electrolyser, current is prioritised and therefore it is connected in parallel to the load [62], [64].

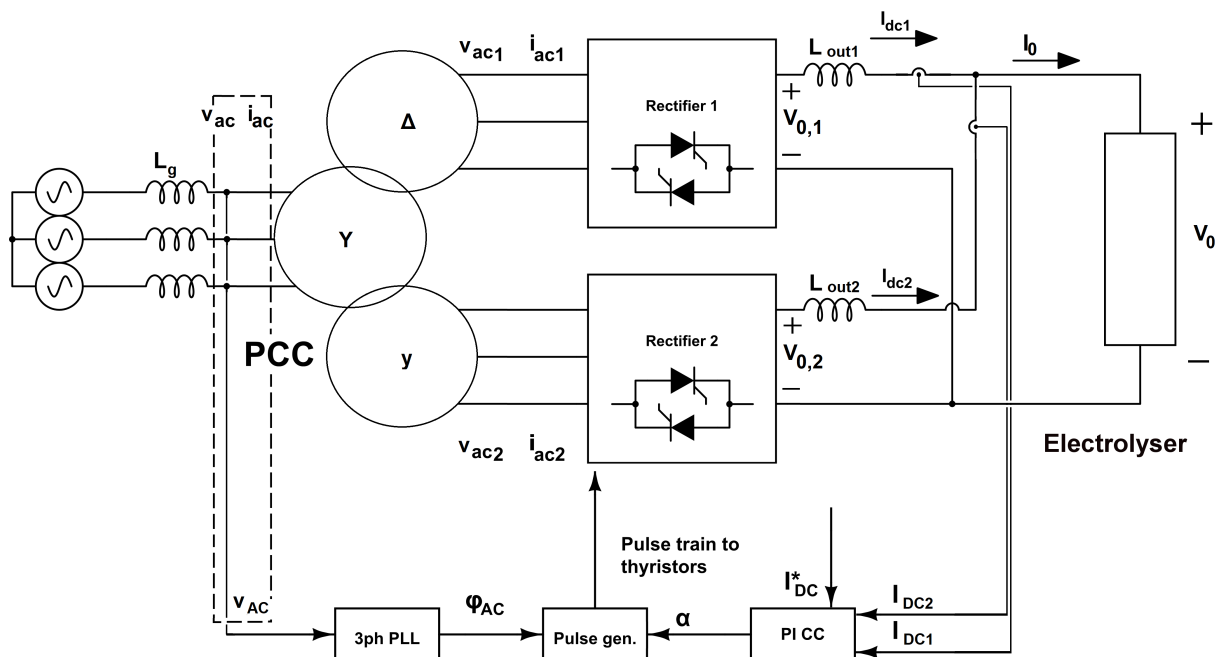


Figure 7.5: Schematic diagram of the 12-pulse thyristor rectifier. The 12-pulse is comprised of a $Y\Delta y$ transformer to step down the voltage level and cancel 5th and 7th order harmonics, two six-pulse rectifiers in parallel output configuration to increase the total current rating and an output filter inductance for each rectifier.

Previously presented in Section 6.2 and shown in (6.9), the amount of hydrogen produced is directly linked to the direct current, which also motivates the use of controllable rectification. The rectifier controller was achieved with the help of a PI (proportional integral) current controller, PLL (phase-locked loop) synchronisation to PCC voltage and pulse generation for the thyristors [65], illustrated in Figure 7.6.

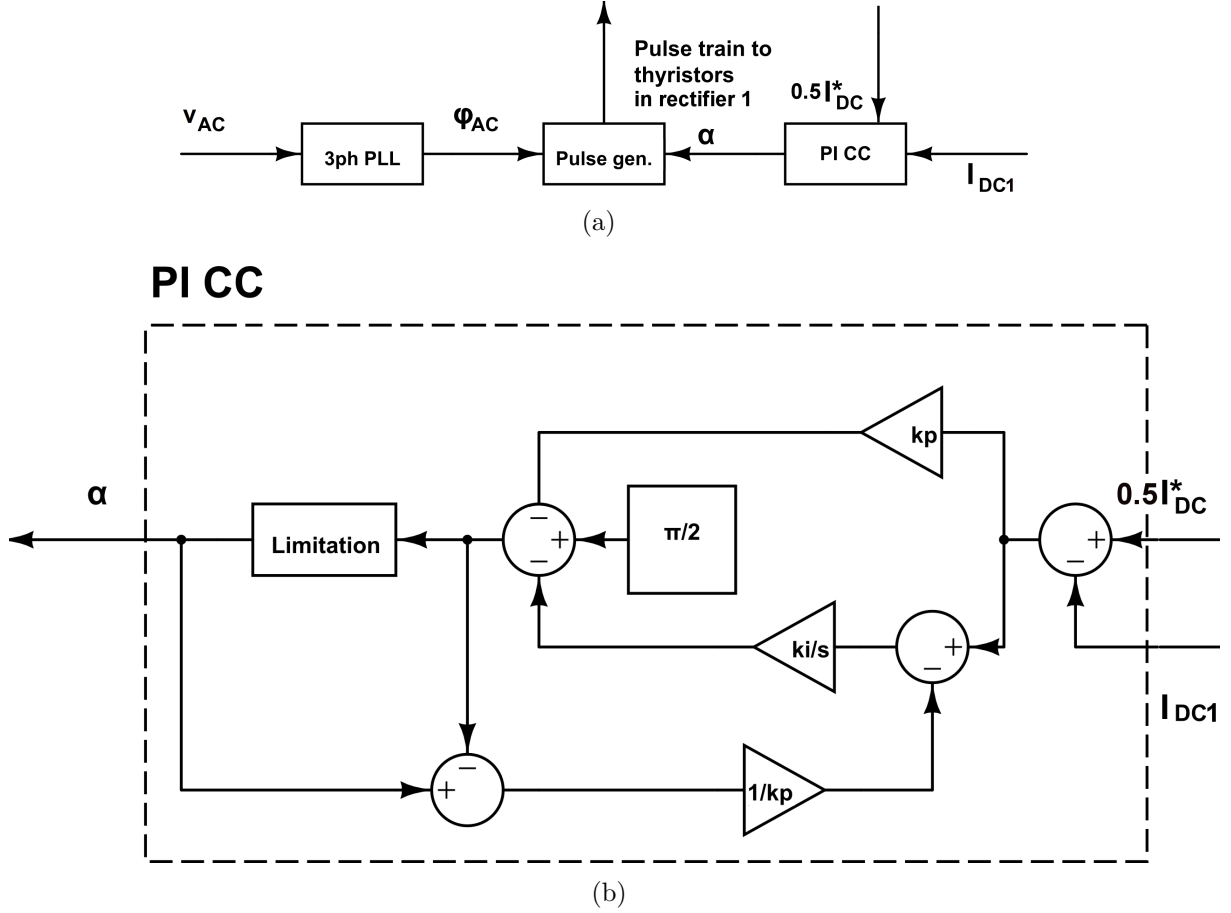


Figure 7.6: a) Block scheme of the pulse generation for rectifier 1 with voltage measurement through a PLL, and b) current control block scheme with anti-windup. The generated controlled firing angle α varies as a response to the input current reference, which in turn decided the commutation delay of each thyristor. Pulse generation is synchronised with the measured voltage phase angle φ_{AC} . A similar control system can be drawn for rectifier 2.

7.1.1 Characteristics of the 12-pulse thyristor rectifier for steady-state electrolyser operation

For the simulations presented in this section, the parameter values are provided in Table 7.1. Figures 7.7 to 7.16 are the voltage and current characteristics in different parts of the rectifier presented in Figure 7.5 during steady-state operation of the electrolyser and converter system. The output current, voltage, power and energy consumption as well as the hydrogen production rate and electrolyser efficiency for different hydrogen production rate demands are also provided in Table 7.2. Steady-state analysis has been performed for two hydrogen production rate demand levels which are 25% and 75% of maximum hydrogen production rate.

For a given fundamental rms current $I_{AC_{f(1)}}$ into the rectifier, at transformer secondaries [63], the expected DC output current amplitude is

$$I_0 = \frac{\pi}{\sqrt{6}} I_{AC_{f(1)}} \quad (7.1)$$

Table 7.1: Parameter values for the 12-pulse thyristor rectifier, which have been kept constant for all simulation cases within Section 7.1.1.

| Parameter description | Parameter value |
|---|---|
| Simulation time | 1 s |
| Initialization time step | 50 ms |
| v_{ac} | $372 \cdot \sin(2\pi ft + \varphi_i + \varphi_0)$ V |
| φ_{ACi} | $0, -\frac{2}{3}\pi$ and $\frac{2}{3}\pi$ for each respective phase |
| f | 50 Hz |
| φ_0 | 0° |
| L_g | None, ideal strong grid |
| n Y: Δ :y | 1: $\sqrt{3}$:1 |
| Transformer winding connections | Y Δ 11 and Yy0 |
| R_{R_p} | 0.05 p.u. |
| R_{R_s} | 0.05 p.u. |
| L_{R_p} | 0.1 p.u. |
| L_{R_s} | 0.1 p.u. |
| Magnetic core saturation in transformer | None, ideal transformer model |
| Iron losses in transformer | Negligible, ideal transformer model |
| PLL peak input voltage | 645 V |
| PLL initial phase angle | 0° |
| PLL k_p | 20π |
| PLL k_i | $(10\pi)^2$ |
| PI CC k_p | 0.005 |
| PI CC k_i | 0.250 |
| L_{out1} | 5 mH |
| L_{out2} | 5 mH |

and for a given input rms phase-voltage V_{AC} the output voltage amplitude V_0 is (same as for the six-pulse rectifier case)

$$V_0 = \left| \frac{3\sqrt{2}}{\pi} \sqrt{3} V_{AC} \cos(\alpha) - \frac{3\omega(L_g + L_T)}{\pi} I_0 \right| \quad (7.2)$$

where L_g is the grid inductance and the term L_T is to account for the transformer equivalent leakage inductance, which can be expressed as

$$L_T = L_{R_p} + L_{R_s} \quad (7.3)$$

where L_{R_p} and L_{R_s} are the primary and secondary leakage inductances of the transformer respectively, which has an apparent power rating of 4 MVA.

Table 7.2: The output current I_0 , output voltage V_0 , output current ripple ΔI_0 , output voltage ripple ΔV_0 , hydrogen production rate v_{H_2} , electrolyser efficiency η^{LHV} , active output power P_0 and energy consumption E_0 for hydrogen production rate reference values of 10%, 25%, 50%, 75% and 100%.

| H ₂ dem. | I_0 | V_0 | ΔI_0 | ΔV_0 | v_{H_2} | η^{LHV} | P_0 | E_0 |
|---------------------|--------|-------|--------------|--------------|------------------|---------------------|---------|-------------|
| 10 % | 375 A | 386 V | 20.6 A | 1.3 V | 3.6 kg/h | 84 % | 145 kW | 40.3 kWh/kg |
| 25 % | 937 A | 411 V | 19.1 A | 0.7 V | 9.2 kg/h | 78 % | 386 kW | 42.0 kWh/kg |
| 50 % | 1875 A | 441 V | 17.0 A | 0.5 V | 18.4 kg/h | 73 % | 827 kW | 44.9 kWh/kg |
| 75 % | 2812 A | 467 V | 14.9 A | 0.4 V | 27.6 kg/h | 69 % | 1314 kW | 47.6 kWh/kg |
| 100 % | 3743 A | 509 V | 11.5 A | 7.2 V | 36.8 kg/h | 63 % | 1905 kW | 51.8 kWh/kg |

Note that for the lower hydrogen production rate demand of 25%, rectifier DC current ripple levels are greater than for the higher demand of 75%. In Figure 7.13 to 7.14, the rectifier DC current ripple is at 40 A for 25% demand and 33 A for 75% demand respectively. The total output current ripple ΔI_0 is lower than the separate rectifier DC current ripples, at 19 A and 15 A for 25% and 75% demand, Figure 7.15. This is due to the overlapping phase shift between rectifier 1 connected to the Δ secondary and rectifier 2 connected to the y secondary: The total current waveform is at minimum for rectifier 1 when it is at maximum for rectifier 2 and vice versa.

7. PEM electrolyser connected to a converter

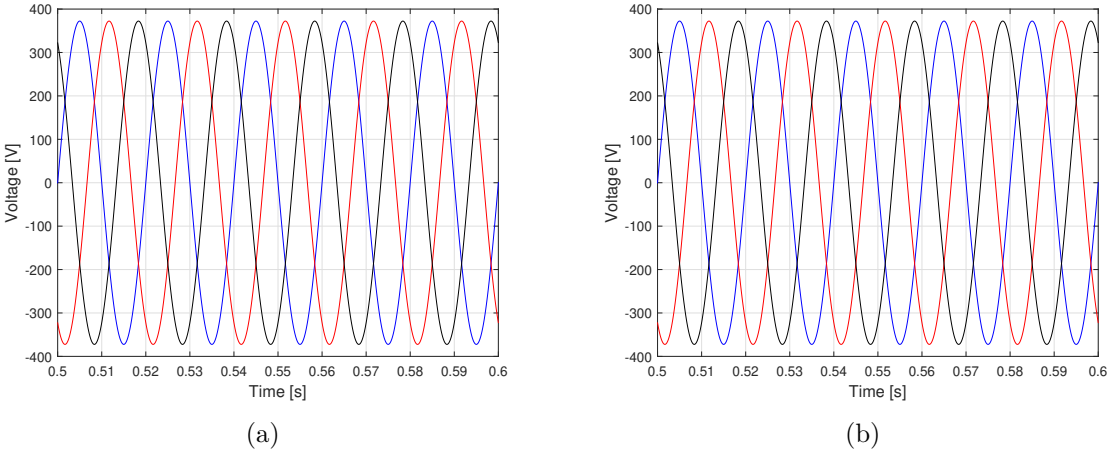


Figure 7.7: Phase voltages at the grid for hydrogen production rate reference of a) 25% and b) 75%.

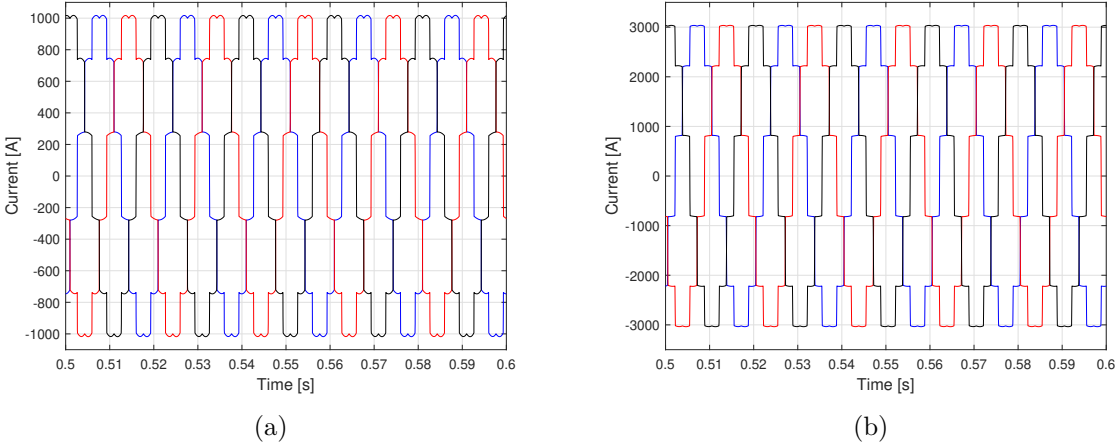


Figure 7.8: Phase currents at the grid for hydrogen production rate reference of a) 25% and b) 75%.

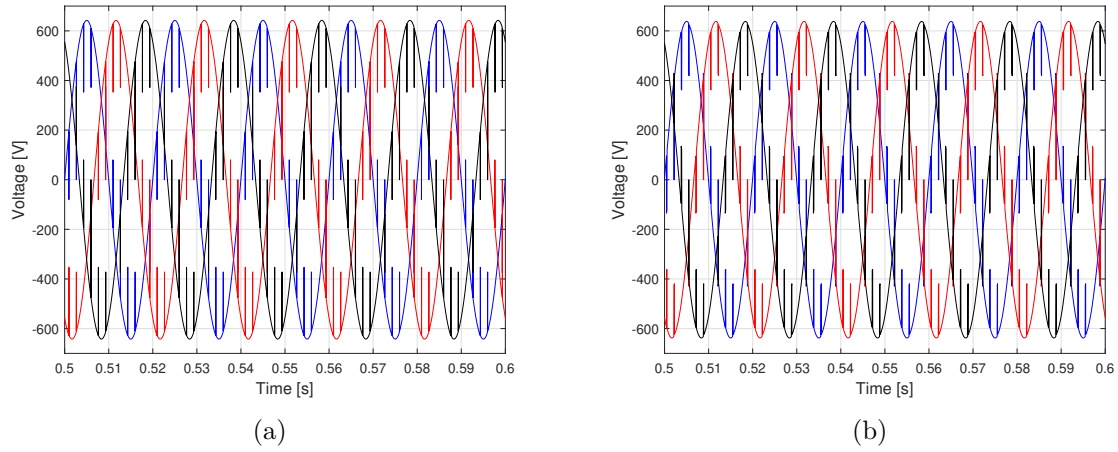


Figure 7.9: Rectifier 1 phase voltages v_{ac1} for hydrogen production rate reference of a) 25% and b) 75%. The irregular spike behaviour is due to the commutation of the current via the Δ -connected transformer leakage inductance L_{R_s} .

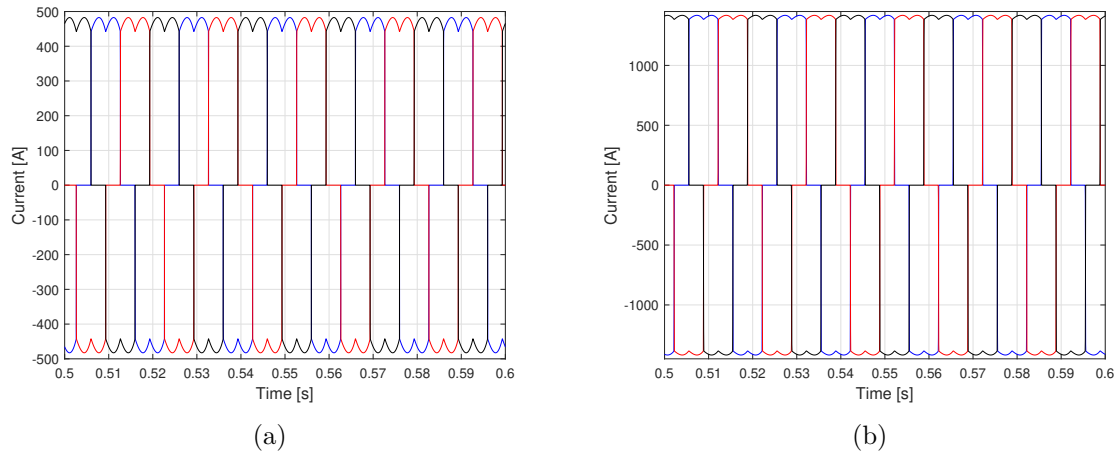


Figure 7.10: Rectifier 1 phase currents i_{ac1} for hydrogen production rate reference of a) 25% and b) 75%.

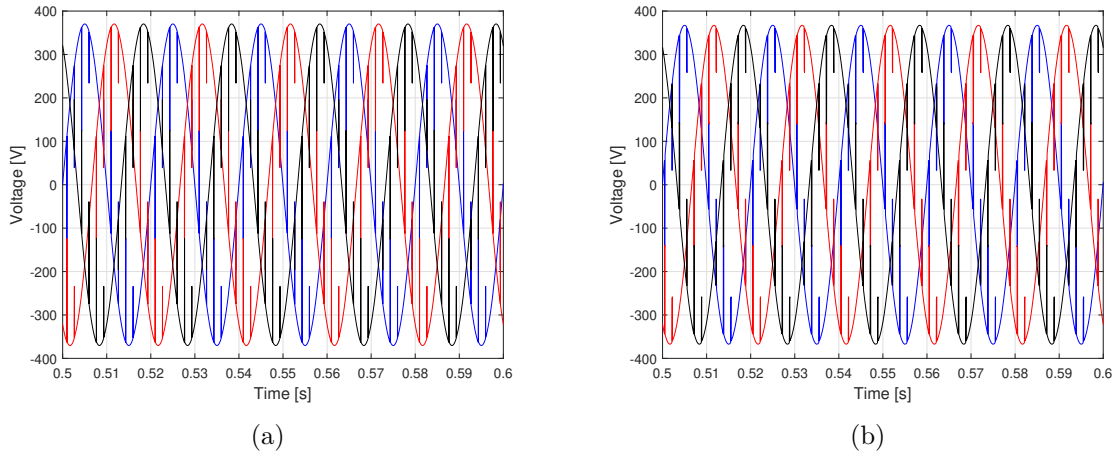


Figure 7.11: Rectifier 2 phase voltages v_{ac2} for hydrogen production rate reference of a) 25% and b) 75%. The irregular spike behaviour is due to the commutation of the current via the y-connected transformer leakage inductance L_{Rs} .

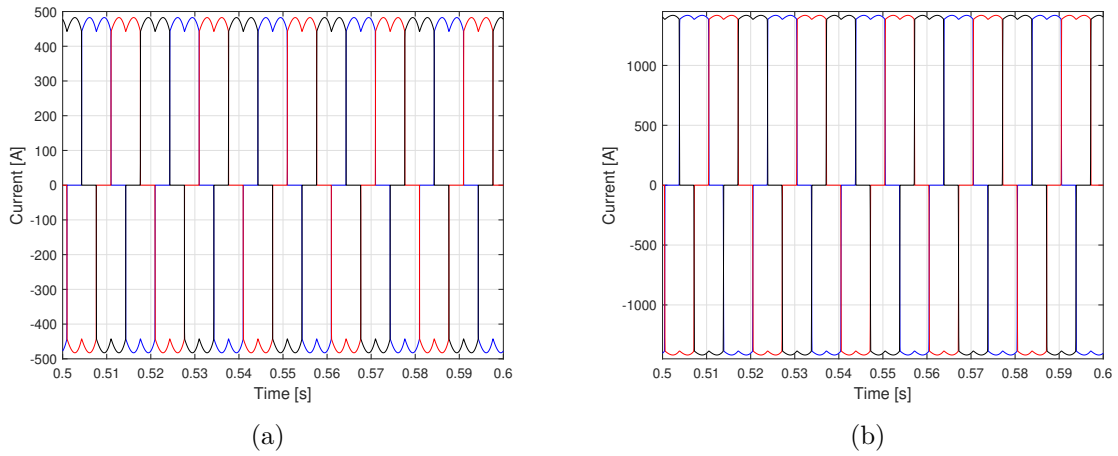


Figure 7.12: Rectifier 2 phase currents i_{ac2} for hydrogen production rate reference of a) 25% and b) 75%.

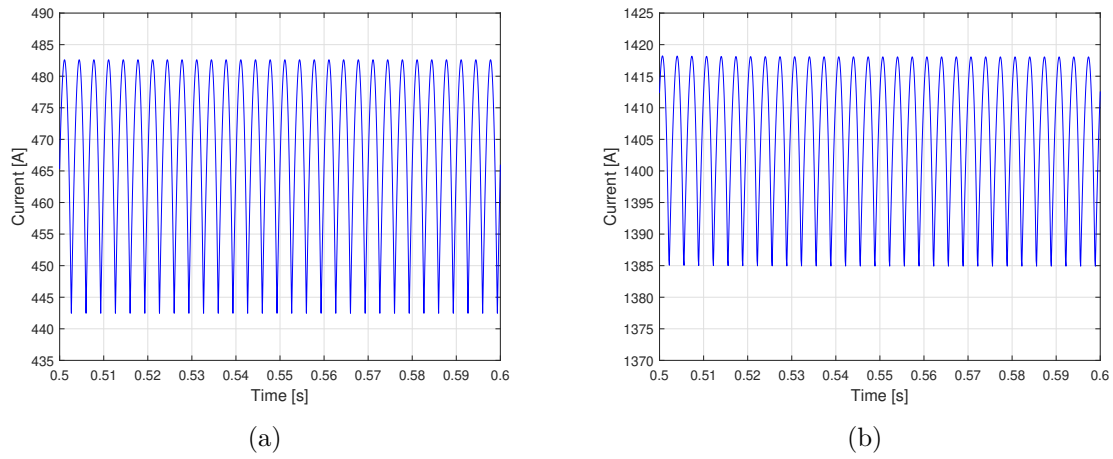


Figure 7.13: Rectifier 1 DC current I_{dc1} for hydrogen production rate reference of a) 25% and b) 75%.

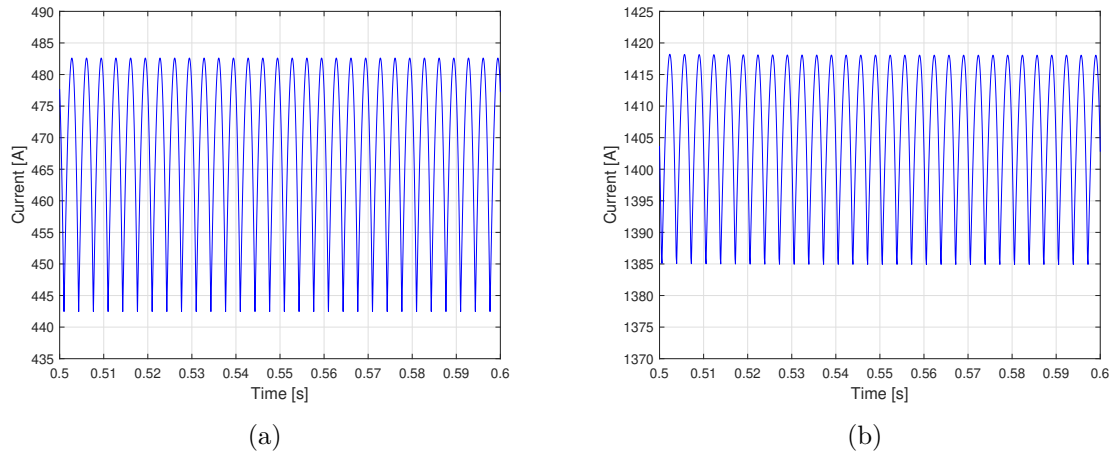


Figure 7.14: Rectifier 2 DC current I_{dc2} for hydrogen production rate reference of a) 25% and b) 75%.

7. PEM electrolyser connected to a converter

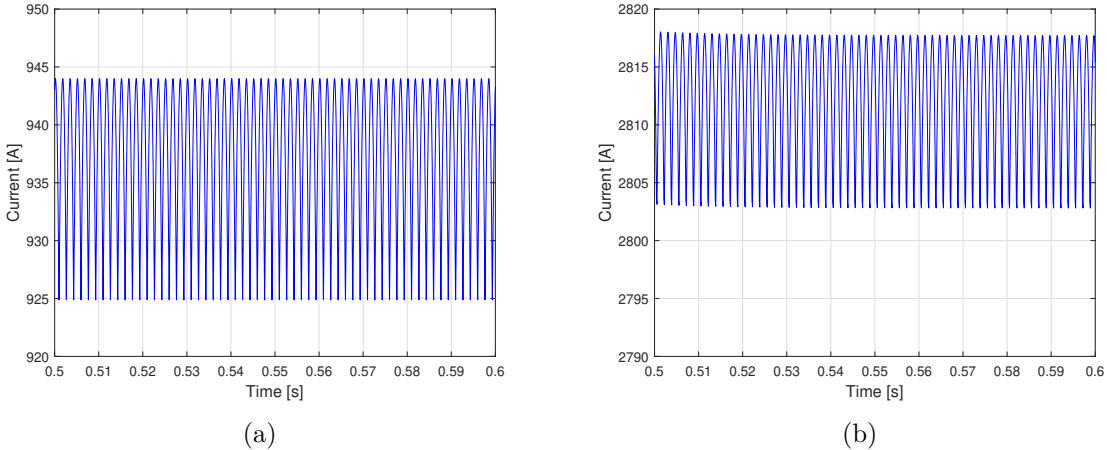


Figure 7.15: Output current I_0 for hydrogen production rate reference of a) 25% and b) 75%.

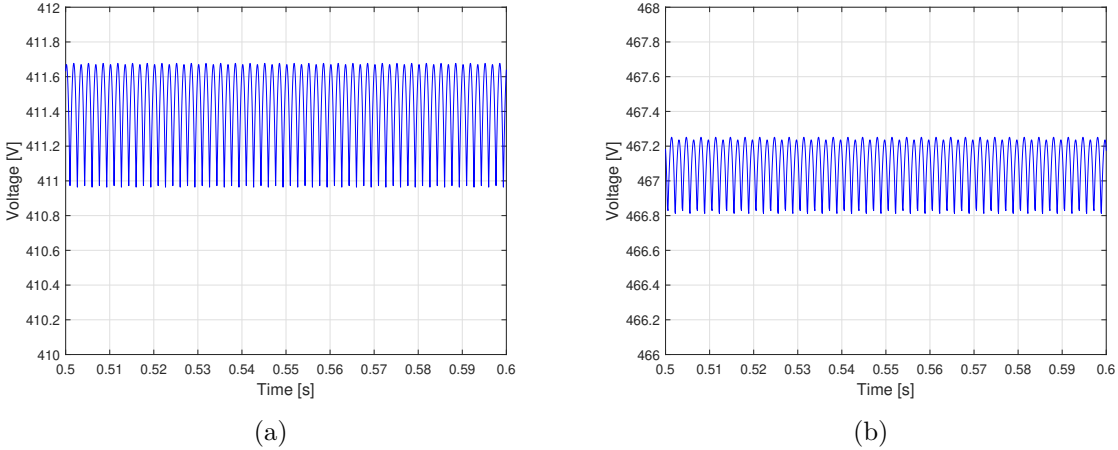


Figure 7.16: Output voltage V_0 for hydrogen production rate reference of a) 25% and b) 75%.

7.1.2 Power requirements and harmonic analysis

For increasing hydrogen production rate, the active power P_{AC} drawn from the PCC increases near-linearly, as seen in Figure 7.17. However, the reactive power Q_{AC} also increases as displayed in Figure 7.17. This effect is not avoidable in this converter type due to the phase difference between voltage component and current component. The current harmonics increase as well, as illustrated in Figure 7.18. Note that these figures were required from the near-ideal data in Table 7.1 with no line impedance, and measured at PCC seen in Figure 7.5.

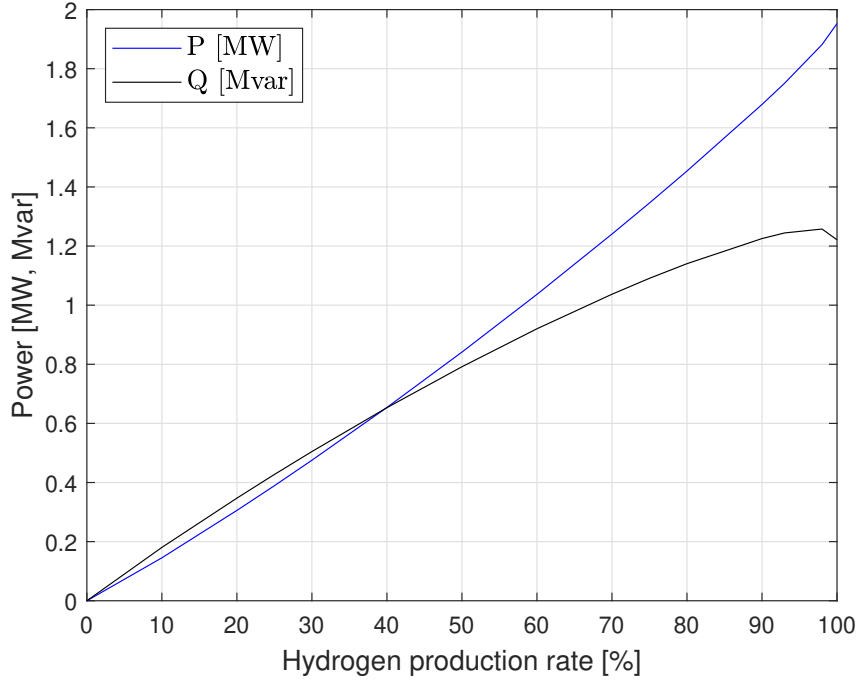


Figure 7.17: The active power P_{AC} and the reactive power Q_{AC} that is required at the PCC as a function of the hydrogen production rate.

The phase currents can each be described with the help of fundamental and harmonic frequencies at the input harmonic grid current rms values $I_{AC_{f(n)}}$, where any of the phase currents at PCC are formulated as

$$\begin{aligned}
 i_{\text{phase}_n}(\omega t) = & \sqrt{2}I_{AC_{f(1)}} \sin(\omega t - \alpha) - \sqrt{2}I_{AC_{f(5)}} \sin(5(\omega t - \alpha)) - \sqrt{2}I_{AC_{f(7)}} \sin(7(\omega t - \alpha)) \\
 & + \sqrt{2}I_{AC_{f(11)}} \sin(11(\omega t - \alpha)) + \sqrt{2}I_{AC_{f(13)}} \sin(13(\omega t - \alpha)) \\
 & - \sqrt{2}I_{AC_{f(17)}} \sin(17(\omega t - \alpha)) - \sqrt{2}I_{AC_{f(19)}} \sin(19(\omega t - \alpha)) \dots
 \end{aligned} \tag{7.4}$$

The required power at PCC will depend on the current, increasing for both P_{AC} and Q_{AC} when the current increases, as displayed in Figure 7.17. However, it is also affected by the grid inductance L_g , with active power P_{AC} and reactive power Q_{AC} decreasing with increasing grid inductance L_g . In the following results, all parameter values provided in Table 7.1 have been kept constant except for grid inductance L_g , which was increased in steps of μH in order to reflect a decreasing short-circuit ratio (SCR), see Table 7.3, to

Table 7.3: Grid inductance values (identical value on all three phases) with corresponding SCR.

| Grid inductance L_g | Corresponding SCR |
|-----------------------|-------------------|
| 0.00 μH | ∞ |
| 1.38 μH | 16 |
| 1.84 μH | 12 |
| 2.76 μH | 8 |
| 5.52 μH | 4 |
| 7.36 μH | 3 |
| 11.03 μH | 2 |
| 22.06 μH | 1 |
| 27.58 μH | 0.8 |
| 29.42 μH | 0.75 |
| 36.77 μH | 0.6 |
| 44.19 μH | 0.5 |

model a weaker grid connection [66]. The grid becomes weaker if the SCR is lower. SCR is derived from the three-phase short-circuit apparent power of the grid S and the rated apparent power of the electrolyser system S_n according to

$$\text{SCR} = \frac{S}{S_n} = \frac{(V_{\text{AC}})^2}{Z_g} \frac{1}{S_n} = \frac{(V_{\text{AC}})^2}{\omega L_g S_n} \quad (7.5)$$

where the grid resistance R_g in the grid impedance $Z_g = \sqrt{R_g^2 + (\omega L_g)^2}$ is equal to zero, and the rated apparent power S_n for the case of the electrolyser is simplified to the rated active power, which is 2 MW.

Current harmonics for 5th, 7th, 11th, 13th, 17th and 19th of fundamental frequency (50 Hz) were measured from the simulated rectifier for varying SCR's, see Table 7.4, where the grid becomes weaker if the SCR is lower. The three-phase line impedances were varied to test different SCR's, and the hydrogen demand was kept constant at 75%. For SCR values below 0.6, the demanded level could not be met. The results of this simulation are displayed in Figure 7.19 and Figure 7.20.

In Table 7.5 and Figure 7.18, the 5th, 7th, 17th and 19th harmonics are cancelled in the 12-pulse thyristor rectifier, as described in Section 7.1. The harmonics which are not cancelled due to this will be the 11th and 13th for low-order harmonics, which also contribute with the largest amplitudes. All non-cancelled orders increase in amplitude for increased hydrogen production demand.

Table 7.4: Fundamental current and current harmonics for different SCR's.

| Grid strength | Fund. amp. 50 Hz | 5 th amp. 250 Hz | 7 th amp. 350 Hz | 11 th amp. 550 Hz | 13 th amp. 650 Hz | 17 th amp. 850 Hz | 19 th amp. 950 Hz |
|---------------|------------------------|-----------------------------------|-----------------------------------|------------------------------------|------------------------------------|------------------------------------|------------------------------------|
| 0.5 SCR | 2949 A | 5 mA | 4 mA | 247 A | 198 A | 2 mA | 1 mA |
| 0.6 SCR | 3100 A | 0 mA | 0 mA | 263 A | 212 A | 0 mA | 0 mA |
| 0.75 SCR | 3100 A | 0 mA | 0 mA | 268 A | 217 A | 0 mA | 0 mA |
| 0.8 SCR | 3101 A | 0 mA | 0 mA | 269 A | 218 A | 0 mA | 0 mA |
| 1 SCR | 3101 A | 0 mA | 0 mA | 272 A | 221 A | 0 mA | 0 mA |
| 2 SCR | 3101 A | 0 mA | 0 mA | 277 A | 226 A | 0 mA | 0 mA |
| 3 SCR | 3101 A | 0 mA | 0 mA | 278 A | 228 A | 0 mA | 0 mA |
| 4 SCR | 3101 A | 0 mA | 0 mA | 278 A | 228 A | 0 mA | 0 mA |
| 8 SCR | 3102 A | 0 mA | 0 mA | 279 A | 229 A | 0 mA | 0 mA |
| 12 SCR | 3102 A | 0 mA | 0 mA | 279 A | 229 A | 0 mA | 0 mA |
| 16 SCR | 3102 A | 0 mA | 0 mA | 280 A | 230 A | 0 mA | 0 mA |

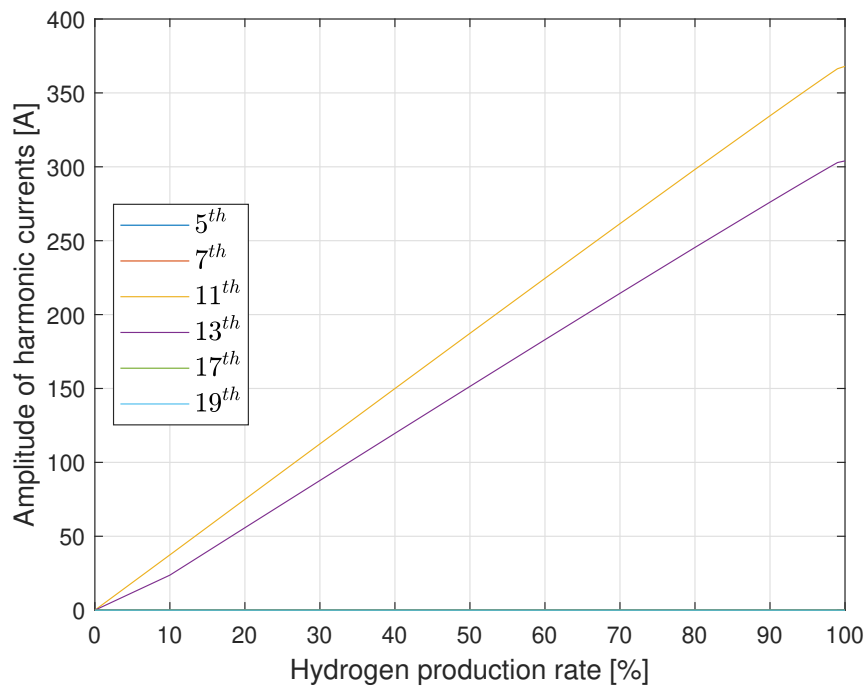
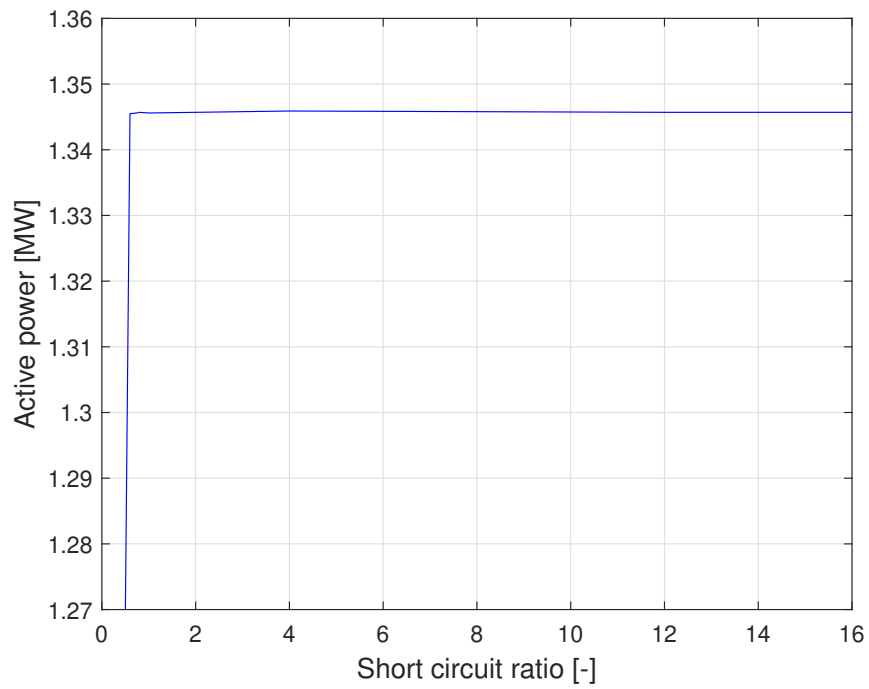


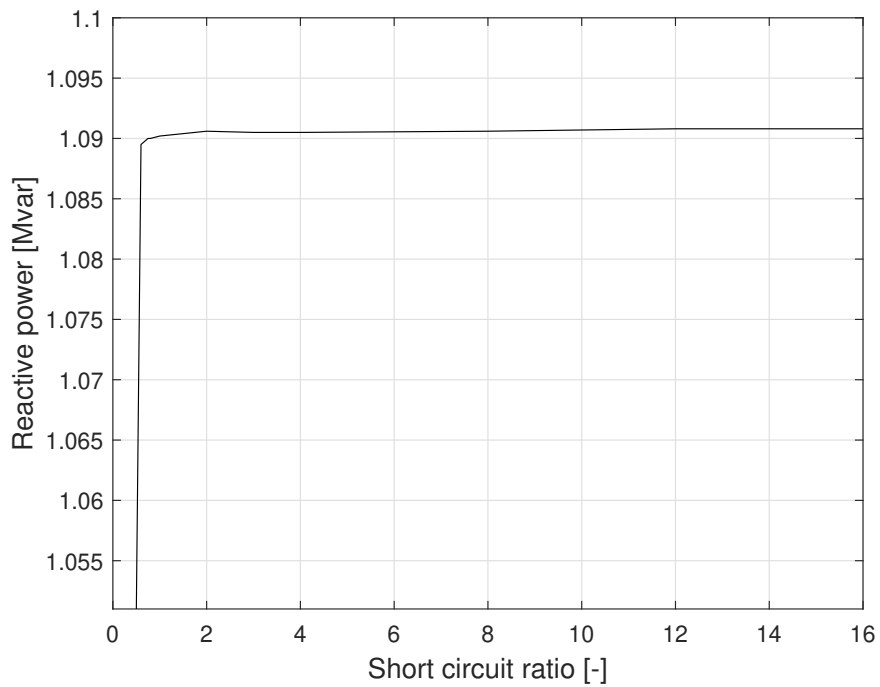
Figure 7.18: The amplitude of the harmonic currents at PCC as a function of hydrogen production rate.

Table 7.5: Fundamental current and current harmonics for 5th, 7th, 11th, 13th, 17th and 19th for hydrogen production rate reference values of 10%, 25%, 50%, 75% and 100%. Simulated for a strong grid (zero line impedance).

| Hydrogen demand | Fundamental amplitude 50 Hz | 5 th amp. 250 Hz | 7 th amp. 350 Hz | 11 th amp. 550 Hz | 13 th amp. 650 Hz | 17 th amp. 850 Hz | 19 th amp. 950 Hz |
|-----------------|--------------------------------|-----------------------------------|-----------------------------------|------------------------------------|------------------------------------|------------------------------------|------------------------------------|
| 10% | 415 A | 0 A | 0 A | 37 A | 24 A | 0 A | 0 A |
| 25% | 1035 A | 0 A | 0 A | 94 A | 72 A | 0 A | 0 A |
| 50% | 2068 A | 0 A | 0 A | 187 A | 151 A | 0 A | 0 A |
| 75% | 3102 A | 0 A | 0 A | 280 A | 230 A | 0 A | 0 A |
| 100% | 4127 A | 0 A | 0 A | 369 A | 305 A | 0 A | 0 A |



(a)



(b)

Figure 7.19: Power at PCC as a function of varying grid strength in a) for active power P_{AC} and in b) for reactive power Q_{AC} with a hydrogen production demand of 75%.

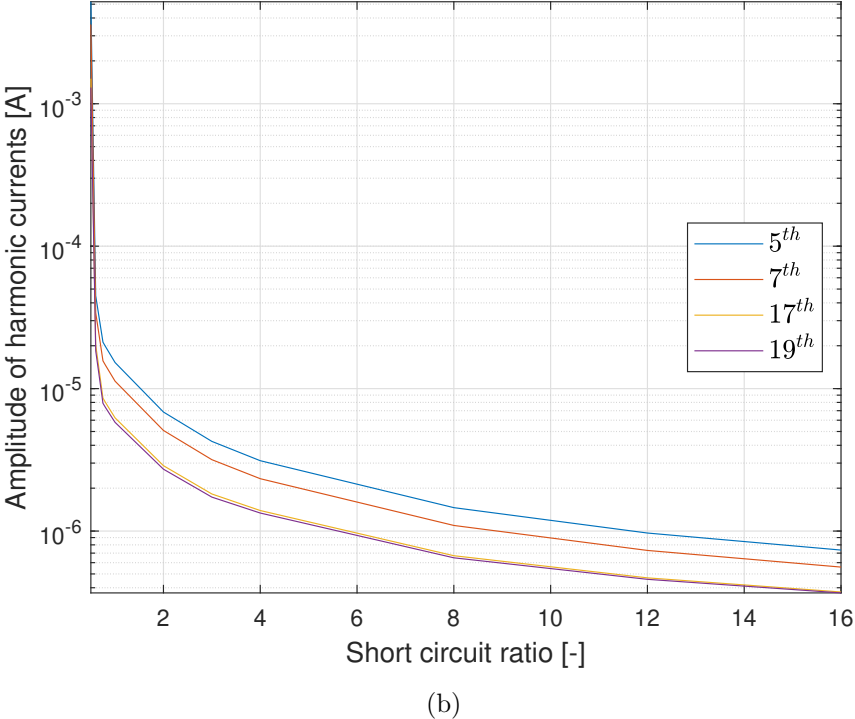
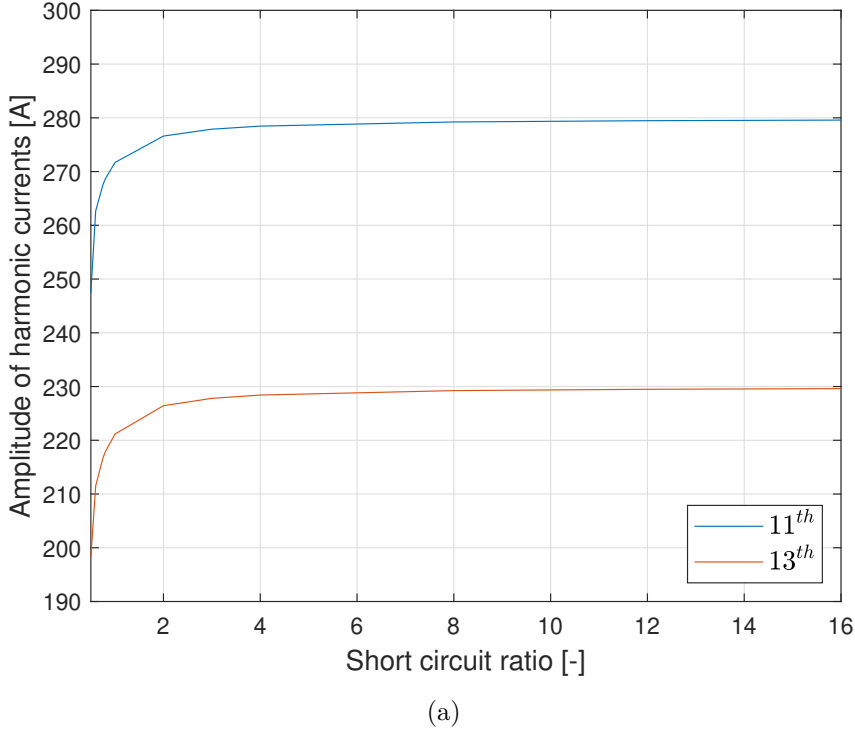


Figure 7.20: Harmonic current amplitudes $\hat{I}_{ACf(n)}$ at PCC for different SCR with a hydrogen production demand of 75%.

7.1.3 Dynamic control response of the 12-pulse rectifier

The 12-pulse thyristor rectifier can be controlled satisfactorily when given a hydrogen production rate reference value, as seen by the simulation displayed in Figure 7.21 to 7.23. The demand is ramped up from 10 to 100 %, and then again to 50% at times 0.2-1.1 s and 1.3-1.8 s respectively. The output current I_0 follows the reference current and thereby the hydrogen production rate reference is followed by the hydrogen production rate.

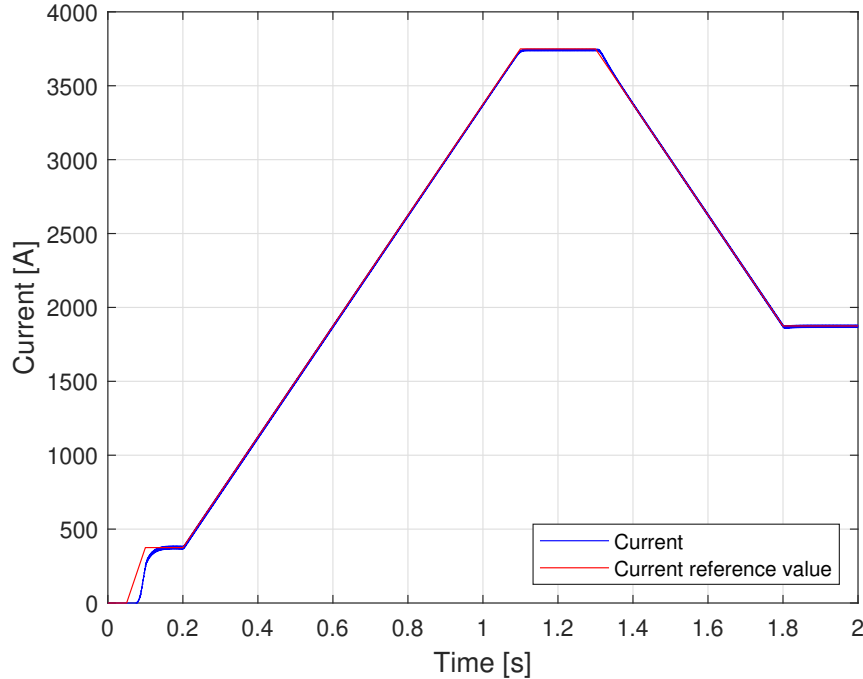


Figure 7.21: Dynamic simulation of the output current I_0 and the output current reference $I_{0,\text{ref}}$ for hydrogen production rate reference of 10%, 50% and 100%.

A phenomenon which is visible at 1.1 s in Figure 7.22 is that the voltage ripple becomes higher. This is because the electrolyser operates in the concentration region which means that V_0 , and therefore the total voltage ripple, increases exponentially. Moreover, the effect of adding a DC reactor ($L_{\text{out}1}$ and $L_{\text{out}2}$) at each output of the thyristor rectifiers is visible in the ripple level of the 12-pulse rectifier output voltage V_0 , which is almost removed entirely, in comparison to the converter output voltage $V_{0,1}$ and $V_{0,2}$. The voltage comparison is shown in Figure 7.24.

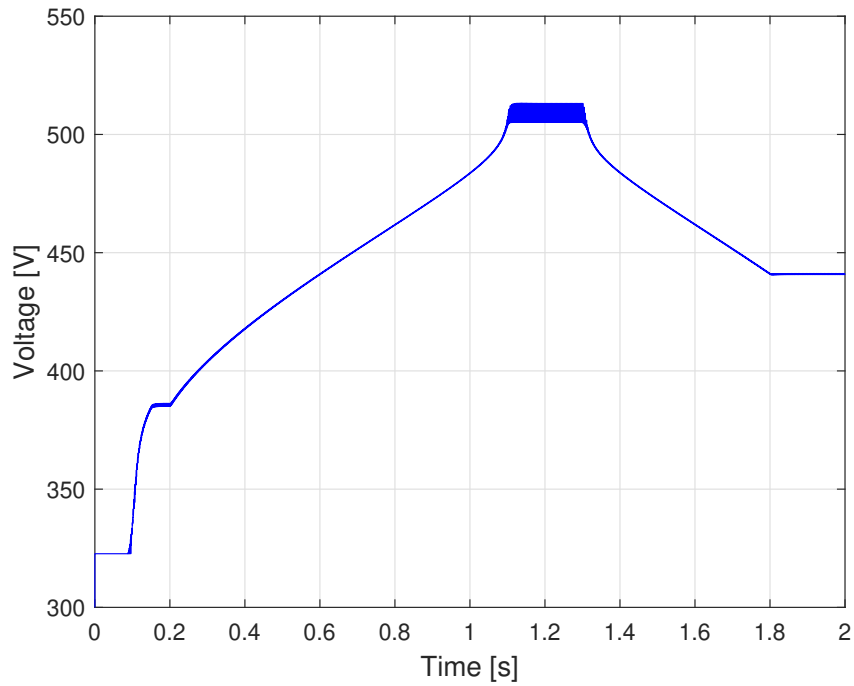


Figure 7.22: Dynamic simulation of the output voltage V_0 and the output voltage reference $V_{0,\text{ref}}$ for hydrogen production rate reference of 10%, 50% and 100%.

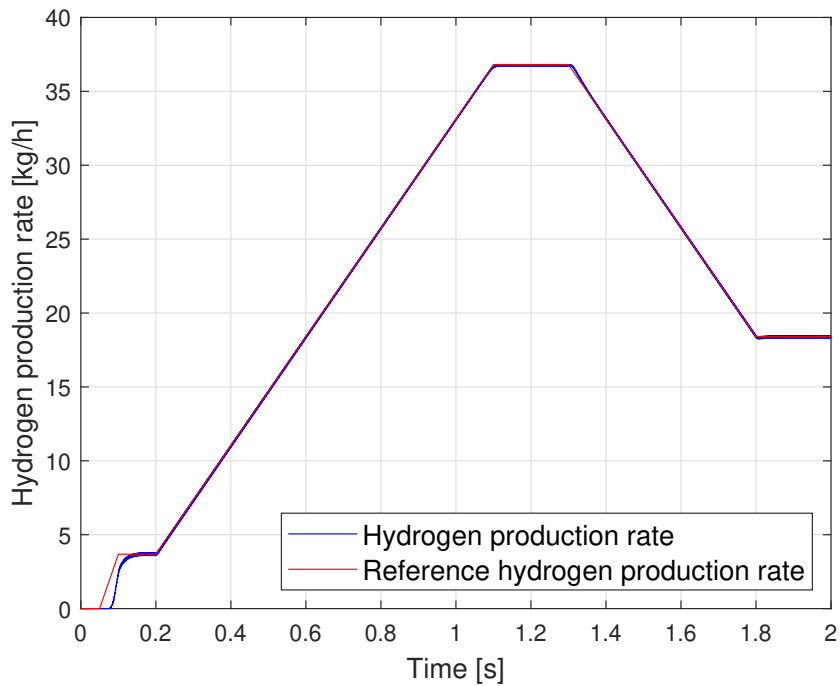
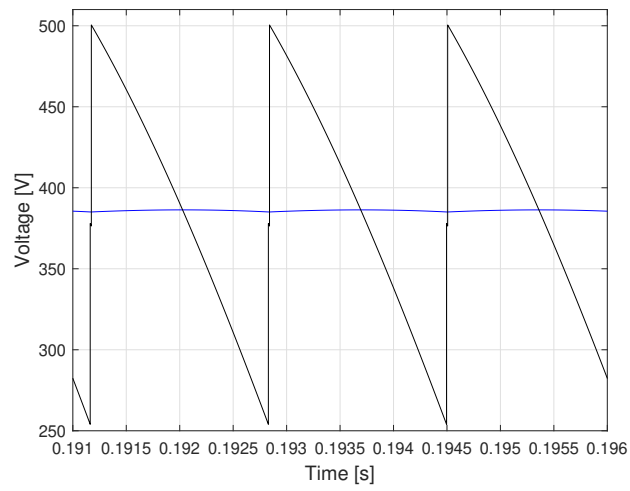
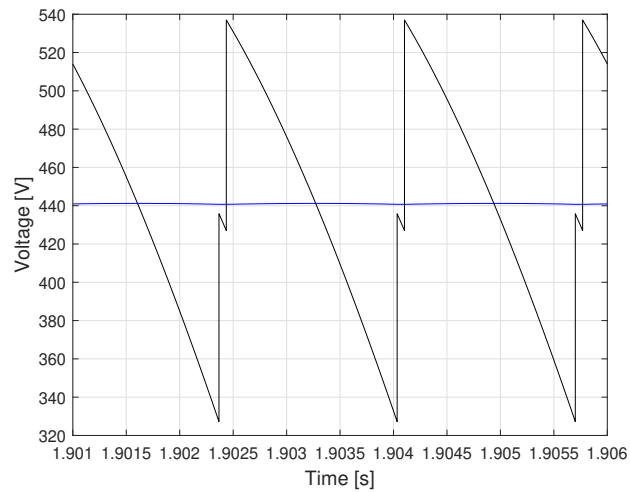


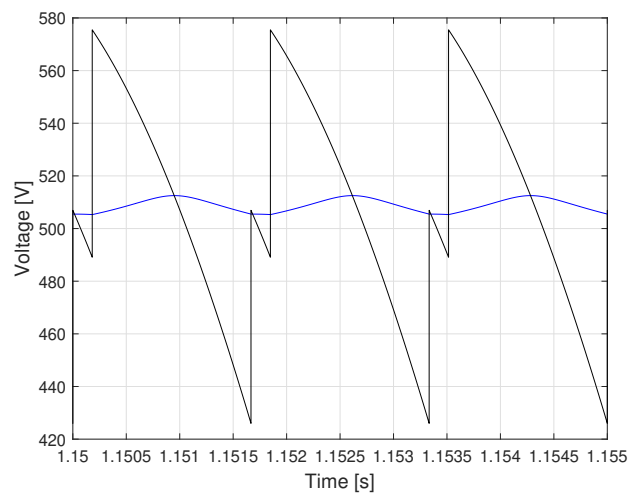
Figure 7.23: Dynamic simulation of the hydrogen production rate v_{H_2} and the hydrogen production rate reference $v_{\text{H}_2,\text{ref}}$ for hydrogen production rate reference of 10%, 50% and 100%.



(a)



(b)



(c)

Figure 7.24: Output voltage V_0 in blue, and the converter voltage $V_{0,1}$ and $V_{0,2}$ in black for hydrogen production rate reference of a) 10%, b) 50% and c) 100%.

7.2 DC/DC converter

As mentioned, electrolysers require a high DC current and a low voltage. If high-power electrolyser units are connected to a high-voltage DC grid, then a high-voltage conversion ratio as well as low output current ripple is required for the converter topology. Furthermore, other desired requirements in a DC/DC converter are high efficiency, low electromagnetic interference (EMI), high-power density, high reliability and low cost. Therefore, the main requirements for a DC-DC converter in electrolyser applications can be listed as [67]:

1. High efficiency;
2. High voltage conversion ratio;
3. Low output current ripple;
4. Low EMI;
5. High power density;
6. Utilised for high-power applications;
7. High reliability;
8. Low cost.

After evaluating different DC/DC converters such as different buck converter topologies, half-bridge DC/DC converter and full-bridge DC/DC converter, the phase-shifted full-bridge (PSFB) DC/DC converter appeared to be one of the most well suited DC/DC converter topologies for high power electrolyser applications. PSFB DC/DC converters are mostly utilised in high power applications and fulfill the requirements 1-7 [68]. The main disadvantage is that they are expensive which is why requirement 8 is not fulfilled.

7.2.1 DC/DC converter topology

The DC/DC converter system which interconnects the electrolyser to the DC-bus is modelled as illustrated in Figure 7.25, where the electrolyser has the same parameter values as the 2 MW PEM electrolyser presented in Table 6.1. As can be seen, the converter system consists of five PSFB DC/DC converter modules which are series-connected on the high-voltage side and parallel-connected on the low-voltage side. This converter system design allows lower voltages to be applied over the transistors while also producing a high output current to the electrolyser with a low output voltage. A high voltage conversion ratio is also enabled with this topology design. The output current I_0 flows through the electrolyser which will give an output voltage V_0 . The schematics of one PSFB DC/DC converter module is shown in Figure 7.26.

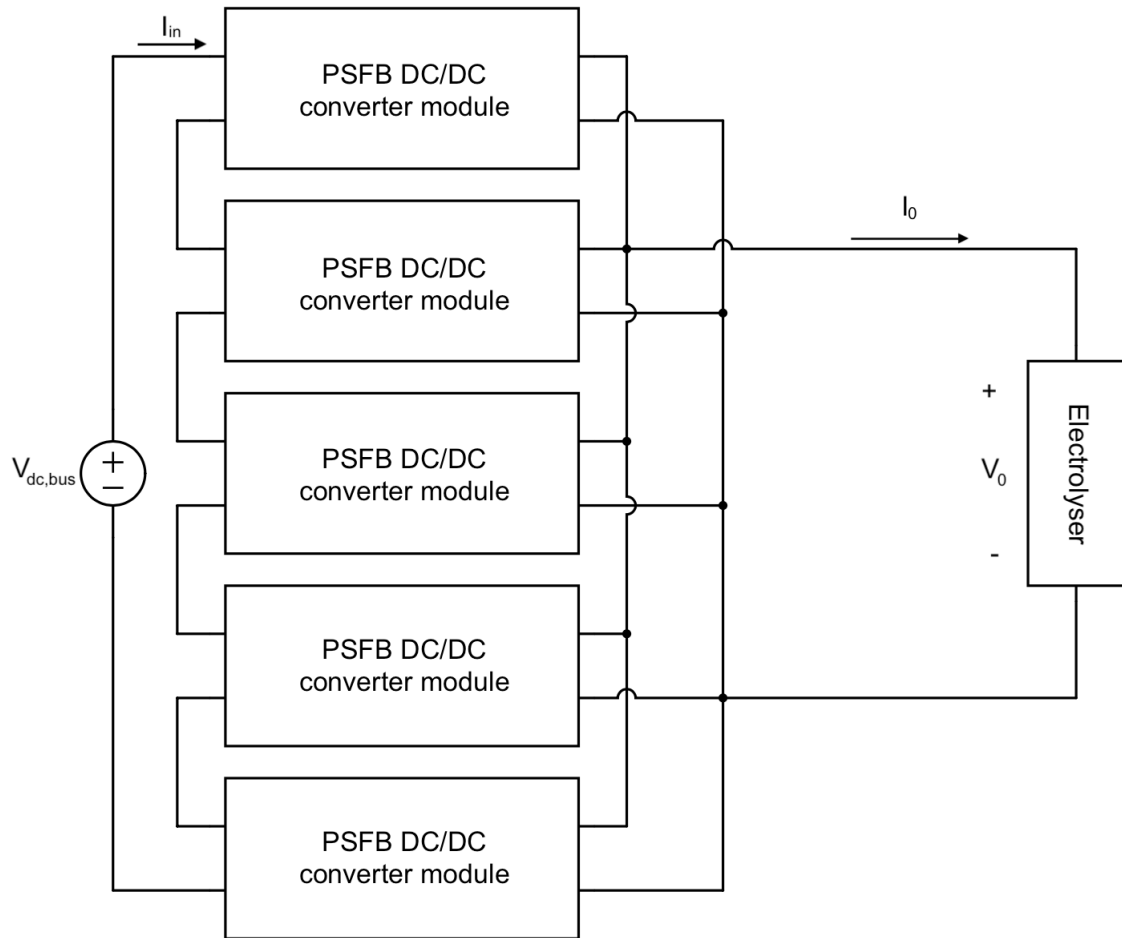


Figure 7.25: Schematic diagram of the PSFB DC/DC converter topology interconnecting the distribution DC-bus and the electrolyser system. The schematics of the PSFB DC/DC converter module can be seen in Figure 7.26.

7.2.2 Phase-shifted full-bridge DC/DC converter module topology

The schematic diagram of the PSFB DC/DC converter module is illustrated in Figure 7.26 and a detailed view of the medium frequency transformer model is illustrated in Figure 7.27. Transistors Q_1 and Q_2 are phase-shifted 180° towards one another and belong to the left phase-leg while transistors Q_3 and Q_4 belong to the right phase-leg, which are phase-shifted 180° towards each other as well. The phase-legs are then phase-shifted with an angle between 0° to 180° which determines the duty cycle, where 0° equals 0% duty cycle while 180° equals 100% duty cycle.

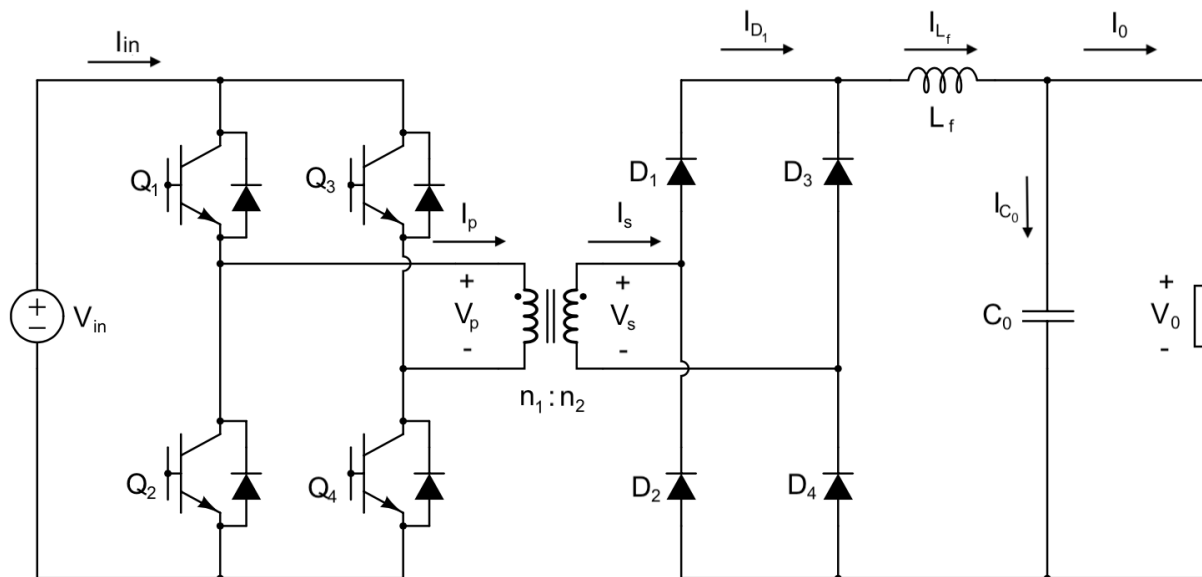


Figure 7.26: Schematic diagram of the PSFB DC/DC converter module.

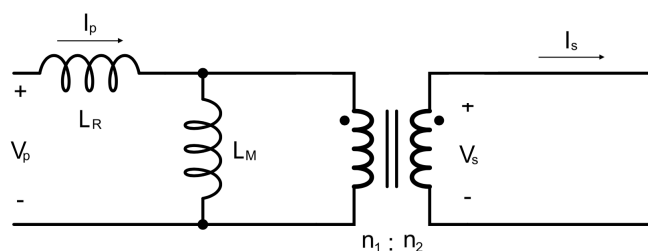


Figure 7.27: Detailed view of the medium frequency transformer model in Figure 7.26.

The duty cycle of a PSFB DC/DC converter can be calculated as

$$D = \frac{n \cdot V_0}{V_{in}} \quad (7.6)$$

where D , n , V_0 and V_{in} are the duty cycle, the turn ratio of the isolated transformer, the output voltage and the input voltage respectively. The PSFB DC/DC converter also

contains filter components which are the filter inductance L_f as well as a filter capacitance C_0 , which can be calculated as

$$L_f \geq \frac{V_{0,\max} \cdot (1 - D_{\max})}{2 \cdot \Delta I_0 \cdot f_{\text{sw}}} \quad (7.7)$$

$$C_0 \geq \frac{\Delta I_0}{16 \cdot \Delta V_0 \cdot f_{\text{sw}}} \quad (7.8)$$

where ΔI_0 and ΔV_0 are the output current ripple and output voltage ripple respectively, while f_{sw} is the switching frequency. The stored leakage inductance energy E_R must be higher than the charging- and discharging energy of the output transistor capacitors C_{oss} in order to attain zero voltage switching (ZVS), and this can be expressed as

$$E_R = \frac{1}{2} L_R \cdot I_2^2 > \left(\frac{4}{3} C_{\text{oss}} + \frac{1}{2} C_T \right) V_{\text{in}}^2 \quad (7.9)$$

where L_R and C_T are the leakage inductance and winding capacitance of the transformer respectively while I_2 is the primary current I_p that flows through the transistors. The minimum size of the leakage inductance L_R can be calculated by applying the transistor current I_2 for half of the maximum load. Finally, the transformer magnetization inductance L_M can be expressed as [68]

$$L_M \geq \frac{n \cdot D_{\max} \cdot V_{\text{in}}}{2 \cdot \Delta I_0 \cdot f_{\text{sw}}} \quad (7.10)$$

7.2.3 Characteristics of the PSFB DC/DC converter for steady-state electrolyser operation

The values of the PSFB DC/DC converter components in Figure 7.26 are presented in Table 7.6 and are calculated as shown in Section 7.2.2. As can be seen, for the maximum and minimum output voltages $V_{0,\max}$ and $V_{0,\min}$, with the transformer turn ratio n and the input voltage V_{in} into consideration, the maximum and minimum duty cycles D_{\max} and D_{\min} can be calculated with (7.6). This will result in D_{\max} and D_{\min} equal to 50% and 31% respectively.

The control system used to control the output current I_0 from the PSFB DC/DC converter in Figure 7.25 to the electrolyser is illustrated in Figure 7.28. As can be seen, a PI-controller was not used as a control system, and is not needed since there is full knowledge of the electrolyser model. First, the reference value of the hydrogen production rate $v_{\text{H}_2,\text{ref}}$ is used as input, along with the temperature T and the pressure p , in the "Reference current calculation" block. Using (6.9), the output current reference $I_{0,\text{ref}}$ is calculated, which is used as input in the "Electrolyser model" block together with the temperature T and the pressure p to calculate the output voltage reference $V_{0,\text{ref}}$. Finally, in the "Reference IGBT signal phase-shift calculation" block, the output voltage reference $V_{0,\text{ref}}$ is divided with the maximum output voltage $V_{0,\max}$ to calculate the quotient of the maximum phase-shift angle, or duty cycle, that results in $V_{0,\max}$. Thereafter, the calculated phase-shift angle will then be used to phase-shift the right phase-leg in Figure 7.26, and then the signals will be sent to the IGBTs Q_1 - Q_4 in Figure 7.26 respectively.

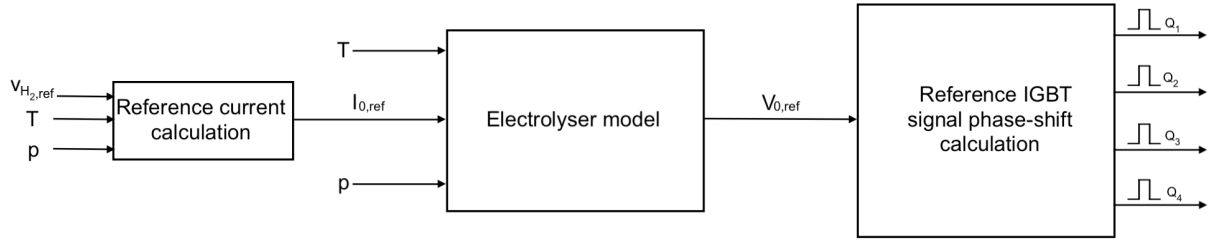


Figure 7.28: Schematic diagram of the control system used for the PSFB DC/DC converter.

Table 7.6: PSFB DC/DC converter parameter values.

| Parameter description | Parameter value |
|-----------------------|-----------------------------------|
| L_f | 3.56 mH |
| C_0 | 28.13 μ F |
| L_R | 0.98 μ H |
| L_M | 30.25 mH |
| C_{oss} | 2.50 nH |
| C_T | 0.00 F |
| f_{sw} | 5.00 kHz |
| $I_{0,max}$ | 3750 A |
| $V_{0,max}$ | 533 V |
| $V_{0,min}$ | 331 V |
| V_{in} | 2.20 kV |
| $V_{dc,bus}$ | 11.00 kV |
| ΔI_0 | $0.01 \cdot I_{0,max}$ |
| ΔV_0 | $\frac{0.10}{16} \cdot V_{0,max}$ |
| $n = n_1 : n_2$ | 33:16 |

For the following simulation results, the hydrogen production rate reference of 25% and 75% were used. The system was connected as illustrated in Figure 7.25. As seen in Table 7.7, different variable values for a hydrogen production rate reference of 25% and 75% are presented for one PSFB DC/DC converter module, as illustrated in Figure 7.26, while different variable values for the PSFB DC/DC converter in Figure 7.25 and the electrolyser are presented in Table 7.8. Firstly, since the maximum hydrogen production rate $v_{H_2,max}$ is equal to 37.8 kg/h, it can be noticed that the hydrogen production rate v_{H_2} for 25% and 75% hydrogen production rate reference is close to the expected theoretical value respectively. Secondly, the output current ripple ΔI_0 is 4.1% and 1.5% of the output current I_0 for 25% and 75% hydrogen production rate reference respectively, which is considered to be very low output current ripples. However, it can also be seen that the output current ripple ΔI_0 is higher than the filter inductor current ripple ΔI_{L_f} of all five PSFB DC/DC converter modules added together, which is a result of the electrolyser model behaviour when there is a high switching current ripple flowing through it. The output voltage ripple ΔV_0 is also considered very low, where it is 0.3% and 0.2% of the output voltage V_0 for 25% and 75% hydrogen production rate reference respectively. Moreover, as can be seen in Table 7.8, the input current I_{in} is relatively low compared to the output current I_0 , which is due to the topology where five modules were series-connected on the high-voltage side and parallel-connected on the low-voltage side to produce a high output current, as illustrated in Figure 7.25. Compared to the bus voltage $V_{dc,bus}$, the output voltage V_0 is

also relatively low, which is due to the high voltage conversion ratio of the PSFB DC/DC converter topology. Finally, the energy consumption E_0 also seems reasonable when compared to the electrolyser products of the different electrolyser manufacturers presented in Table 4.2, Table 4.4 and Table 4.6 in Section 4.2. The electrolyser efficiency η^{LHV} can also be seen to decrease for an increase in the hydrogen production rate reference, which is expected according to the illustration seen in Figure 6.4 where η^{LHV} decreases for an increase in the current density J .

Table 7.7: The filter inductor current I_{L_f} , the output voltage V_0 , the filter inductor current ripple ΔI_{L_f} and the output voltage ripple ΔV_0 of one PSFB DC/DC converter module for hydrogen production rate reference value of 25% and 75%.

| Variable | H ₂ demand 25% | H ₂ demand 75% |
|------------------|---------------------------|---------------------------|
| I_{L_f} | 188 A | 547 A |
| V_0 | 423 V | 477 V |
| ΔI_{L_f} | 7.2 A | 7.4 A |
| ΔV_0 | 1.4 V | 1.1 V |

Table 7.8: The output current I_0 , the output current ripple ΔI_0 , the input current I_{in} , the hydrogen production rate v_{H_2} , the electrolyser efficiency η^{LHV} , the output power P_0 and the energy consumption E_0 of the PSFB DC/DC converter and the electrolyser for hydrogen production rate reference value of 25% and 75%.

| Variable | H ₂ demand 25% | H ₂ demand 75% |
|---------------------|---------------------------|---------------------------|
| I_0 | 940 A | 2736 A |
| ΔI_0 | 38 A | 40 A |
| I_{in} | 38 A | 120 A |
| v_{H_2} | 9.5 kg/h | 27.6 kg/h |
| η^{LHV} | 78% | 69% |
| P_0 | 397 kW | 1306 kW |
| E_0 | 41.9 kWh/kg | 47.4 kWh/kg |

The filter inductor current I_{L_f} is presented in Figure 7.29, and as seen there is a ripple ΔI_{L_f} . The output current I_0 also has a ripple ΔI_0 and is presented in Figure 7.30. The primary and secondary transformer currents I_p and I_s are presented in Figure 7.31 and Figure 7.32 respectively. Furthermore, the diode current I_{D_1} and the capacitor current I_{C_0} are presented in Figure 7.33 and Figure 7.34 respectively. Finally, the output voltage V_0 as well the primary and secondary transformer voltages V_p and V_s are presented in Figure 7.35, Figure 7.36 and Figure 7.37. The waveforms of the PSFB DC/DC converter module are behaving as expected for a PSFB DC/DC converter.

The PSFB DC/DC converter seems to be a well-suited converter for electrolyser applications as it fulfills seven of the eight suggested requirements for DC/DC converters in electrolyser applications. It can also be observed on the results of the PSFB DC/DC converter that the output current ripple ΔI_0 and output voltage ripple ΔV_0 are very low. This is preferable since current ripples with high switching frequency can have a negative effect on different components inside the electrolyser system, which were not modelled in this work, such as an increase in the loss of life according to [67].

Hence, if this is the case, additional filter would be needed to remove high frequency components which would increase the cost. Another advantage this converter topology has is that no reactive power is consumed, and therefore there is no need for reactive power compensation. Finally, the chosen DC/DC converter topology, as illustrated in Figure 7.25, seemed to be an accomplished design. This enabled lower voltages over the IGBTs, since the distribution DC-bus voltage $V_{dc,bus}$ otherwise would have been too high. But more importantly, it also enabled a high output current, low output voltage and at the same time a low current at the distribution DC-bus, which minimises the risk of exceeding the thermal constraints of the distribution cable as well as removes the need to install larger and more expensive cables.

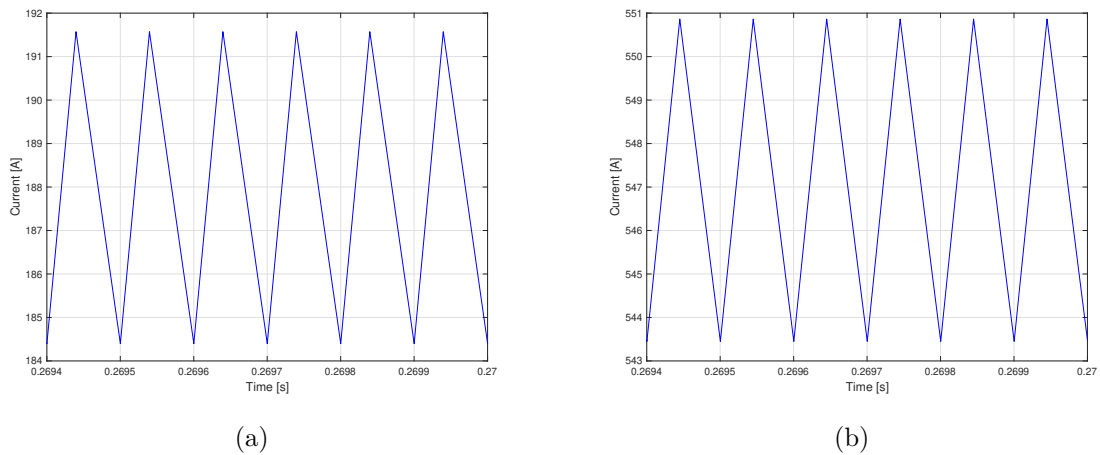


Figure 7.29: Filter inductor current I_{L_f} for hydrogen production rate reference of a) 25% and b) 75%.

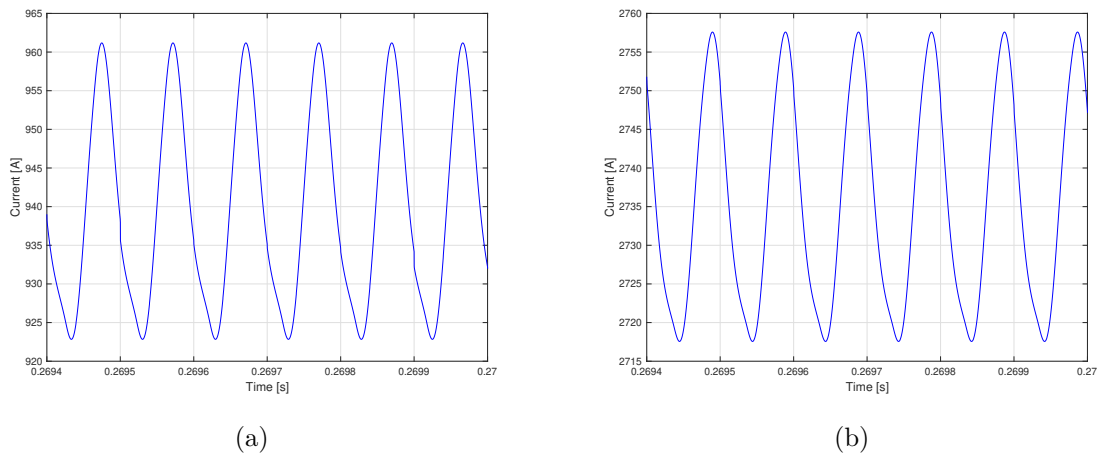
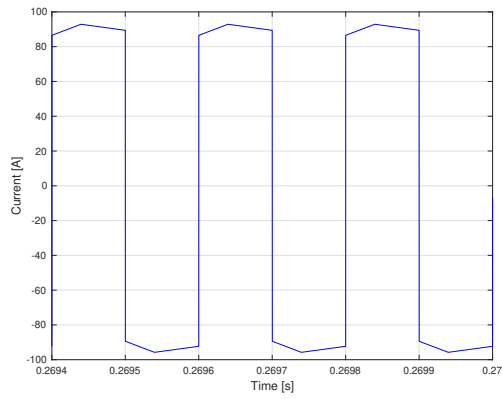
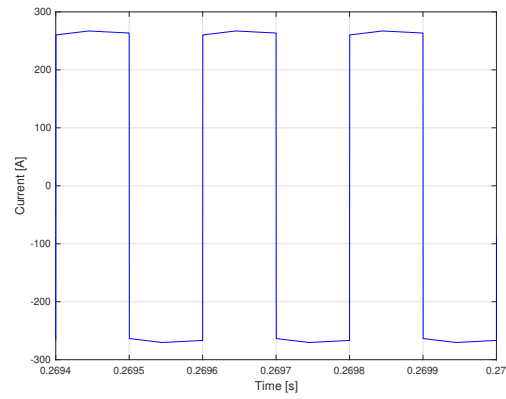


Figure 7.30: Output current I_0 for hydrogen production rate reference of a) 25% and b) 75%.

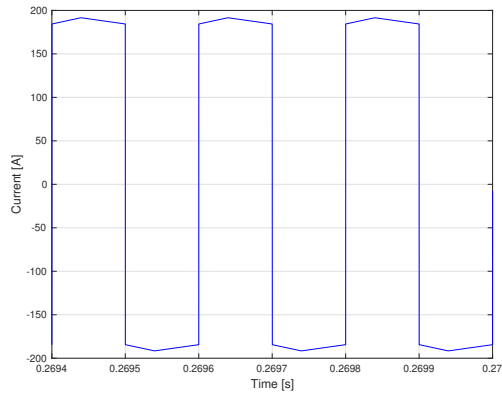


(a)

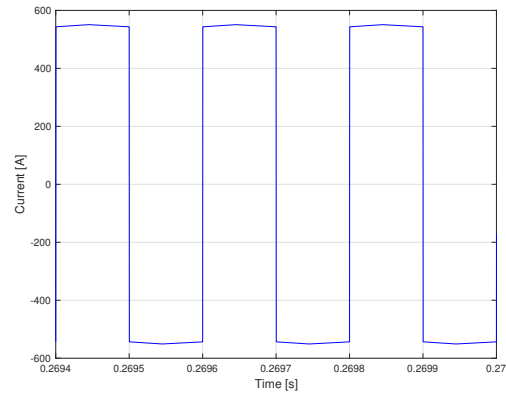


(b)

Figure 7.31: Primary transformer current I_p for hydrogen production rate reference of a) 25% and b) 75%.

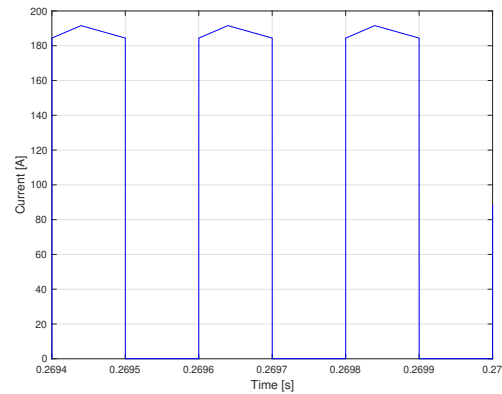


(a)

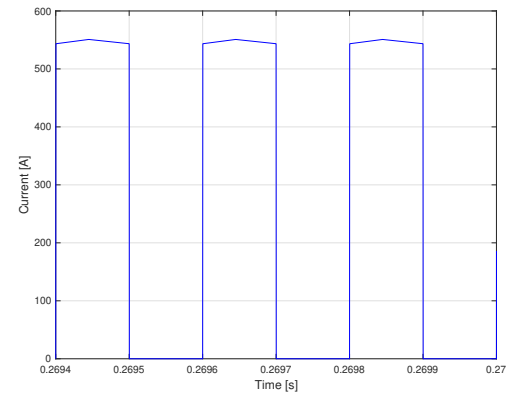


(b)

Figure 7.32: Secondary transformer current I_s for hydrogen production rate reference of a) 25% and b) 75%.



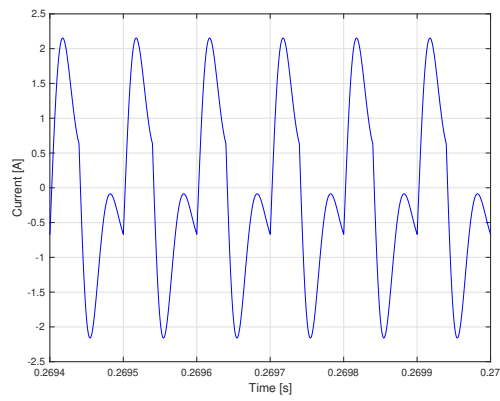
(a)



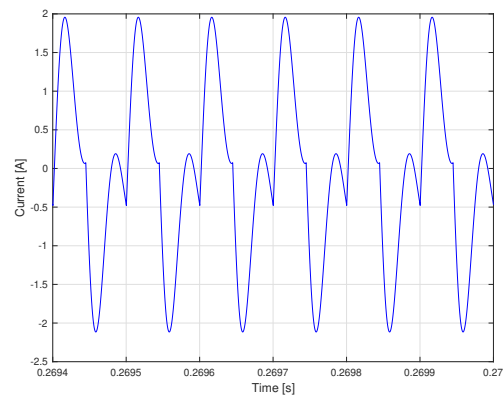
(b)

Figure 7.33: Diode current I_{D_1} for hydrogen production rate reference of a) 25% and b) 75%.

7. PEM electrolyser connected to a converter

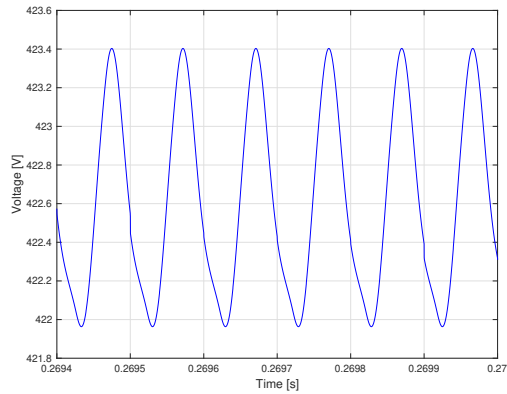


(a)

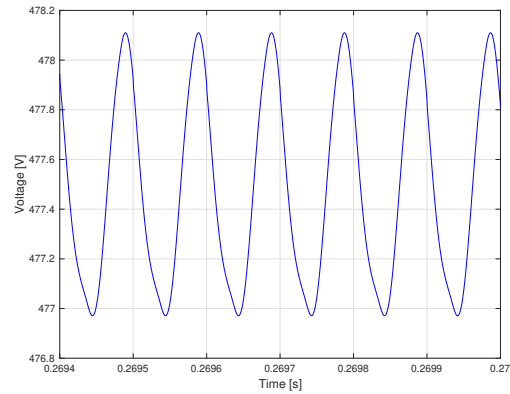


(b)

Figure 7.34: Capacitor current I_{C_0} for hydrogen production rate reference of a) 25% and b) 75%.

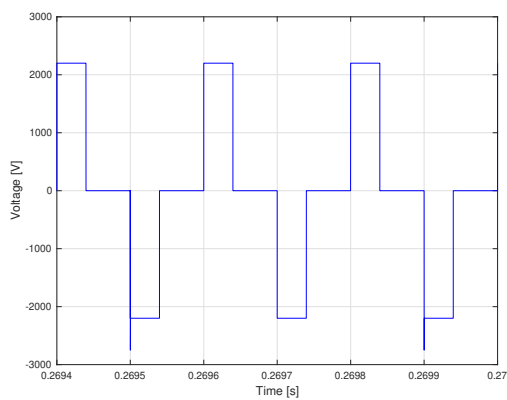


(a)

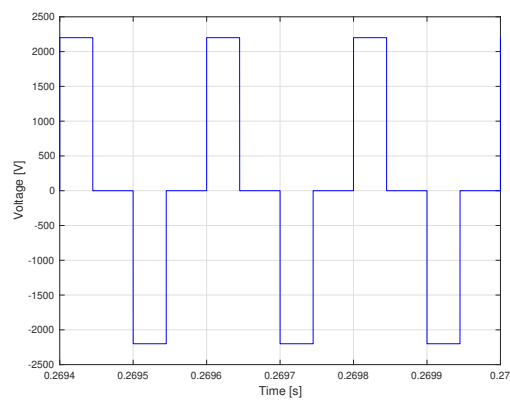


(b)

Figure 7.35: Output voltage V_0 for hydrogen production rate reference of a) 25% and b) 75%.

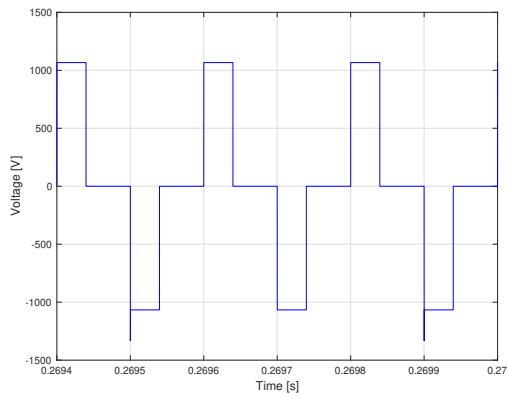


(a)

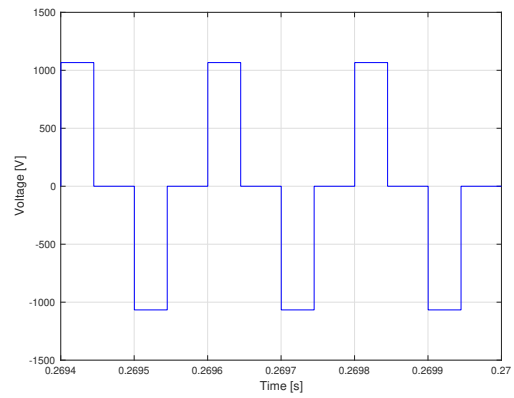


(b)

Figure 7.36: Primary transformer voltage V_p for hydrogen production rate reference of a) 25% and b) 75%.



(a)



(b)

Figure 7.37: Secondary transformer voltage V_s for hydrogen production rate reference of a) 25% and b) 75%.

7.2.4 Dynamic control response of the PSFB DC/DC converter

The dynamic simulation results of the PSFB DC/DC converter connected with the electrolyser, as illustrated in Figure 7.25, are shown in Figure 7.38, 7.39 and 7.40 for the output current I_0 , the output voltage V_0 and the hydrogen production rate v_{H_2} respectively. The hydrogen production rate reference started at 10%, and was then ramped up from 10% to 100% between 0.2 s and 0.4 s. Finally, the hydrogen production rate reference was ramped down from 100% to 50% between 0.6 s and 0.8 s. As can be seen, the values follow the reference values when it is changed. The mean values of the output current I_0 , the output voltage V_0 and the hydrogen production rate v_{H_2} presented in Table 7.9 can also be compared to their respective reference values in Table 7.10. The output current ripple ΔI_0 and the output voltage ripple ΔV_0 are also presented in Table 7.9 for the different steady-state hydrogen production rate reference values. As can be seen, the output current ripple ΔI_0 is much lower for a reference value of 100% hydrogen production rate compared to 10% and 50%. The reason for this can be because when the hydrogen production rate reference value is 100%, the electrolyser is operating in the concentration region which will result in an exponential increase of the voltage as a function of the current. Therefore, since the PSFB DC/DC converter is designed so that the output voltage ripple ΔV_0 is equal to 3.3 V for 100% hydrogen production rate reference value, a low output current ripple ΔI_0 will be enough to result in that output voltage ripple. But the output current ripple ΔI_0 is still considered to be very low for 10% and 50% as well. Furthermore, the output voltage ripple ΔV_0 is also considered to be very low for the different hydrogen production rate reference values. Finally, the hydrogen production rate reference $v_{\text{H}_2,\text{ref}}$ and the corresponding output current reference $I_{0,\text{ref}}$ for the dynamic simulation response is also illustrated in Figure 7.41.

Table 7.9: The output current I_0 , the output voltage V_0 , the input current I_{in} , the output current ripple ΔI_0 , the output voltage ripple ΔV_0 , the hydrogen production rate v_{H_2} , the electrolyser efficiency η^{LHV} , the output power P_0 and the energy consumption E_0 of the PSFB DC/DC converter and the electrolyser for hydrogen production rate reference value of 10%, 50% and 100%.

| Variable | H ₂ demand 10% | H ₂ demand 50% | H ₂ demand 100% |
|---------------------|---------------------------|---------------------------|----------------------------|
| I_0 | 381 A | 1832 A | 3749 A |
| V_0 | 396 V | 452 V | 530 V |
| I_{in} | 14 A | 75 A | 180 A |
| ΔI_0 | 15 A | 40 A | 0.9 A |
| ΔV_0 | 1.0 V | 1.2 V | 3.3 V |
| v_{H_2} | 3.8 kg/h | 18.5 kg/h | 37.8 kg/h |
| η^{LHV} | 84% | 73% | 63% |
| P_0 | 151 kW | 828 kW | 1986 kW |
| E_0 | 39.3 kWh/kg | 44.8 kWh/kg | 52.6 kWh/kg |

Table 7.10: The output current reference $I_{0,\text{ref}}$, the output voltage reference $V_{0,\text{ref}}$ and the hydrogen production rate reference $v_{\text{H}_2,\text{ref}}$ of the PSFB DC/DC converter and the electrolyser for hydrogen production rate reference value of 10%, 50% and 100%.

| Variable | H ₂ demand 10% | H ₂ demand 50% | H ₂ demand 100% |
|-----------------------------|---------------------------|---------------------------|----------------------------|
| $I_{0,\text{ref}}$ | 375 A | 1875 A | 3750 A |
| $V_{0,\text{ref}}$ | 396 V | 453 V | 533 V |
| $v_{\text{H}_2,\text{ref}}$ | 3.8 kg/h | 18.9 kg/h | 37.8 kg/h |

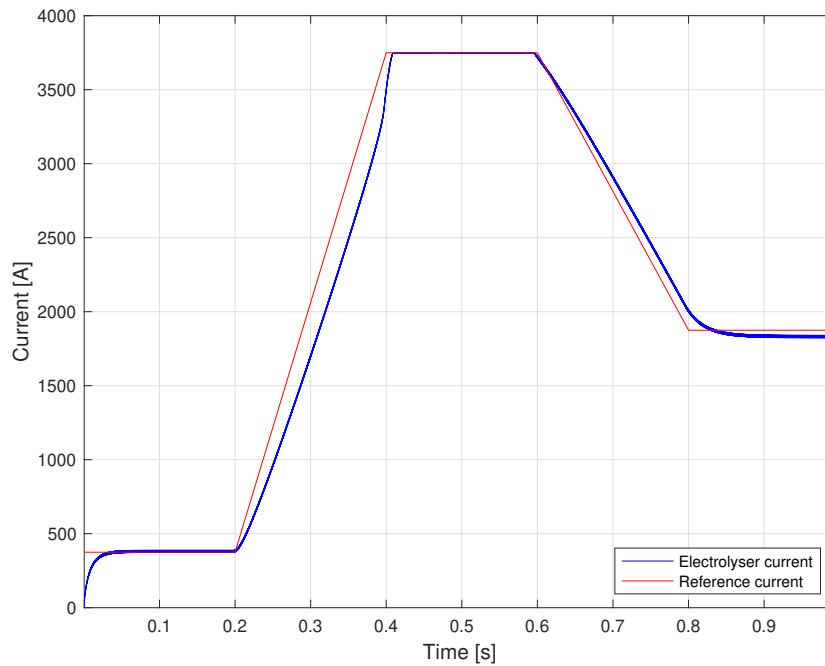


Figure 7.38: Dynamic simulation of the output current I_0 and the output current reference $I_{0,\text{ref}}$ for hydrogen production rate reference of 10%, 50% and 100%.

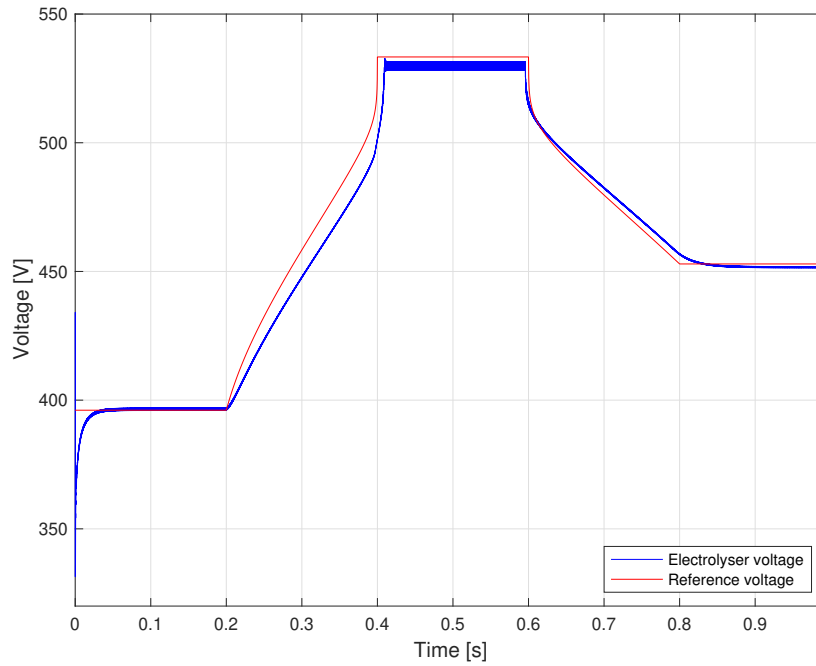


Figure 7.39: Dynamic simulation of the output voltage V_0 and the output voltage reference $V_{0,\text{ref}}$ for hydrogen production rate reference of 10%, 50% and 100%.

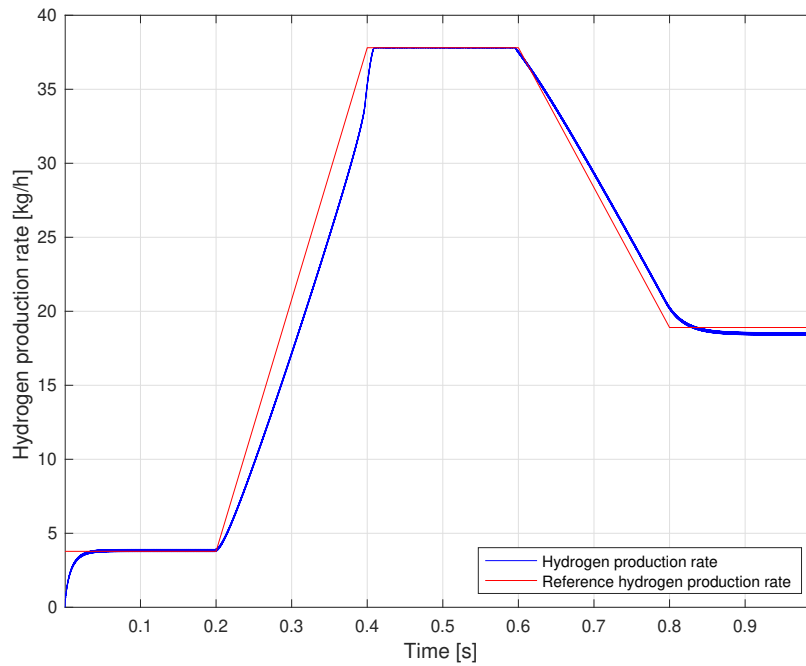


Figure 7.40: Dynamic simulation of the hydrogen production rate v_{H_2} and the hydrogen production rate reference $v_{\text{H}_2,\text{ref}}$ for hydrogen production rate reference of 10%, 50% and 100%.

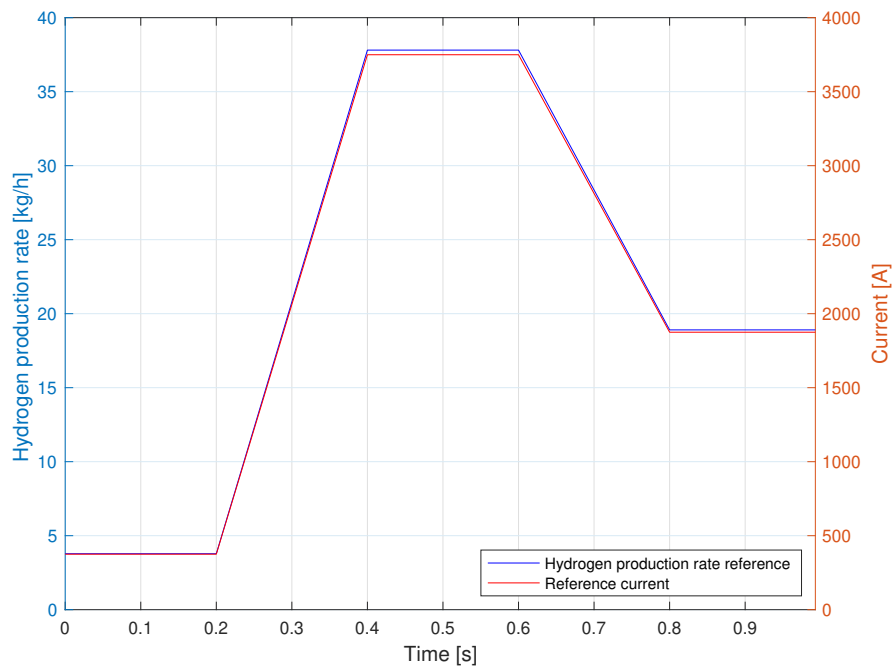


Figure 7.41: Dynamic simulation of the hydrogen production rate reference $v_{\text{H}_2,\text{ref}}$ and the output current reference $I_{0,\text{ref}}$ for hydrogen production rate reference of 10%, 50% and 100%.

7.2.5 The effect of leakage inductance on the PSFB DC/DC converter

Different cases were made where the leakage inductance L_R was increased in order to observe the effect that it has on the PSFB DC/DC converter. Other parameter values were not altered for these different cases. Different variable values for different leakage inductances are presented in Table 7.11 and Table 7.12 of one PSFB DC/DC converter module and of the PSFB DC/DC converter as well as the electrolyser respectively. As can be seen, an increase in the leakage inductance L_R will result in a decrease in the filter inductor current I_{L_f} and the output current I_0 as well as in the output voltage V_0 . This will therefore also result in a decrease in the hydrogen production rate v_{H_2} , the output power P_0 and energy consumption E_0 . The reason for this behaviour is because higher values of the leakage inductance L_R will result in higher voltage drops across the inductor, which will lower the output voltage V_0 and therefore the output current I_0 . Thus, if the leakage inductance L_R is increased, the medium frequency transformer has to be modified accordingly in order to consider the higher voltage drops. It is therefore of great importance to choose the leakage inductance value low enough for the medium frequency transformer design to take the voltage drop into consideration. However, it must also be chosen high enough that the energy stored in the leakage inductor E_R is greater than the charging- and discharging energy of the output transistor capacitors C_{oss} in order to attain ZVS. The output power P_0 as a function of the the leakage inductance L_R ratio is also illustrated in Figure 7.42, where it can be seen that the output power P_0 decreases almost linearly with an increase of the leakage inductance L_R . Another thing that is noticed in Table 7.11 and Table 7.12 is that the output voltage ripple ΔV_0 and the output current ripple ΔI_0 decrease much. This can be because the current is low enough that the electrolyser will begin to operate in the activation region, since the hydrogen production rate reference value for these cases was 25%, which will affect the output ripples differently. As also can be seen is that the filter inductor ripple ΔI_{L_f} is not highly affected by the increase of the leakage inductance L_R , and that is because that ripple is not dependent on which region the electrolyser operates in compared to the output ripples.

Table 7.11: The filter inductor current I_{L_f} , the output voltage V_0 , the filter inductor current ripple ΔI_{L_f} and the output voltage ripple ΔV_0 of one PSFB DC/DC converter module for different leakage inductance values when the hydrogen production rate reference value is 25%.

| Variable | L_R | $5 \cdot L_R$ | $15 \cdot L_R$ | $30 \cdot L_R$ |
|------------------|-------|---------------|----------------|----------------|
| I_{L_f} | 188 A | 172 A | 143 A | 116 A |
| V_0 | 423 V | 420 V | 414 V | 408 V |
| ΔI_{L_f} | 7.2 A | 7.2 A | 7.1 A | 7.1 A |
| ΔV_0 | 1.4 V | 0.6 V | 0.7 V | 0.8 V |

Table 7.12: The output current I_0 , the output current ripple ΔI_0 , the hydrogen production rate v_{H_2} , the output power P_0 and the energy consumption E_0 of the PSFB DC/DC converter and the electrolyser for different leakage inductance values when the hydrogen production rate reference value is 25%.

| Variable | L_R | $5 \cdot L_R$ | $15 \cdot L_R$ | $30 \cdot L_R$ |
|--------------|-------------|---------------|----------------|----------------|
| I_0 | 940 A | 860 A | 716 A | 582 A |
| ΔI_0 | 38 A | 16 A | 16 A | 16 A |
| v_{H_2} | 9.5 kg/h | 8.7 kg/h | 7.2 kg/h | 5.9 kg/h |
| P_0 | 397 kW | 361 kW | 296 kW | 237 kW |
| E_0 | 41.9 kWh/kg | 41.6 kWh/kg | 41.0 kWh/kg | 40.4 kWh/kg |

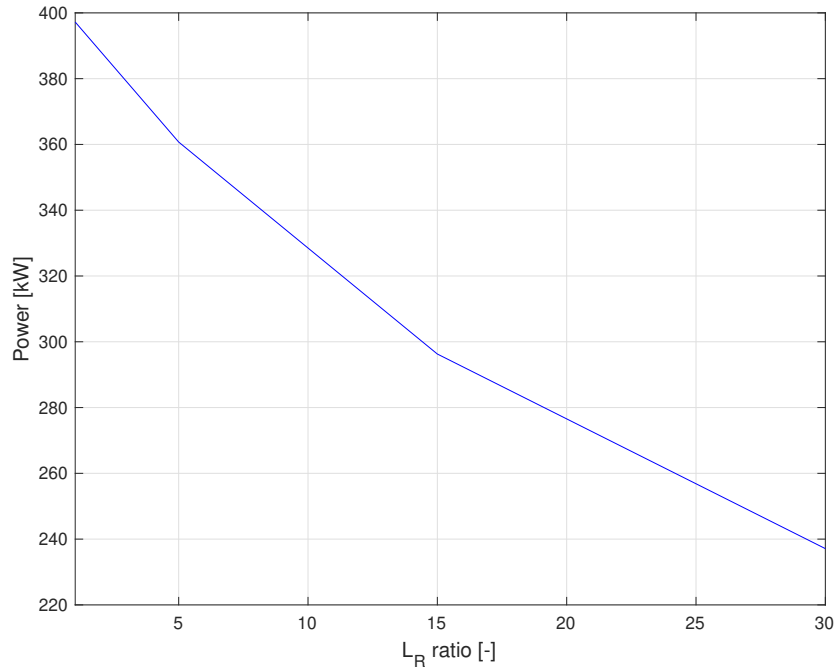


Figure 7.42: Output power P_0 as a function of the leakage inductance L_R ratio when the hydrogen production rate reference value is 25%.

7.3 Summary

In this chapter, two converters, a 12-pulse thyristor rectifier which was interfaced with an AC distribution system via a transformer and a PSFB DC/DC converter that operates on a DC distribution system, have been modelled and simulated.

Successful 12-pulse thyristor rectifier behaviour was achieved where the expected current waveform shape in the grid side current i_{ac} , similar to a six-step up and down staircase, could be observed for both 25% and 75% hydrogen production rate reference. Commutations of the thyristors is also visible in the AC voltage input to the rectifiers. For each distorting spike, current commutation starts in each phase-linked thyristor pair, contributing to their respective output currents I_{dc1} and I_{dc2} . By the 12-pulse design and three-phase setup, lower-order harmonics (up to the 19th harmonic) cancellation was confirmed. However, the amplitudes of the 11th and 13th harmonic were not

cancelled. 11th and 13th harmonic amplitude values compared to fundamental frequency amplitude f_1 is consistent with theoretical expectation ($\frac{1}{11}f_1$ and $\frac{1}{13}f_1$ of the fundamental amplitude). There is thus a need of tuned filter-compensation for the 11th and 13th harmonic amplitude. Decreasing grid strength was modelled by increasing the value of grid impedance, which was modelled as a reactance with the grid inductance L_g (the grid impedance had zero resistance). The result of this simulation was that demand, which was modelled for 75%, could be met at a steady-state output down to a SCR of 0.6, and at lower ratios the output current was lower than the reference value ($I_0 < I_{DC}^*$). Therefore, high-power thyristor rectifiers should preferably be connected to a strong grid to decrease the line voltage drop that results in a limited output power of the rectifier. The transformer turn ratio can also be changed to be able to feed the desired output voltage to the electrolyser even when the voltage drop of the grid increases with the power. For the 12-pulse thyristor rectifier, ripple cancellation at the output voltage V_0 was successfully implemented with DC reactors and it responded correctly to dynamic control.

The PSFB DC/DC converter was one of the most suitable DC/DC converter topologies as it fulfilled seven of the eight suggested requirements DC/DC converters should have for electrolyser applications. Current and voltage waveforms for one PSFB DC/DC converter module behaved as expected. Simulations also showed that the PSFB DC/DC converter had low output current ripple ΔI_0 and low output voltage ripple ΔV_0 for hydrogen production rate reference values of 10%, 25%, 50%, 75% and 100%, which is preferable. Another advantageous quality is that there is no reactive power consumption, hence no need for reactive power compensation. Furthermore, the topology of the PSFB DC/DC converter where five PSFB DC/DC converter modules were series-connected on the high-voltage side and parallel-connected on the low-voltage side was an accomplished design. It enabled a high voltage conversion ratio, a high output current I_0 and a low output voltage V_0 while at the same time decreasing the voltage across the IGBTs as well as the current flow at the distribution DC-bus. Moreover, good dynamic control response of the PSFB DC/DC converter was also achieved. Finally, an increase in the leakage inductance L_R , while the other parameters were unaltered, resulted in a higher voltage drop over the inductor which decreased the output voltage V_0 and therefore the output current I_0 . Thus, the leakage inductance L_R has to be chosen accordingly so that the voltage drop is considered by the medium frequency transformer design and so that ZVS can be attained.

8

Implementation and structure of electrolyser station on GW-scale

To supply the needed hydrogen to different sectors such as the steel industry or the chemical industry, electrolyser stations with a high production capacity are needed in the future. Thus, the electric power needed for each electrolyser station will be in the range of 100 MW up to GW-scale. A station handling this amount of power will be connected to the sub-transmission or the transmission grid. This chapter will discuss how the structure of large electrolyser stations can be designed and what the main requirements will be.

8.1 Electrolyser station requirements at PCC

When considering the electrolyser station as a load, it might affect the grid operation due to its significantly large size. Similarly, the AC grid properties affect the design choices of the electrolyser station. The integration to the AC grid of the proposed large electrolyser station is shown in Figure 8.1.

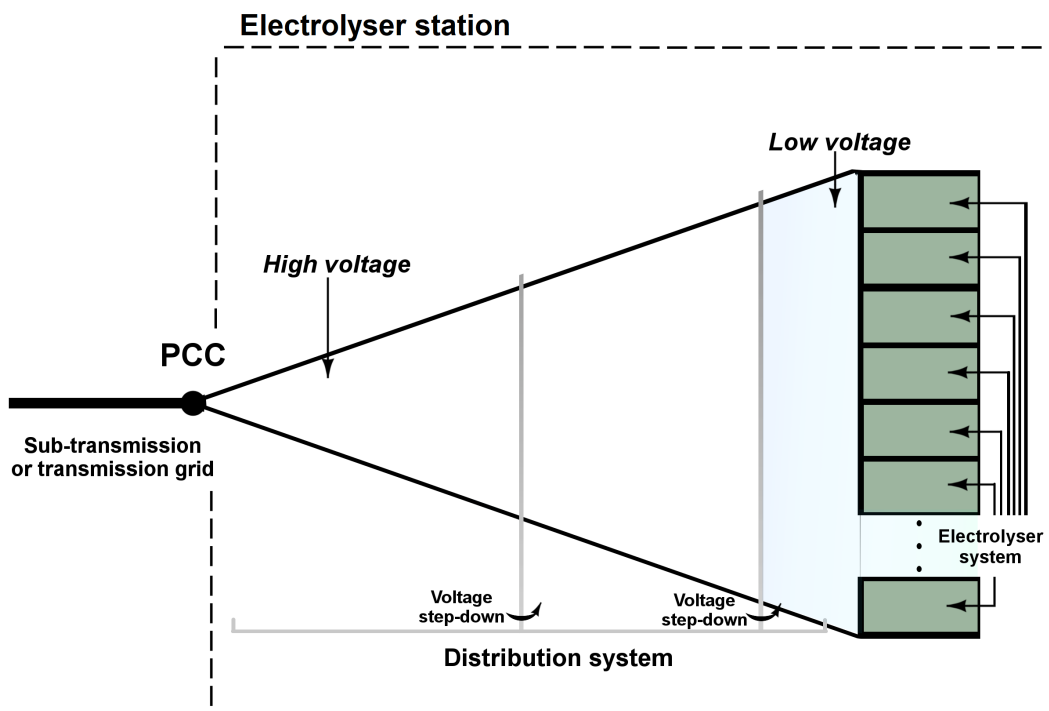


Figure 8.1: Schematic view of an electrolyser station connected to PCC.

It consists of the distribution of the power from the PCC that is connected to the incoming HVAC line at transmission or subtransmission level. At the other end of the distribution system, a large number of electrolyser systems are connected. Thus, the power must be distributed to a number of electrolyser systems and the voltage level must also be reduced. Therefore, a number of transformers will be used inside the distribution system.

When designing an electrolyser station, it is important to fulfill a number of requirements to be able to connect to the transmission line. Firstly, the power factor should be equal to one. This means that only active power should be consumed from the PCC, while the reactive power that is produced from the distribution system and the electrolyser systems should be compensated by either reactive power compensation filters or by an active reactive-power compensator, such as a STATCOM. Moreover, the harmonic current at the PCC should be below the threshold in the grid codes. When using thyristor rectifiers, low-frequency harmonic currents are produced. These harmonics must be removed by either passive harmonic filters or active power filters. The electrolyser station is also expected to not cause any power and voltage fluctuations, flicker and other operational issues associated with the type of load that a GW electrolyser station is.

For different installation points at the grid, the particular grid strength should be evaluated to minimise the risk of not being able to supply the electrolyser station with needed power. For any given point of interconnection, critical grid components would be shared on the transmission line between the installation point, PCC and generation buses [69]. Preferably, when planning for renewable generation integration on the grid, especially in combination with building renewable hydrogen generation stations, SCR analysis provides a good reference as to how the grid strength can be improved [66], [69], [70]. To achieve completely renewable hydrogen production, enough VRE capacity, foremost solar and wind power, is needed to supply the GW-scale electrolyser station, which makes grid planning and location of installation critical.

Another way to handle the amount of active power and relatively quickly adapt the hydrogen production rate is to install the station in a modular way, as shown in Figure 8.1. By using modules, where each module in the station is an electrolyser system of a couple MW, the station active power is easily expandable. Additionally, serviceability increases if one or a couple of modules can be taken out of service while the rest of them are powered on. If all of these requirements are considered, adhering to grid codes and utilising the most of VRE's and renewable hydrogen generation combined can be achieved.

8.2 Internal requirements of electrolyser station

As presented in Chapter 5, renewable hydrogen can be applied in several sectors in the future such as the chemical industry or the steel industry. According to IRENA [25], future electrolyser stacks could reach sizes up to 10 MW. Hence, electrolyser plants on GW-scale would consist of hundreds of electrolyser systems. But before it can be economically beneficial to begin the construction and operation of GW-scale electrolyser stations, the CAPEX and the OPEX of the total system must be on an attractive level to make the investment. Today, the cost is too high to be able to compete against non-renewable

hydrogen production technologies [25]. Nonetheless, electrolyser stations will probably be built on a smaller scale initially, with a plant-design that enables facilitating an extension in later stage. Once electrolyser stations are integrated and connected to future hydrogen-based industries, it must be able to meet the hydrogen demand uninterruptedly. Disturbances or faults inside the electrolyser station that interrupts the hydrogen production would also interrupt the production of hydrogen-dependent industries, which can be extremely costly. Thus, high reliability and availability of the electrolyser station is of great importance. Achieving these requirements can be done by utilising redundancy of the most important devices such as the transformers. Moreover, switchgears and sensors have to be installed as well in order to provide protection and monitoring of the plant. Finally, the electrolyser station should be service friendly, preferably with a separate service building included and with the possibility to perform services without shutting down the electrolyser station. It is preferable if the electrolyser systems operate at low DC voltage levels below 1500 V as well. Another important requirement is that the electrolyser must have good dynamic performance with the ability to change the hydrogen production based on the demand or what the power system can provide.

8.3 Structure of electrolyser station

Electrolyser stations on GW-scale can have different structures. In this section, four proposed structure designs from an electric point of view will be presented and evaluated to get an idea of which options could be viable. For the following cases, the transformer leakage impedances were assumed to be 0.1 p.u. Furthermore, the electrolyser station was assumed to have an apparent power rating of 1200 MVA and an active power rating of 1 GW, with no reactive power compensation. This was based on the maximum active and reactive power consumed from PCC for the 12-pulse thyristor rectifier with the 2 MW PEM electrolyser, presented in Figure 7.17, as well as under the assumption that the power increases linearly with the power rating of the electrolyser system. Moreover, the bus which the electrolyser systems are connected to was assumed to have a current rating of 3 kA. The maximum allowed short-circuit current is also assumed to be below 63 kA [71]. Finally, the electrolyser systems in the electrolyser station were assumed to have a power rating of 10 MW.

As mentioned, four cases will be investigated in which cases 1 and 2, the 400/150 kV transformers are parallel-connected between the 400 kV and the 150 kV bus. Each 400/150 kV transformer for these two cases were assumed to have an apparent power rating of 570 MVA, due to the assumption that they operate at 70% of nominal rating for a nominal power consumption of 1 GW for the electrolyser station. The difference between the two cases is that case 1 has a bus voltage, which the electrolyser systems are connected in parallel to, of 33 kV while case 2 has a bus voltage of 66 kV. For cases 3 and 4, the 400/150 kV transformers are not parallel-connected, and therefore have an apparent power rating of 400 MVA. The bus voltage is 33 kV for case 3 and 66 kV for case 4.

8.3.1 Case 1

The proposed structure of an electrolyser station for case 1 is illustrated in Figure 8.2. As can be seen, it consists of three 400/150 kV transformers connected in parallel

between the 400 kV and the 150 kV bus. The purpose of several transformers is to attain redundancy in case of transformer failure. Moreover, there are a number of 150/33 kV transformers connected to the 150 kV bus to handle the current at each 33 kV bus. Therefore, the electrolyser systems will be divided so that equal number of electrolyser systems are connected in parallel to each 33 kV bus.

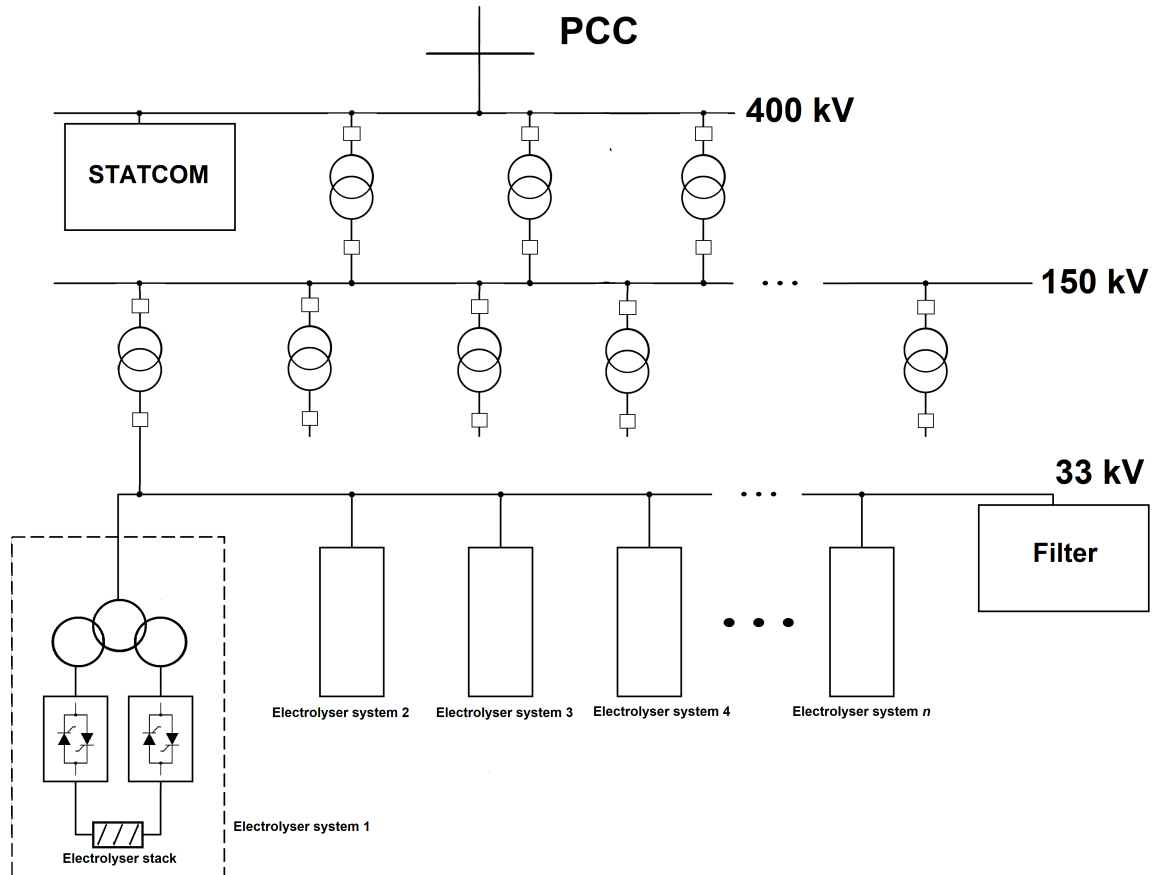


Figure 8.2: The structure of the electrolyser station and its integration to the sub-transmission or the transmission grid for case 1.

First, the short-circuit current (SCC) has to be determined to calculate the number of 150/33 kV transformers that are required. Assuming that a three-line-to-ground (3LG) fault occurs at one of the 33 kV buses, the fault voltage V_F can be expressed as

$$V_F = I_{SCC} \cdot Z_F \quad (8.1)$$

which is equal to 33 kV in this case. The fault impedance Z_F can also be expressed as

$$Z_F = Z_{T_{1,tot}} + Z_{T_2} \quad (8.2)$$

where $Z_{T_{1,tot}}$ is the total impedance of the 400/150 kV parallel-connected transformers, equal to Z_{T_1} divided by three, while Z_{T_2} is the 150/33 kV transformer impedance. Moreover, since the transformer impedances are assumed in per unit values, the base impedance Z_B can be calculated as

$$Z_B = \frac{V_F^2}{S_{n,T}} \quad (8.3)$$

where $S_{n,T}$ is the rated apparent power of the 400/150 kV and 150/33 kV transformers, equal to 570 MVA and the rated apparent power of the electrolyser station $S_{n,el}$ of 1200 MVA divided by the number of 150/33 kV transformers x respectively. The reason why the rated apparent power of the 150/33 kV transformers is equal to $S_{n,el}$ divided with x is because the rated apparent power $S_{n,el}$ will be equally divided for all the 150/33 kV transformers. Finally, the nominal current at the bus $I_{n,bus}$ which the electrolyser systems are connected in parallel to can be expressed as

$$I_{n,bus} = \frac{S_{n,el}/x}{\sqrt{3}V_{bus}} \quad (8.4)$$

where V_{bus} is the bus voltage which the electrolyser systems are connected in parallel to. Combining (8.1)-(8.4), the nominal current at the 33 kV bus $I_{n,bus}$ and the SCC I_{SCC} can be plotted as a function of the number of transformers connected to the 150 kV bus x , as illustrated in Figure 8.3. As can be seen, the number of 150/33 kV transformers x must be equal to or higher than 7 to attain a nominal current at the 33 kV bus $I_{n,bus}$ below 3 kA. This will result in a SCC I_{SCC} of 27 kA, which fulfills the assumed requirement that SCC should be below 63 kA. Thus, if a lower SCC I_{SCC} is required, then the number of transformers connected to the 150 kV bus x should increase. Since the electrolyser station consists of 100 electrolyser systems of 10 MW, each 33 kV bus will have approximately 14 electrolyser systems connected in parallel.

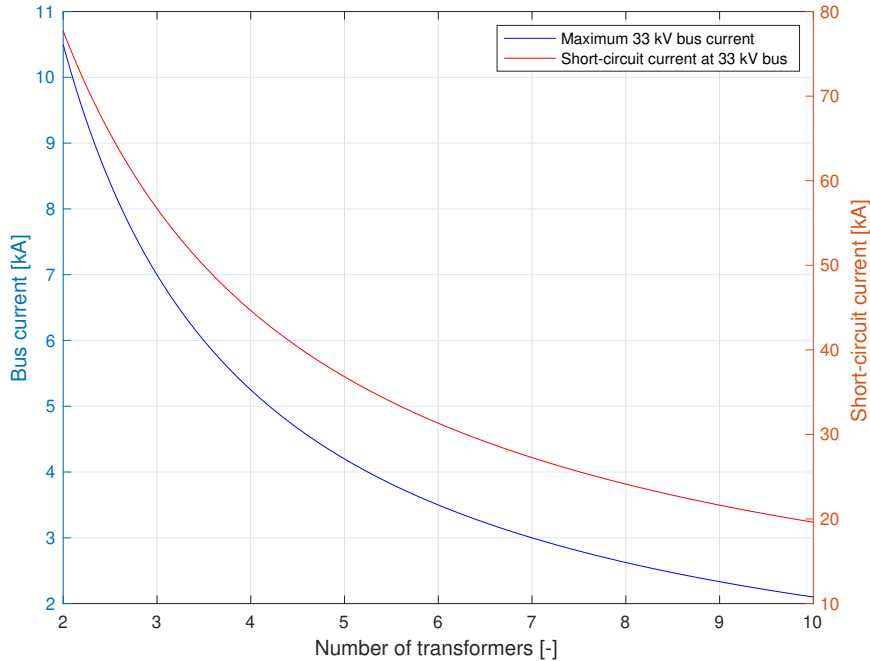


Figure 8.3: The nominal current at the 33 kV bus $I_{n,bus}$ and the SCC I_{SCC} as a function of the number of transformers connected to the 150 kV bus x for case 1.

The reactive power produced from the electrolyser systems could be compensated with a STATCOM of equal capacity. Based on the results in Section 7.1.2, the maximum reactive power drawn from PCC for a 2 MW electrolyser system is 1258 kvar when a 12-pulse thyristor rectifier is used. Moreover, it is also assumed that the increase in reactive power is linearly proportional to the rated power of the electrolyser system. Thus, the

reactive power drawn from PCC for a 1 GW electrolyser station is approximately equal to 629 Mvar, which would also be the required size of the STATCOM in Figure 8.2. The size of the STATCOM will be equal for all the cases. However, this size only considers the reactive power from the electrolyser systems. In reality, the transformers will produce reactive power as well, which would therefore require a larger STATCOM. Each bus is also assumed to have a filter that removes the harmonics produced from the electrolyser systems.

8.3.2 Case 2

For this case, the bus voltage V_{bus} which the electrolyser systems are connected to has been changed from 33 kV as in case 1 to 66 kV, as illustrated in Figure 8.4. However, the configuration as well as the assumptions are still the same as in case 1, which is why (8.1)-(8.4) can be used to plot the number of 150/66 kV transformers x , the nominal current at the bus $I_{n,\text{bus}}$ and the SCC I_{SCC} .

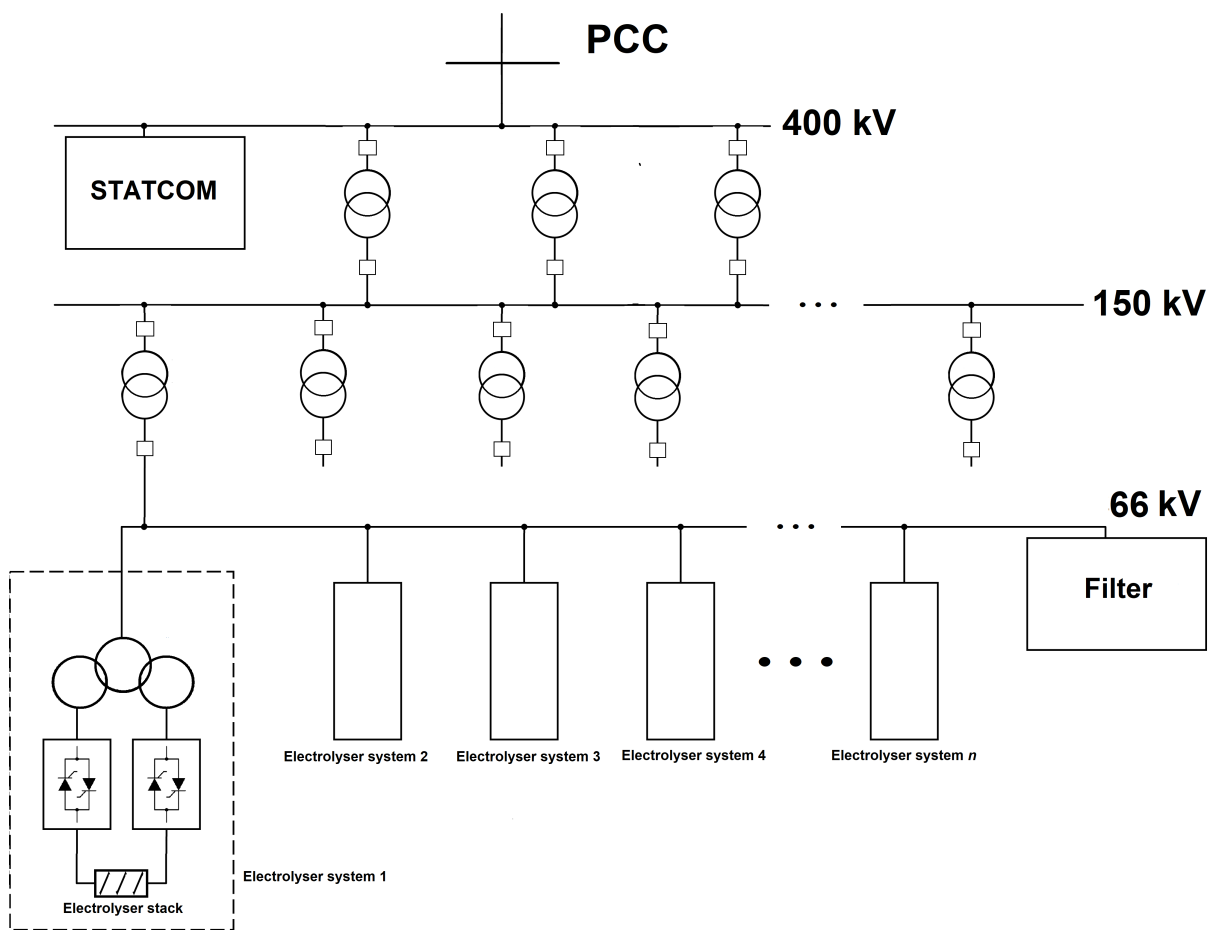


Figure 8.4: The structure of the electrolyser station and its integration to the sub-transmission or the transmission grid for case 2.

As illustrated in Figure 8.5, the number of 150/66 kV transformers x must be equal to or higher than 4 to attain a nominal bus current $I_{n,\text{bus}}$ below 3 kA. The SCC I_{SCC} for x equal to 4 will be 22 kA. However, compared to the configuration in case 1, it can be noticed that the requirement on the number of transformers connected to the 150 kV bus x decreased almost by half. Thus could this configuration be less costly compared to the

configuration used in case 1 since the installation costs will decrease. Moreover, each 66 kV bus can have 25 electrolyser systems connected in parallel to it, as compared to case 1 where a maximum of 14 electrolyser systems could be connected in parallel to each 33 kV bus.

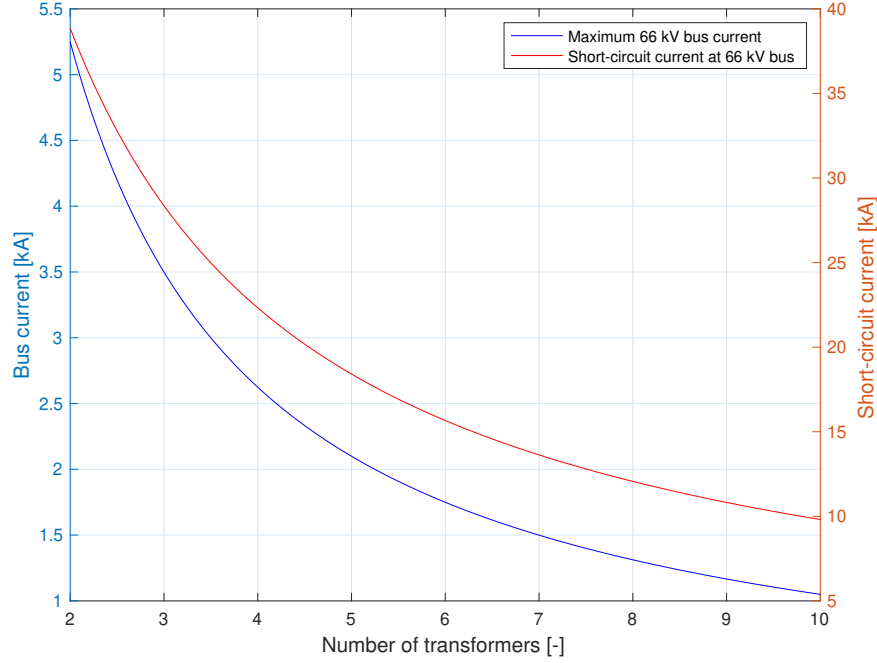


Figure 8.5: The nominal current at the 66 kV bus $I_{n,bus}$ and the SCC I_{SCC} as a function of the number of transformers connected to the 150 kV bus x for case 2.

8.3.3 Case 3

As illustrated in Figure 8.6, the configuration for this case differ compared to cases 1 and 2 in that the three 400/150 kV transformers are no longer connected in parallel between the 400 kV and the 150 kV bus. Nonetheless, (8.1)-(8.4) can still be used for this configuration to plot the number of 150/33 kV transformers x , the nominal current at the bus $I_{n,bus}$ and the SCC I_{SCC} , as illustrated in Figure 8.7. But, since the three 400/150 kV transformers are not parallel-connected anymore, there will be three 150 kV buses instead of one. Thus, the total impedance of the 400/150 kV transformers $Z_{T_1,tot}$ will be equal to the transformer impedance Z_{T_1} . They also do not have to operate at 70% of their rating for maximum load, since there is no redundancy. Therefore, the apparent power rating of the 400/150 kV transformers for this case will be the rated apparent power of the electrolyser station $S_{n,el}$ divided by three, which is equal to 400 MVA. As seen in Figure 8.7, the number of 150/33 kV transformers x must be equal to or higher than 7 to attain a nominal bus current $I_{n,bus}$ below 3 kA, as for case 1. However, the SCC I_{SCC} for case 3 decreased to 21 kA compared to case 1. Finally, the advantage this configuration has compared to the ones presented in cases 1 and 2 is that the 400/150 kV transformers are not connected in parallel. Hence, if a fault occurs on one of the 150 kV buses, only one third of the hydrogen production will be interrupted. However, in cases 1 and 2, the entire electrolyser station will be interrupted until the fault at the 150 kV bus is cleared.

But there will be no redundancy in case of 400/150 kV transformer failure which is the advantage of the configuration in cases 1 and 2.

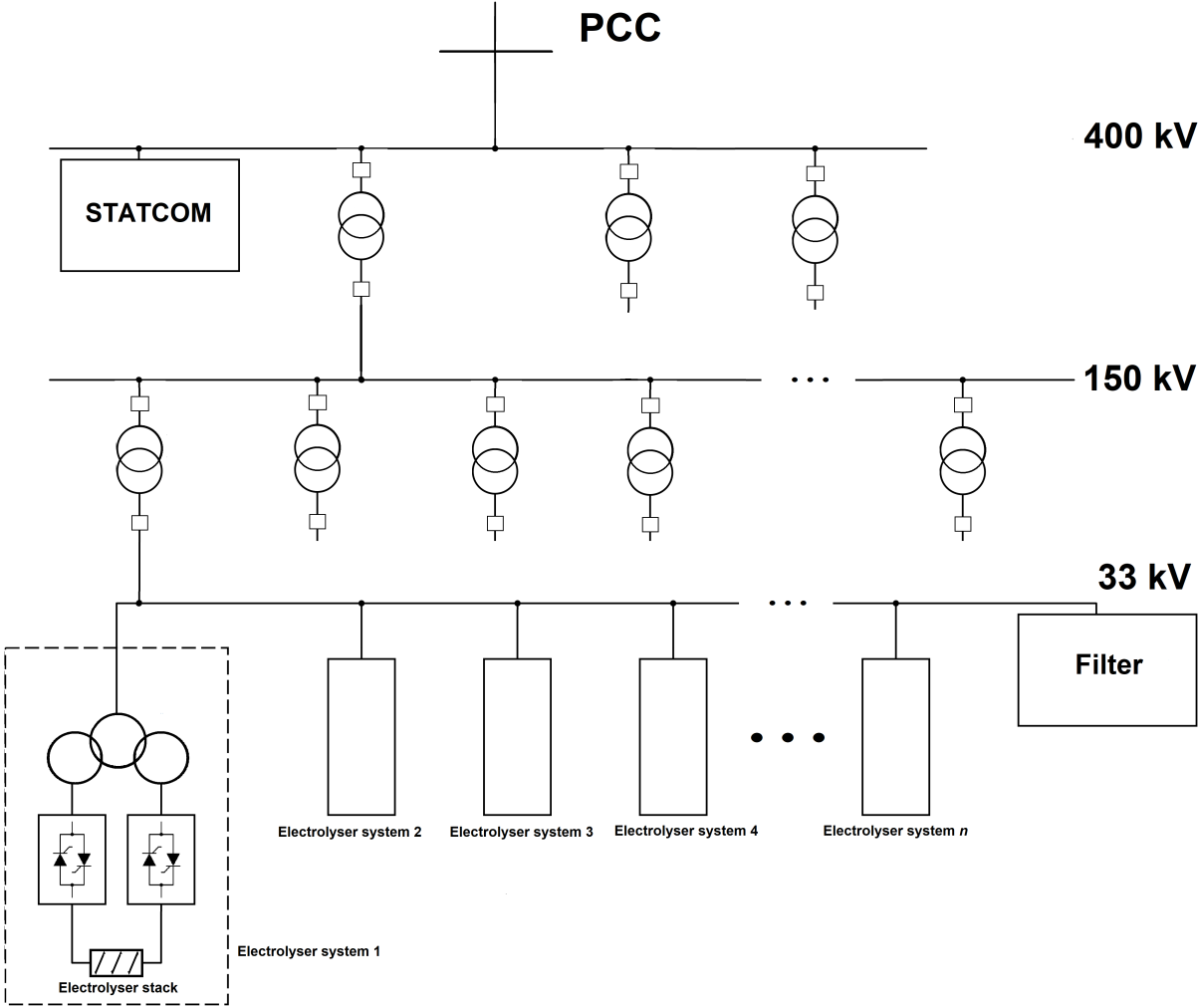


Figure 8.6: The structure of the electrolyser station and its integration to the sub-transmission or the transmission grid for case 3.

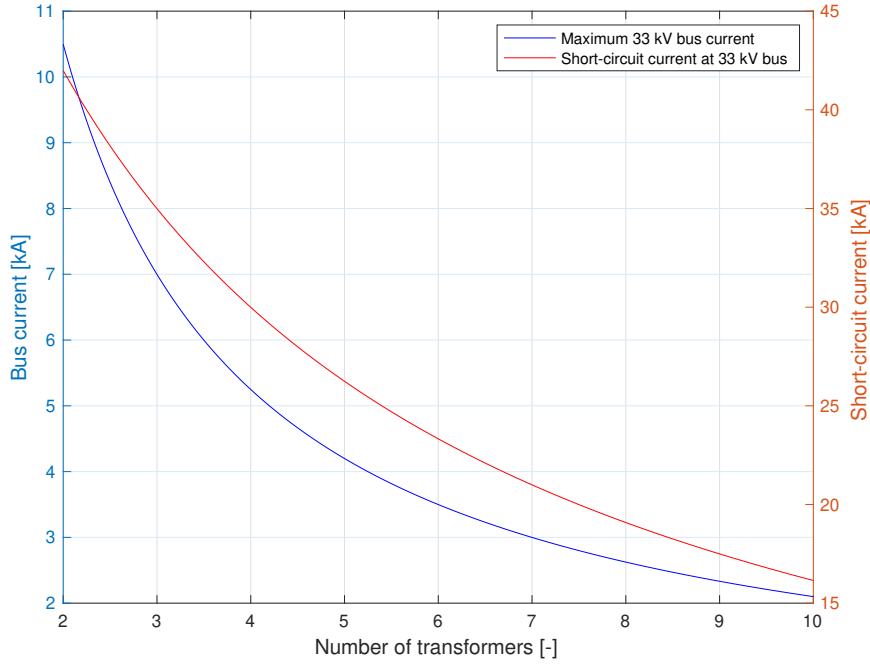


Figure 8.7: The nominal current at the 33 kV bus $I_{n,bus}$ and the SCC I_{SCC} as a function of the number of transformers connected to one of the 150 kV buses x for case 3.

8.3.4 Case 4

The configuration used for case 4, which is illustrated in Figure 8.8, is the same as for case 3 shown in Figure 8.6, except that the bus voltage V_{bus} which the electrolyser systems are connected to is 66 kV instead of 33 kV. However, the total impedance of the 400/150 kV transformers $Z_{T_1,tot}$ as well as the apparent power rating S_{n,T_1} is the same as for case 3. Therefore, by using (8.1)-(8.4) the number of 150/66 kV transformers x , the nominal current at the bus $I_{n,bus}$ and the SCC I_{SCC} can be plotted which is shown in Figure 8.9. As for case 2, the number of 150/66 kV transformers x must be equal to or higher than 4 in order to attain a nominal bus current $I_{n,bus}$ below 3 kA. However, the SCC I_{SCC} is lower compared to the other three cases, being equal to 15 kA for x equal to 4, which could decrease the costs as circuit-breakers with lower rating will be required. It also has the advantage as case 3 that the 400/150 kV transformers are not parallel-connected, therefore increasing the reliability and availability of the system in case of a fault at the 150 kV bus. However, this also results in the same disadvantage as case 3 has for a 400/150 kV transformer failure. The comparison between cases 1-4 is presented in Table 8.1, where it can be seen that the configuration used for case 4 gives the lowest number of 150 kV connected transformers x , the nominal current at the bus $I_{n,bus}$ and the SCC I_{SCC} . Thus, a configuration similar to the one in Figure 8.8 for case 4, where the 400/150 kV transformers are not parallel-connected and a higher bus voltage which the electrolyser systems are connected to is used, seems beneficial from an economic point of view. A better configuration would also be if the 400/150 kV transformer redundancy advantage of cases 1 and 2 could be attained as well. Furthermore, it is also presented in Table 8.1 that the apparent power rating of the 400/150 kV transformers is higher for cases 1 and 2 compared to cases 3 and 4, which is due to redundancy. Finally, the apparent power rating of the 150/66 kV transformers for cases 2 and 4 are higher than the apparent

power rating of the 150/33 kV transformers for cases 1 and 3. This is because fewer transformers x , which the rated apparent power of the electrolyser station $S_{n,el}$ will be equally divided to, are required to attain a nominal bus current $I_{n,bus}$ below 3 kA. It must also be observed and considered that a decrease in the SCC I_{SCC} , with the nominal bus current $I_{n,bus}$ unchanged, will decrease the SCR.

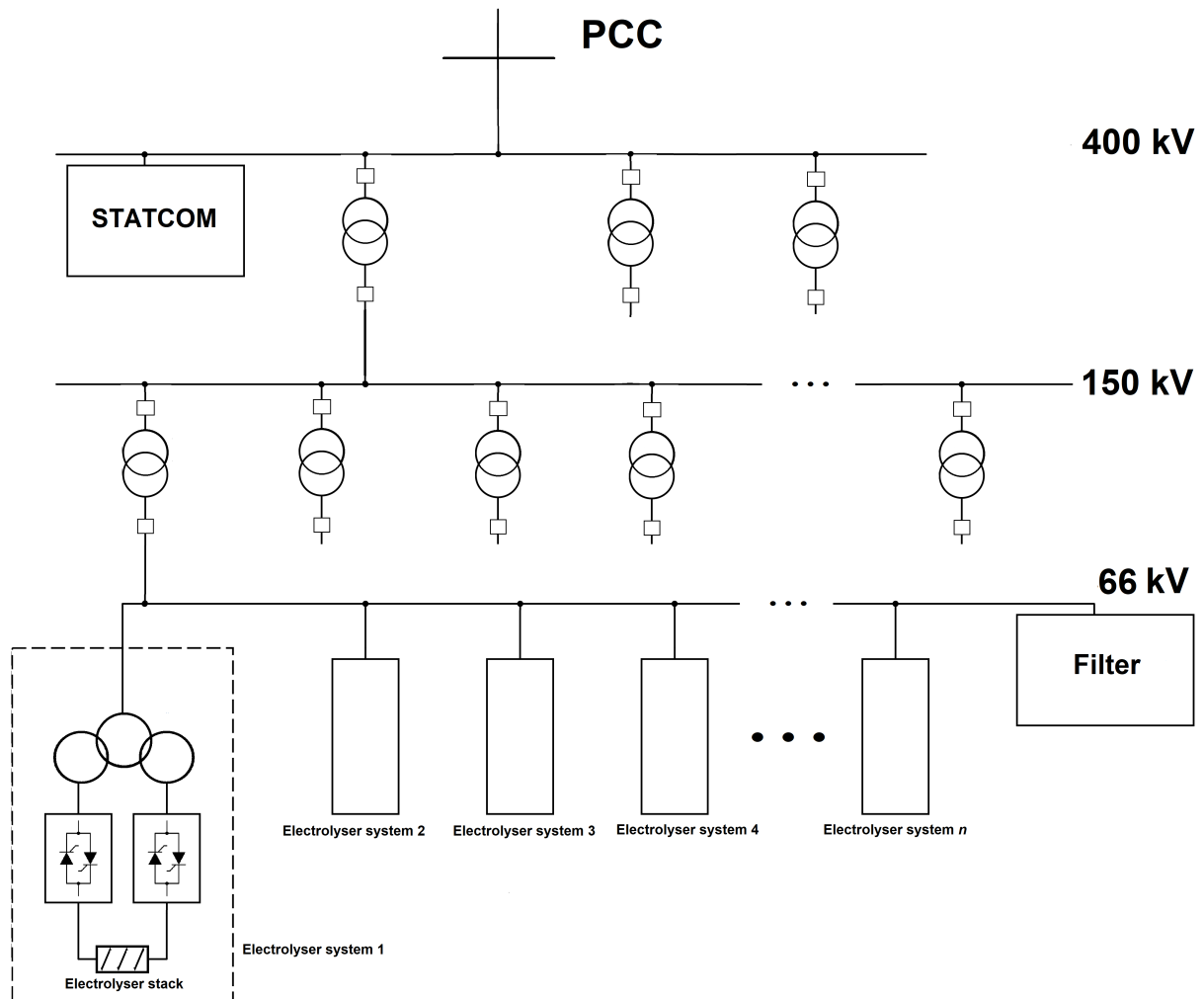


Figure 8.8: The structure of the electrolyser station and its integration to the sub-transmission or the transmission grid for case 4.

Table 8.1: Structure comparison of electrolyser station cases 1-4.

| Parameter | Case 1 | Case 2 | Case 3 | Case 4 |
|-------------|---------|---------|---------|---------|
| V_{bus} | 33 kV | 66 kV | 33 kV | 66 kV |
| $I_{n,bus}$ | 3.0 kA | 2.6 kA | 3.0 kA | 2.6 kA |
| I_{SCC} | 27 kA | 22 kA | 21 kA | 15 kA |
| S_{n,T_1} | 570 MVA | 570 MVA | 400 MVA | 400 MVA |
| S_{n,T_2} | 172 MVA | 300 MVA | 172 MVA | 300 MVA |
| x | 7 | 4 | 7 | 4 |

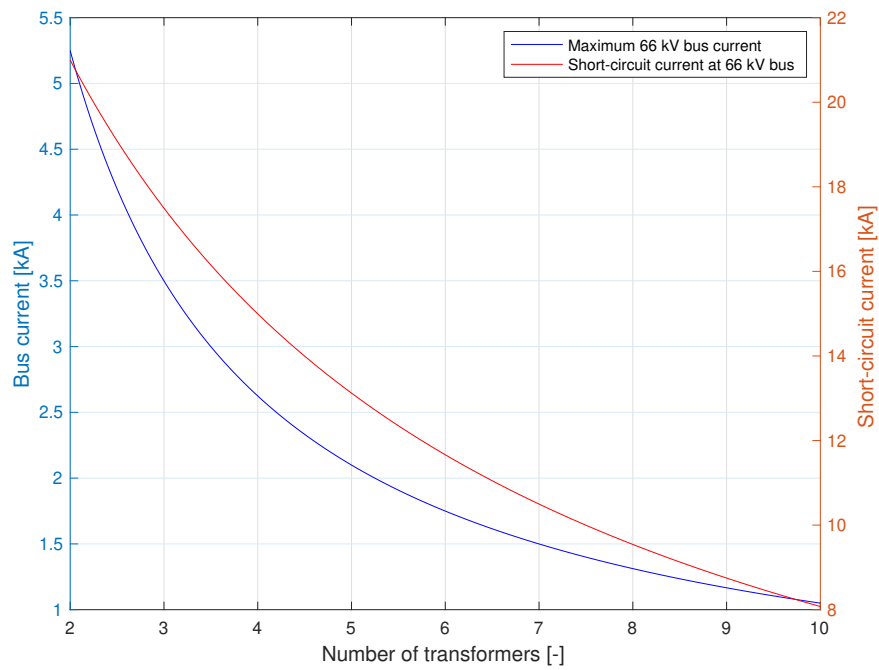


Figure 8.9: The nominal current at the 66 kV bus $I_{n,bus}$ and the SCC I_{SCC} as a function of the number of transformers connected to one of the 150 kV buses x for case 4.

9

Conclusion and future work

9.1 Conclusion

In this report, a study on the global hydrogen demand, electrolyser manufacturers as well as hydrogen applications in both near-time and future perspective were investigated. Renewable hydrogen produced from electrolysis has a potential to increase immensely in the near future in order to support the decarbonisation of several sectors. Furthermore, a PEM electrolyser was modelled in MATLAB Simulink and it behaved as expected. Simulations showed that the cell voltage increased with the current density which is why the efficiency decreased for higher current densities as well. It was also demonstrated through simulations that possible course of actions to increase the efficiency of the electrolyser are to decrease the membrane thickness or to increase the temperature. Moreover, the membrane area or the number of cells connected in series can be increased to develop larger electrolyser stacks and allow higher hydrogen production rate. Another alternative is also to expand the limiting current density in order to allow higher current densities and therefore higher hydrogen production rates. It would also be preferable to increase the limiting current density so that a high current density can be acquired without operating in the concentration region due to the exponential voltage increase.

The behaviour of the 12-pulse thyristor rectifier was successful as it displayed low output current ripple, low output voltage ripple and good dynamic control response. Low-order harmonics cancellation, except 11th and 13th harmonics, was also achieved. However, due to the large demand in current amplitude, the 12-pulse thyristor rectifier developed increasing reactive power levels as demand increases for its 11th and 13th harmonic current amplitudes. For any application requiring a lower current output, this behaviour would be less of a concern. But for any industrial electrolyser plant, designing power conversion from the AC distribution grid with a 12-pulse thyristor rectifier must include tuned LC-filters, which increases the cost. Operational issues due to grid strength are expected to be more prominent if the converter is modelled with all losses included, and at a grid voltage of higher value than at the secondary sides of the transformer. Additionally, with VRE technologies becoming increasingly common, part of the reactive power that is needed for thyristor rectifier operation might be needed as extra power just for the electrolyser plant operation.

The PSFB DC/DC converter seems to be a suitable converter for electrolyser applications as it fulfilled seven of the eight suggested requirements for DC/DC converters in electrolyser applications. The simulations demonstrated that it has low output current ripple and low output voltage ripple. Another advantage is also that there is

no reactive power consumption. Moreover, the PSFB DC/DC converter topology design was accomplished as it enabled a high output current and a low output voltage while also enabling an applicable voltage across the IGBTs as well as a low current flow at the distribution DC-bus, which is favourable. Finally, the model demonstrated that dynamic control response functioned accordingly as well.

When designing an electrolyser station on GW-scale, both requirements at PCC and internal requirements must be fulfilled. Furthermore, four electrolyser structure designs were proposed, where case 4 seemed most beneficial as it enabled lower number of transformers, nominal bus current and short-circuit current. However, redundancy of the 400/150 kV transformers was not fulfilled with this design approach.

9.2 Future work

Further investigations as future work would be to advance the electrolyser model even further with regards to:

- More accurate modelling of the electrolyser components, with consideration of parameters such as the resistance and the stray capacitance of the electrodes;
- Design and simulation of common electrolyser system architecture components;
- Thermodynamics;
- Pressure dynamics.

Components inside the electrolyser such as the electrodes and the membrane should be modelled more accurately with consideration of choice of material or other significant characteristics such as the resistance and the stray capacitance of the electrodes. These were not considered which would increase the ohmic overvoltage contribution and possibly affect the ripple respectively. Moreover, since the temperature and pressure were assumed constant, an investigation on the thermodynamics and pressure dynamics of the electrolyser would be recommended. Finally, the electrolyser system should be modelled with its common system architecture components such as feed water supply, gas separator and compressor, which would enable more real-based simulation results. This would also enable to further investigate how ripple will affect the electrolyser system. Specific things that should be evaluated in detail are the lifetime, components durability, performance and efficiency.

Accuracy of both converter simulation models, the 12-pulse thyristor rectifier and the PSFB DC/DC converter, should be improved. Adding details to all components such as electrical losses would improve and produce more accurate simulation results compared to those presented in this work. Moreover, investigating optimisation of the converters such as cost and volume would be preferable. A separate study of the impact on the grid for the thyristor rectifier with a more detailed model of the line impedance would be recommended as well. Finally, for the PSFB DC/DC converter, it would be proposed to model it as an interleaved PSFB DC/DC converter to investigate if the ripple can be lowered. This could require smaller filter components and therefore decrease the expenses.

In order to find viable electrolyser station designs, a more detailed design analysis

is recommended. The design analysis should consider more common components that are required such as switchgears, relays, current and voltage transformers. The reactive power consumption should also include the entire electrolyser station and not only the electrolyser systems within. Finally, the transformer impedances, apparent power rating and nominal bus current should be estimated with more accurate data.

Bibliography

- [1] P. Hoffman and B. Dorgan, ‘*Tomorrow’s Energy, Revised and Expanded Edition: Hydrogen, Fuel Cells, and the Prospects for a Cleaner Planet*,’ 2nd ed., Cambridge, Massachusetts, USA: MIT Press, 2012. [Online]. Available: <https://ebookcentral.proquest.com/lib/chalmers/reader.action?docID=3339385> Accessed: 07/11/2020.
- [2] J. Turner et al., ‘Renewable hydrogen production,’ *International Journal of Energy Research*, vol. 32, no. 5, pp. 379–407, Nov. 2007. DOI: 10.1002/er.1372.
- [3] IRENA, ‘Renewable power-to-hydrogen,’ IRENA, Abu Dhabi, United Arab Emirates, ISBN 978-92-9260-145-4, 2019. [Online]. Available: https://www.irena.org/-/media/Files/IRENA/Agency/Publication/2019/Sep/IRENA_Power-to-Hydrogen_Innovation_2019.pdf Accessed: 05/12/2020.
- [4] Q. Hassan, ‘Optimisation of solar-hydrogen power system for household applications,’ *International Journal of Hydrogen Energy*, vol. 45, no. 58, pp. 33 111–33 127, Nov. 2020. DOI: <https://doi.org/10.1016/j.ijhydene.2020.09.103>.
- [5] E.M. Gray et al., ‘Hydrogen storage for off-grid power supply,’ *International Journal of Hydrogen Energy*, vol. 36, no. 1, pp. 654–663, Jan. 2011. DOI: <https://doi.org/10.1016/j.ijhydene.2010.09.051>.
- [6] GE Gas Power, ‘Can GE’s gas turbines run on hydrogen fuel?,’ 2021. [Online]. Available: <https://www.ge.com/power/gas/fuel-capability/hydrogen-fueled-gas-turbines/> Accessed: 05/12/2020.
- [7] J.D. Holladay, J. Hu, D.L. King and Y. Wang, ‘An overview of hydrogen production technologies,’ *Catalysis Today*, vol. 139, no. 4, pp. 244–260, Jan. 2009. DOI: 10.1016/j.cattod.2008.08.039.
- [8] T. E. Lipman and A. Z. Weber, *Fuel Cells and Hydrogen Production: A Volume in the Encyclopedia of Sustainability Science and Technology*. 2nd ed., New York, NY, USA: Springer, 2019. [Online]. Available: <https://search.ebscohost.com/login.aspx?direct=true&AuthType=sso&db=cat07472a&AN=clec.SPRINGERLINK9781493977895&site=eds-live&scope=site&custid=s3911979&authtype=sso&group=main&profile=eds> Accessed: 05/12/2020.
- [9] Office of Energy Efficiency & Renewable Energy, ‘Hydrogen storage,’ n.d. [Online]. Available: <https://www.energy.gov/eere/fuelcells/hydrogen-storage> Accessed: 12/09/2020.

- [10] Clean Energy Institute at the University of Washington, ‘What is a lithium-ion battery and how does it work?’, 2020. [Online]. Available: <https://www.cei.washington.edu/education/science-of-solar/battery-technology/> Accessed: 10/11/2020.
- [11] A. Mayyas, M. Wei and G. Levis, ‘Hydrogen as a long-term, large-scale energy storage solution when coupled with renewable energy sources or grids with dynamic electricity pricing schemes,’ *International Journal of Hydrogen Energy*, vol. 45, no. 33, pp. 16 311–16 325, Jun. 2020. DOI: <https://doi.org/10.1016/j.ijhydene.2020.04.163>.
- [12] A. Godula-Jopek and D. Stolten, *Hydrogen Production : By Electrolysis*. 1st ed., Hoboken, NJ, USA: John Wiley & Sons, 2015. [Online]. Available: <https://search.ebscohost.com/login.aspx?direct=true&AuthType=sso&db=cat07472a&AN=clec.EBC1956440&site=eds-live&scope=site&custid=s3911979&authtype=sso&group=main&profile=eds> Accessed: 15/11/2020.
- [13] J. Koponen, V. Ruuskanen, A. Kosonen, M. Niemelä and J. Ahola, ‘Effect of converter topology on the specific energy consumption of alkaline water electrolyzers,’ *IEEE Transactions on Power Electronics*, vol. 34, no. 7, pp. 6171–6182, Oct. 2018. DOI: 10.1109/TPEL.2018.2876636.
- [14] IEEE, ‘IEEE Code of Ethics,’ IEEE Policies, Section 7 - Professional Activities (Part A - IEEE Policies), 2020. [Online]. Available: <https://www.ieee.org/about/corporate/governance/p7-8.html> Accessed: 26/01/2021.
- [15] TRIMIS European Commission, ‘Nordic hydrogen corridor: Zero emission transport between the capitals of the nordic countries with fuel cell vehicles,’ 2017. [Online]. Available: <https://trimis.ec.europa.eu/project/nordic-hydrogen-corridor-zero-emission-transport-between-capitals-nordic-countries-fuel-cell>.
- [16] W. Nummelin, ‘EU: Släpp Navalnyj omedelbart,’ *Svenska Dagbladet*, January, 21, 2021. [Online]. Available: <https://www.svd.se/eu-parlamentet-vill-straaffaryssland/om/forgiftningen-av-navalnyj> Accessed: 22/01/2021.
- [17] Royal Swedish Academy of Engineering Sciences, ‘Future forum - räcker elen till?’, 2021. [Online]. Available: <https://www.iva.se/event/future-forum/>.
- [18] TRIMIS European Commission, ‘Hydrogen in gas grids: A systematic validation approach at various admixture levels into high-pressure grids,’ 2020. [Online]. Available: <https://trimis.ec.europa.eu/project/hydrogen-gas-grids-systematic-validation-approach-various-admixture-levels-high-pressure>.
- [19] P. Charlier, ‘Hydrogen tanker crashes and explodes on freeway in Changhua City,’ *Taiwan English News*, September, 30, 2020. [Online]. Available: <https://taiwanenglishnews.com/hydrogen-tanker-crashes-and-explodes-on-freeway-in-changhua-city/> Accessed: 28/01/2021.
- [20] J. Riccioli, ‘A massive boom’: Explosion at Waukesha gas company reverberated through the city and left one injured,’ *Milwaukee Journal Sentinel*, December, 12, 2019. [Online]. Available: <https://eu.jsonline.com/story/communities/waukesha/news/waukesha/2019/12/12/explosion-rocks-airgas-waukesha-cause-unclear/4412254002/> Accessed: 28/01/2021.

- [21] L. Sung-hyun and C. Jeehyun, ‘Tank explosion poses setback for Seoul’s push for hydrogen economy,’ *Pulse by Maeil Business News Korea*, May, 24, 2019. [Online]. Available: <https://pulsenews.co.kr/view.php?year=2019&no=346776> Accessed: 28/01/2021.
- [22] J. Conca, ‘Natural gas and the new deathprint for energy,’ *Forbes*, January, 25, 2018. [Online]. Available: <https://www.forbes.com/sites/jamesconca/2018/01/25/natural-gas-and-the-new-deathprint-for-energy/?sh=5ca082945e19> Accessed: 28/01/2021.
- [23] G. Newsholme, P. Bellaby, R. Flynn and M. Ricci, ‘Hydrogen: Too dangerous to base our future upon?’ *Institution of Chemical Engineers Symposium Series*, 2006. [Online]. Available: <https://www.icheme.org/media/9792/xix-paper-04.pdf> Accessed: 10/01/2021.
- [24] G. Chisholm and L. Cronin, ‘Hydrogen From Water Electrolysis,’ in *Storing Energy: With Special Reference to Renewable Energy Sources*. 1st ed., T.M. Letcher, Amsterdam, The Netherlands: Elsevier, 2016, ch. 16, pp. 315-343. [Online]. Available: <https://www.sciencedirect.com/science/article/pii/B9780128034408000166?via%5C%3Dihub> Accessed: 11/03/2021.
- [25] IRENA, ‘Green hydrogen cost reduction,’ IRENA, Abu Dhabi, United Arab Emirates, ISBN 978-92-9260-295-6, 2020. [Online]. Available: https://irena.org/-/media/Files/IRENA/Agency/Publication/2020/Dec/IRENA_Green_hydrogen_cost_2020.pdf Accessed: 11/03/2021.
- [26] ———, ‘Hydrogen from renewable power,’ IRENA, Abu Dhabi, United Arab Emirates, ISBN 978-92-9260-077-8, 2018. [Online]. Available: https://www.irena.org/-/media/Files/IRENA/Agency/Publication/2018/Sep/IRENA_Hydrogen_from_renewable_power_2018.pdf Accessed: 11/03/2021.
- [27] S. Sood et al., ‘Generic dynamical model of pem electrolyser under intermittent sources,’ *Energies*, vol. 13, no. 24, Dec. 2020. DOI: <https://doi.org/10.3390/en13246556>.
- [28] IEA, ‘The future of hydrogen,’ IEA, Paris, France, 2019. [Online]. Available: https://iea.blob.core.windows.net/assets/9e3a3493-b9a6-4b7d-b499-7ca48e357561/The_Future_of_Hydrogen.pdf Accessed: 05/03/2021.
- [29] IRENA, ‘Hydrogen: A renewable energy perspective,’ IRENA, Abu Dhabi, United Arab Emirates, ISBN 978-92-9260-151-5, 2019. [Online]. Available: https://www.irena.org/-/media/Files/IRENA/Agency/Publication/2019/Sep/IRENA_Hydrogen_2019.pdf Accessed: 11/03/2021.
- [30] Nel, 2021. [Online]. Available: <https://nelhydrogen.com> Accessed: 15/02/2021.
- [31] McPhy, 2021. [Online]. Available: <https://mcphy.com/en/> Accessed: 15/02/2021.
- [32] ITM Power, 2021. [Online]. Available: <https://www.itm-power.com> Accessed: 15/02/2021.
- [33] Siemens, ‘The foreground needs a background,’ 2021. [Online]. Available: <https://new.siemens.com/global/en/company/about/history/specials/170-years-of-siemens.html> Accessed: 22/02/2021.

- [34] —, ‘Renewable-energy power plants,’ 2021. [Online]. Available: <https://new.siemens.com/global/en/company/about/history/technology/power-generation-and-distribution/renewable-energy-power-plants.html> Accessed: 22/02/2021.
- [35] Siemens Energy, ‘Siemens energy company presentation,’ 2020. [Online]. Available: <https://assets.siemens-energy.com/siemens/assets/api/uuid:fc59adb3-bc23-4642-a227-d5d30f7e4c4e/company-presentation-siemens-energy-en.pdf> Accessed: 16/02/2021.
- [36] Ú. Guerra, ‘Siemens gamesa and siemens energy to unlock a new era of offshore green hydrogen production,’ 2021. [Online]. Available: <https://www.siemensgamesa.com/en-int/newsroom/2021/01/210113-siemens-gamesa-press-release-siemens-energy-agreement-green-hydrogen> Accessed: 22/02/2021.
- [37] A. Benzinger, ‘Siemens energy and air liquide to develop a large scale electrolyzer partnership for sustainable hydrogen production,’ 2021. [Online]. Available: <https://press.siemens-energy.com/global/en/pressrelease/siemens-energy-and-air-liquide-develop-large-scale-electrolyzer-partnership> Accessed: 22/02/2021.
- [38] Stadtwerke Mainz AG, ‘Energiepark mainz,’ 2017. [Online]. Available: <https://www.energiepark-mainz.de/en/> Accessed: 17/05/2021.
- [39] U. Kreutzer, ‘World’s largest power-to-gas plant of its kind: A blueprint for sector coupling?’, 2018. [Online]. Available: <https://www.siemens-energy.com/global/en/news/magazine/2020/the-future-of-energy-interview-power-to-x.html> Accessed: 17/05/2021.
- [40] J. Bentein, ‘Green hydrogen,’ *New Technology Magazine*, January, 27, 2014. [Online]. Available: https://issuu.com/jwnenergy/docs/ntm_01022014 Accessed: 17/02/2021.
- [41] Cummins, ‘Cummins closes on its acquisition of hydrogenics,’ 2019. [Online]. Available: <https://www.cummins.com/news/releases/2019/09/09/cummins-closes-its-acquisition-hydrogenics> Accessed: 17/02/2021.
- [42] Seeking alpha, ‘Hydrogenics corporation 2018 q4 - results - earnings call slides,’ 2019. [Online]. Available: <https://seekingalpha.com/article/4249048-hydrogenics-corporation-2018-q4-results-earnings-call-slides> Accessed: 18/02/2021.
- [43] —, ‘Hydrogenics corporation 2017 q4 - results - earnings call slides,’ 2018. [Online]. Available: <https://seekingalpha.com/article/4154572-hydrogenics-corporation-2017-q4-results-earnings-call-slides> Accessed: 18/02/2021.
- [44] B. Motz and C. Witty, ‘Hydrogenics reports fourth quarter and full year 2014 results,’ 2015. [Online]. Available: <https://www.globenewswire.com/fr/news-release/2015/03/04/712264/10123127/en/Hydrogenics-Reports-Fourth-Quarter-and-Full-Year-2014-Results.html> Accessed: 18/02/2021.
- [45] Cummins, ‘Cummins hydrogen day,’ 2020. [Online]. Available: <https://www.cummins.com/new-power/applications/about-hydrogen/hydrogenday> Accessed: 16/02/2021.

- [46] J. Mills, ‘Cummins closes on nproxx joint venture for hydrogen storage,’ *Businesswire*, November, 13, 2020. [Online]. Available: <https://www.businesswire.com/news/home/20201113005546/en/Cummins-Closes-on-NPROXX-Joint-Venture-for-Hydrogen-Storage> Accessed: 19/02/2020.
- [47] L. Collins, ‘World’s largest green-hydrogen plant inaugurated in Canada by Air Liquide,’ *Recharge News*, January, 27, 2021. [Online]. Available: <https://www.rechargenews.com/transition/worlds-largest-green-hydrogen-plant-inaugurated-in-canada-by-air-liquide/2-1-952085> Accessed: 19/02/2020.
- [48] DNV GL, ‘Oil and gas forecast to 2050,’ DNV GL, Høvik, Norway, 2017. [Online]. Available: <https://eto.dnv.com/2017/oilgas> Accessed: 08/03/2021.
- [49] IRENA, ‘Green hydrogen: A guide to policy making,’ IRENA, Abu Dhabi, United Arab Emirates, ISBN 978-92-9260-286-4, 2020. [Online]. Available: https://irena.org/-/media/Files/IRENA/Agency/Publication/2020/Nov/IRENA_Green_hydrogen_policy_2020.pdf Accessed: 06/03/2021.
- [50] —, ‘Reaching zero with renewables,’ IRENA, Abu Dhabi, United Arab Emirates, ISBN 978-92-9260-269-7, 2020. [Online]. Available: https://www.irena.org/-/media/Files/IRENA/Agency/Publication/2020/Sep/IRENA_Reaching_zero_2020.pdf Accessed: 10/03/2021.
- [51] HYBRIT, ‘Hybrit - fossil-free steel,’ 2017. [Online]. Available: <https://dh5k8ug1gwbyz.cloudfront.net/uploads/2021/02/Hybrit-broschure-engelska.pdf> Accessed: 26/05/2021.
- [52] Fossilfritt Sverige, ‘Strategi för fossilfri konkurrenskraft: Vätgas,’ Fossilfritt Sverige, Stockholm, Sverige, 2021. [Online]. Available: <https://fossilfritt Sverige.se/wp-content/uploads/2021/01/Vatgasstrategi-for-fossilfri-konkurrenskraft-1.pdf> Accessed: 07/03/2021.
- [53] DNV GL, ‘Maritime forecast to 2050,’ DNV GL, Høvik, Norway, 2019. [Online]. Available: https://sustainableworldports.org/wp-content/uploads/DNV-GL_2019_Maritime-forecast-to-2050-Energy-transition-Outlook-2019-report.pdf Accessed: 09/03/2021.
- [54] ARUP, ‘Future of rail 2050,’ Arup, London, England, 2019. [Online]. Available: <https://www.arup.com/perspectives/publications/research/section/future-of-rail-2050> Accessed: 11/03/2021.
- [55] Baker McKenzie, ‘Shaping tomorrow’s global hydrogen market,’ Baker McKenzie, Chicago, IL, USA, 2020. [Online]. Available: https://www.bakermckenzie.com/-/media/files/insight/publications/2020/01/hydrogen_report.pdf?la=en Accessed: 11/03/2021.
- [56] F. Marangio, M. Santarelli and M. Cali, ‘Theoretical model and experimental analysis of a high pressure pem water electrolyser for hydrogen production,’ *International Journal of Hydrogen Energy*, vol. 34, no. 3, pp. 1143–1158, Feb. 2009. DOI: <https://doi.org/10.1016/j.ijhydene.2008.11.083>. Accessed: 05/02/2021.
- [57] A. S. Tijani, M. F. A. Ghani, I. K. Muritala, A. H. A. Rahim and F. A. B. Mazlan, ‘Electrochemical characteristics of (pem) electrolyzer under influence of charge transfer coefficient,’ *International Journal of Hydrogen Energy*, vol. 44, no. 50, pp. 27 177–27 189, Oct. 2019. DOI: <https://doi.org/10.1016/j.ijhydene.2019.08.188>. Accessed: 05/02/2021.

- [58] S. Toghiani et al., ‘Optimization of operating parameters of a polymer exchange membrane electrolyzer,’ *International Journal of Hydrogen Energy*, vol. 44, no. 13, pp. 6403–6414, Mar. 2019. DOI: <https://doi.org/10.1016/j.ijhydene.2019.01.186>. Accessed: 05/02/2021.
- [59] Z. Abdin, C. J. Webb and E. M. Gray, ‘Modelling and simulation of a proton exchange membrane (pem) electrolyser cell,’ *International Journal of Hydrogen Energy*, vol. 40, no. 39, pp. 13 243–13 257, Oct. 2015. DOI: <https://doi.org/10.1016/j.ijhydene.2015.07.129>. Accessed: 05/02/2021.
- [60] M. G. Santarelli, M. F. Torchio and P. Cochis, ‘Parameters estimation of a pem fuel cell polarization curve and analysis of their behavior with temperature,’ *Journal of Power Sources*, vol. 159, no. 2, pp. 824–835, Sep. 2006. DOI: <https://doi.org/10.1016/j.jpowsour.2005.11.099>. Accessed: 05/02/2021.
- [61] K. Harrison, ‘MW-scale PEM-based electrolyzers for RES applications,’ NREL, Washington, D.C, USA, NREL/TP-5B00-79055, 2021. [Online]. Available: <https://www.nrel.gov/docs/fy21osti/79055.pdf> Accessed: 01/04/2021.
- [62] N. G. Hingorani, L. Gyugyi and M. E. El-Hawary, *Understanding FACTS : concepts and technology of flexible AC transmission systems*. Piscataway, NJ, USA: IEEE Press, 2000.
- [63] N. Mohan, T. M. Undeland and W. P. Robbins, *Power electronics: converters, applications and design*. Hoboken, NJ, USA: Wiley, 2003.
- [64] S. Kim, S.-W. Han, G.-J. Han and Y.-H. Cho, ‘Initial firing angle control of 12-pulse parallel connected thyristor dual converter for urban railway power substations,’ *2016 International Symposium on Power Electronics, Electrical Drives, Automation and Motion (SPEEDAM)*, pp. 645–650, Jun. 2016. DOI: <https://doi.org/10.1109/SPEEDAM.2016.7525954>. Accessed: 26/04/2021.
- [65] F. Blaabjerg, *Control of Power Electronic Converters and Systems: Volume 1*. Cambridge, MA, USA: Academic Press, 2018.
- [66] A. Subburaj and S. Bayne, ‘Battery and wind system in weak/strong grid analysis,’ *IEEE Industry Application Society - 51st Annual Meeting, IAS 2015, Conference Record*, Oct. 2015. DOI: <https://doi.org/10.1109/IAS.2015.7356938>. Accessed: 28/04/2021.
- [67] D. Guilbert, A. Scipioni and S. M. Collura, ‘DC/DC converter topologies for electrolyzers: State-of-the-art and remaining key issues,’ *International Journal of Hydrogen Energy*, vol. 42, no. 38, pp. 23 966–23 985, Sep. 2017. DOI: <https://doi.org/10.1016/j.ijhydene.2017.07.174>. Accessed: 13/04/2021.
- [68] N. Hassanzadeh, F. Yazdani, S. Haghbin and T. Thiringer, ‘Design of a 50 kw phase-shifted full-bridge converter used for fast charging applications,’ *IEEE*, Apr. 2018. DOI: [10.1109/VPPC.2017.8330881](https://doi.org/10.1109/VPPC.2017.8330881). Accessed: 20/04/2021.
- [69] A. Ekic et al., ‘Impact analysis of power network structure on grid strength,’ *2018 North American Power Symposium (NAPS), Power Symposium (NAPS), 2018 North American*, Sep. 2018. DOI: [10.1109/NAPS.2018.8600573](https://doi.org/10.1109/NAPS.2018.8600573).
- [70] Y. Li et al., ‘Research on capacity planning of renewable energy grid integration based on effective short circuit ratio,’ *2020 IEEE Sustainable Power and Energy Conference (iSPEC), Sustainable Power and Energy Conference (iSPEC), 2020 IEEE*, Nov. 2020. DOI: <https://doi.org/10.1109/iSPEC50848.2020.9351108>.

- [71] ABB, 'Medium voltage indoor circuit breakers,' 2021. [Online]. Available: <https://new.abb.com/medium-voltage/apparatus/circuit-breakers/indoor-CB>
Accessed: 05/06/2021.

A

Appendix

In this appendix the electrolyser model in MATLAB Simulink, the 12-pulse thyristor rectifier model in PLECS and the PSFB DC/DC converter model in PLECS, as illustrated in Figure A.1-A.3, together with their respective MATLAB simulation initialisation files are presented.

A.1 PEM Electrolyser model

```
%% Electrolyser system
%%%%%%%%%%%%%%%%%%%%%%%%%%%%%%%%%%%%%%%%%%%%%%%%%%%%%%%%%%%%%%%%%%%%%%%%
% Main program for electrolyser system.
clear all
clc
%%%%%%%%%%%%%%%%%%%%%%%%%%%%%%%%%%%%%%%%%%%%%%%%%%%%%%%%%%%%%%%%%%%%%%%%
T0=20; % Reference temperature [Celsius]
T=4*T0; % Temperature [Celsius]

p0=1; % Reference pressure [bar]
p=30*p0; % Pressure [bar]

deltaH=285840; % Change of enthalpy [J/mol]
deltaS=163.2; % Change of entropy [J/(mol*K)]
deltaG=deltaH-deltaS*(273.15+T); % Gibbs free energy [J/mol]
F=96485; % Faraday constant [C/mol]
R=8.3144; % Universal gas constant [J/(mol*K)]
Ru=8.3144e-2; % Universal gas constant [bar*L/(mol*K)]

% Vact:
alpha_an=0.5; % Anode charge transfer coefficient [-]
alpha_ca=0.5; % Cathode charge transfer coefficient [-]
j0_an=1e-2; % The anode exchange current density [A/cm^2]
j0_ca=1e1; % The cathode exchange current density [A/cm^2]

% Vrev
Vrev0=deltaG/(2*F); % Reversible voltage [V]

% Vohm
lambda=18; % Molecules of water per sulphonic group [-]
```

```

delta_mem=127e-4; % Membrane thickness [cm]
sigma_mem=(0.005139*lambda-0.00326)*exp(1268*(1/303-1/(273.15+T)));
% Conductivity of the membrane [S/cm]
A_mem=1250; % Area of the membrane [cm^2]
Rmem=delta_mem/(A_mem*sigma_mem); % Membrane resistance [ohm]

% Vcon
j_1=3.0; % Limiting current density [A/cm^2]

I0_max=A_mem*j_1; % Maximum electroyser current [A]
P0_max=2e6; % Maximum electroyser power [W]
V0_max=P0_max/I0_max; % Maximum electroyser voltage [V]
Vcell_max=1.92; % Maximum cell voltage [V]
ns=V0_max/Vcell_max; % Series configuration of cells [-]

% Simulation
Tstart=0; % Starting time for the simulation [s]
Tstop=1; % End time for the simulation [s]

Hydrogen_demand=100; % Hydrogen production demand of maximum [%]
I_ref=(Hydrogen_demand/100)*(I0_max-0.5); % Reference current [A]

sim('Electrolyser',[Tstart,Tstop])

```

%%%

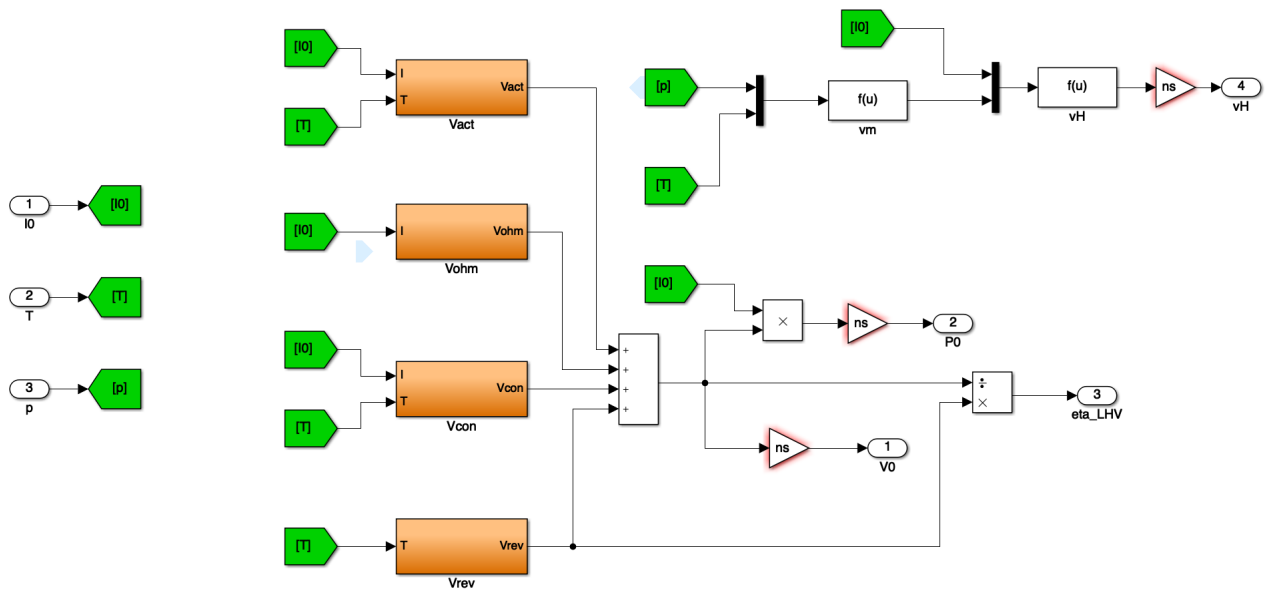


Figure A.1: The PEM electrolyser model as modelled in MATLAB Simulink.

A.2 12-pulse thyristor rectifier model

```

%% 12-pulse thyristor rectifier with electrolyser

```

```
%%%%%%%%%%%%%%%%%%%%%%%%%%%%%%%%%%%%%%%%%%%%%%%%%%%%%%%%%%%%%%%%%%%%%%%%%
% Main program for 12pTR AC/DC converter with electrolyser system.
clc; clf; clear all; close all;
%%%%%%%%%%%%%%%%%%%%%%%%%%%%%%%%%%%%%%%%%%%%%%%%%%%%%%%%%%%%%%%%%%%%%%%%%
Tstart=0; % Start time for the simulation [s]
Tstop=1; % End time for the simulation [s]
Tstep=0.05; %initiate the PLL:s, rectifiers start to conduct [s]
hydrogen_demand = 100; % Hydrogen production demand of maximum [%]

% Converter parameters
V_ac = 372; % V
f = 50; % Hz
omega = f*2*pi; Phi=0; % rad of sinusoidal and initial offset.
Power = 4e6; % MVA
nTurns=[1 1*sqrt(3) 1]; % -
run('Trf_windings');

% PLL & PI controller settings
kp = 0.0050; %Proportional gain of current controller(s)
ki = 0.2500; %Integral gain of current controller(s)
L_out = 10e-03;

Electrolyser_init
sim('thyristorConv_v4_0', [Tstart, Tstop])
%%%%%%%%%%%%%%%%%%%%%%%%%%%%%%%%%%%%%%%%%%%%%%%%%%%%%%%%%%%%%%%%%%%%%%%%%
```

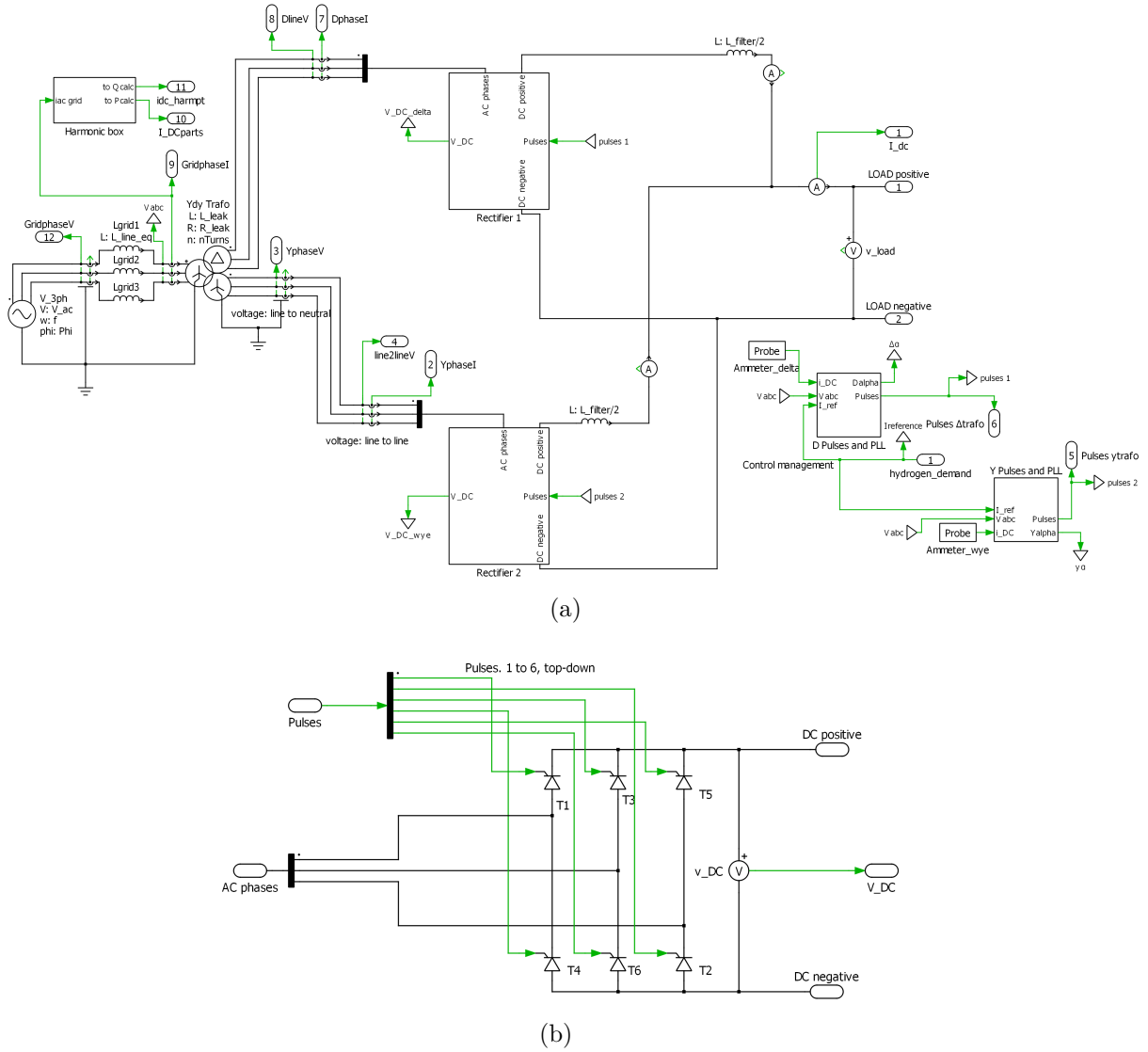


Figure A.2: The 12-pulse thyristor rectifier model as modelled in PLECS in a), with the two six-pulse rectifiers demonstrated in b).

A.3 Phase-shifted full-bridge DC/DC converter model

```

%% Phase shifted full-bridge with electrolyser
%%%%%%%%%%%%%%%%%%%%%%%%%%%%%%%%%%%%%%%%%%%%%%%%%%%%%%%%%%%%%%%%%%%%%%%%
% Main program for PSFB DC/DC converter with electrolyser system.
clear all
clc
%%%%%%%%%%%%%%%%%%%%%%%%%%%%%%%%%%%%%%%%%%%%%%%%%%%%%%%%%%%%%%%%%%%%%%%%
D_max=0.5; % Maximum duty cycle [-]
fsw=5e3; % Switching frequency [Hz]
Tsw=1/fsw; % Switching period [s]

I0_max=3750; % Maximum electrolyser current [A]
    
```

```

P0_max=2e6; % Maximum electrolyser power [W]

Vdc_bus=11e3; % DC bus voltage [V]
V0_max=P0_max/I0_max; % Maximum output voltage [V]
Vin=2.2e3; % Input voltage per PSFB [V]
n_PSFb=Vdc_bus/Vin;
% Number of PSFB connected in series at HV side and parallel
% at LV side [-]
I_PSFb_max=I0_max/n_PSFb; % Maximum PSFB output current [A]
deltaI0=0.01*I_PSFb_max; % Current ripple [A]
deltaV0=0.1/16*V0_max; % Voltage ripple [V]

n_turn=D_max*Vin/V0_max; % Turns ratio [-]
Coss=2.5e-9; % MOSFET output capacitor of the SiC switch [F]
C_T=0; % Transformer capacitance [F]
E_R=4/3*Coss*Vin^2+1/2*C_T*Vin^2;
% The required energy in the leakage inductance [J]
Lf=V0_max*(1-D_max)/(2*deltaI0*fsw); % Filter inductance [H]
L_R=2*E_R/(0.5*I_PSFb_max/n_turn)^2;% Leakage inductance [H]
Lm=n_turn*D_max*Vin/(2*deltaI0*fsw);% Magnetizing inductance [H]
C0=deltaI0/(16*deltaV0*fsw);% Filter capacitance [F]

f_cutoff=1/(2*pi*sqrt(Lf*C0)); % Cut-off frequency [Hz]
f_sample=10e6; % Sampling frequency for delay block to solve
% algebraic loop [Hz]

% Simulation
Tstart=0; % Starting time for the simulation [s]
Tstop=0.3; % End time for the simulation [s]

Hydrogen_demand=100; % Hydrogen production demand of maximum [%]
I_ref=(Hydrogen_demand/100)*(I0_max-0.5); % Reference current [A]
Phase_shift_max=180*D_max; % Maximum phase shift [Degrees]
Phase_shift_max_time=Phase_shift_max/360*Tsw; % Maximum phase
% time shift [s]

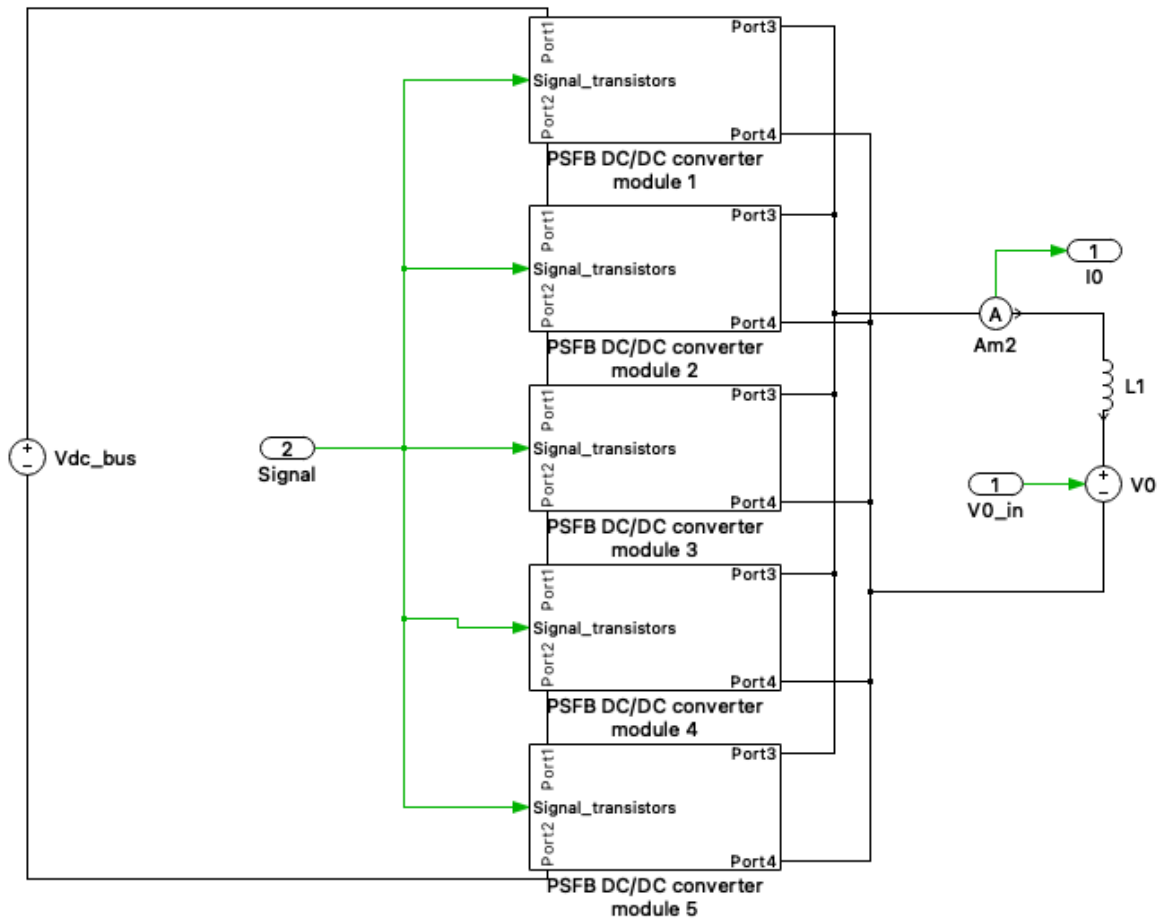
Electrolyser_init
sim('PSFB_electrolyser',[Tstart,Tstop])

```

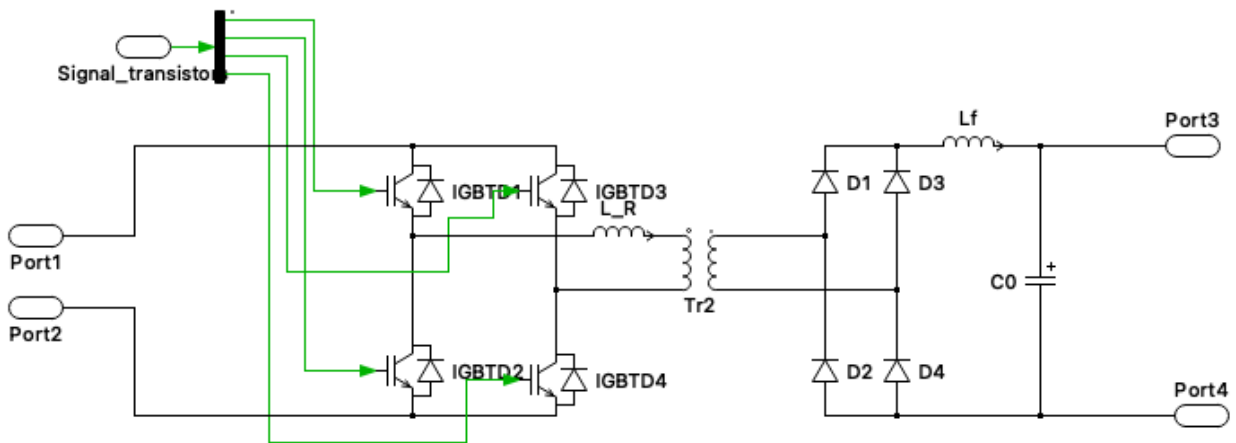
```

%%%%%%%%%%%%%%%%%%%%%%%%%%%%%%%%%%%%%%%%%%%%%%%%%%%%%%%%%%%%%%%%%%%%%%%%

```



(a)



(b)

Figure A.3: The PSFB DC/DC converter model as modelled in PLECS in a), with the PSFB DC/DC converter module model demonstrated in b).

DEPARTMENT OF ELECTRICAL ENGINEERING
CHALMERS UNIVERSITY OF TECHNOLOGY
Gothenburg, Sweden
www.chalmers.se



CHALMERS
UNIVERSITY OF TECHNOLOGY